M.Sc. Annasha Dutta

Small non-coding RNAs in regeneration of *Schmidtea mediterranea*

Doctoral dissertation

Supervisor: Dr. hab. Paulina Jackowiak, prof. ICHB PAN

Poznań, March 2025

Laboratory of Single Cell Analyses

Institute of Bioorganic Chemistry Polish Academy of Sciences

I dedicate this doctoral thesis to my parents, Swapan Kumar Dutta and Malaya Dutta, and my husband, Supratik Roy.

Acknowledgements

It is with great pleasure that I extend my deepest gratitude to Dr. hab. Paulina Jackowiak for giving me the opportunity to work on this project and be part of the Laboratory of Single Cell Analyses. Being a member of this team has been a truly rewarding experience, fostering both my scientific growth and personal satisfaction. I am profoundly grateful for her unwavering support, encouragement, kindness, and intellectual stimulation, primarily through inspiring discussions. Her patience and guidance have shaped my journey as a PhD student, and under her mentorship, I have always felt at home.

My heartfelt appreciation also goes to Anastasiia Zaremba, my academic sister and closest confidante during my time in the laboratory. Her expertise in bioinformatics and scientific acumen have profoundly influenced my doctoral dissertation, and without her, this work would not have been possible.

I would like to extend my sincere thanks to my colleagues from the Laboratory of Single Cell Analyses, the Laboratory of Genomics, and the Department of Molecular and Systems Biology at IBCH PAS. I have greatly benefited from the scientific and professional advice of Prof. Marek Figlerowicz and Dr. hab. Luiza Handschuh. It was a pleasure collaborating on various experiments with Dr. Anna Samelak-Czajka, Magdalena Trybus, Marcin Osuch, and Dr. inż. Małgorzata Marcinkowska-Swojak. Additionally, the companionship of Karolina, Joanna, Magda, Ola, and Czarek made my PhD journey all the more enjoyable.

I am also deeply grateful to Dr. hab. Anna Kurzyńska-Kokorniak, Dr. hab. Mariola Dutkiewicz, and Agnieszka Markowska for their invaluable help and support throughout my doctoral studies.

My warmest thanks go to Raneet, Martyna, Monidipa, Alessandra, and Linh, with whom I shared both the joys and challenges of the PhD journey. Their presence made my life in Poznań an extraordinary experience that I will cherish forever. I would also like to thank Banadeep, Somedeb, Arindam, Sandro, Shrena, and Diptashikha, some of my closest friends who have always stood by me through the thick and thin of life.

Lastly, my heartfelt appreciation goes to my husband, Supratik Roy, for his unwavering support, both intellectually and emotionally, and for always having my back. I am also deeply grateful to my parents and in-laws, my brother, and my sister-in-law for their immense emotional and mental support throughout this journey.

This work was financed by the National Science Centre, Poland, through a grant no. 2019/35/B/NZ2/02658 granted to Dr. hab. Paulina Jackowiak.

I acknowledge the use of the infrastructure developed under the project NEBI - National Research Center for Imaging in the Biological and Biomedical Sciences, POIR.04.02.00-00-C004/19, co-financed through the European Regional Development Fund (ERDF) in the frame of Smart Growth Operational Programme 2014-2020 (Measure 4.2 Development of modern research infrastructure of the science sector).

Abstract

Planarians like *Schmidtea mediterranea* are flatworms known for their extraordinary regenerative abilities and hence have been the subject of scientific study for over two centuries. Recent discoveries have unveiled multiple cellular and molecular mechanisms that drive this process. However, many questions remain open, particularly concerning the role of small non-coding RNAs (ncRNAs), a group of molecules that includes some of the most significant regulators of metazoan gene expression. Considering that the *S. mediterranea* shares homologous genes with humans, including those that are associated with Mendelian diseases when disrupted, a deeper understanding of the molecular mechanisms in this organism can provide universal insights.

The major objective of this study was to identify and characterize small ncRNAs involved in *S. mediterranea* regeneration, with particular focus on the RNA fragments – molecules derived from mature constitutive ncRNAs. To achieve this goal, the research focused on developing a strategy to disrupt the pool of small ncRNA in regenerating planarians and assess the impact of this disruption across multiple physiological levels. Accordingly, the ncRNA-processing ribonuclease **Smed Elac2** was stably depleted in an asexual strain of *S. mediterranea*, and the resulting effects were examined at phenotypic, anatomical, cellular, gene expression, and small ncRNA levels.

Following *Smed ELAC2* knockdown a delay in eye regeneration and abnormal ventral nerve cord development was observed at the phenotypic and anatomic levels, respectively. The cellular-level analysis of *Smed ELAC2* knockdown worms led to the discovery of multinucleated cells (**MuNs**) in planarians. While the established differentiative cell populations remained unaffected, *Smed ELAC2* disruption resulted in a progressive increase in the nuclearity of MuNs during regeneration. In-depth characterization of MuNs using imaging flow cytometry and fluorescence-activated cell sorting (FACS), revealed them to be large homeostatic cells with a potential epidermal progenitor-like identity. Differential gene expression and gene ontology analyses upon *Smed ELAC2* knockdown identified key dysregulated processes, including the overall negative regulation of cell proliferation and migratory pathways, developmental processes, and synaptic transmission—crucial elements in the regeneration context. This study identified a small non-coding RNA essential for proper regeneration timing: the **5′ tRNA half Gly-GCC**, which was drastically reduced following *Smed ELAC2* knockdown. This reduction highlighted a previously unknown role of Smed Elac2 in the production of 5′ tRNA half Gly-GCC. Functional *in vivo* studies further uncovered that this small ncRNA silenced the

expression of a receptor-type tyrosine phosphatase gene. The overexpression of this gene upon *Smed ELAC2* knockdown appeared to be linked to the increase in nuclearity of MuNs at the cellular level and the negative regulation of cell migratory pathways at the gene expression level.

In summary, the mechanistic link between Smed Elac2 and 5′ tRNA half Gly-GCC, the functional significance of 5′ tRNA half Gly-GCC, and the identification of MuNs provide new insights in planarian regeneration and open avenues for further research of the conserved role of small ncRNA across diverse biological contexts.

Streszczenie

Wypławki takie jak *Schmidtea mediterranea*, są płazińcami znanymi ze swoich niezwykłych zdolności regeneracyjnych i dlatego stanowią przedmiot badań naukowych od ponad dwóch stuleci. Odkrycia dokonane na przestrzeni ostatnich lat ujawniły wiele mechanizmów komórkowych i molekularnych, leżących u podstaw regeneracji. Nadal jednak wiele pytań pozostaje otwartych. Dotyczą one zwłaszcza roli krótkich niekodujących RNA (ang. *non-coding RNAs*, ncRNA), czyli grupy obejmującej najważniejsze cząsteczki regulujące ekspresję genów u *Metazoa*. Biorąc pod uwagę fakt, że *S. mediterranea* posiada geny będące homologami genów człowieka, w tym tych, których zaburzenia prowadzą do wystąpienia chorób dziedzicznych, lepsze zrozumienie procesów zachodzących u tego organizmu może dostarczyć wiedzy na temat uniwersalnych mechanizmów molekularnych.

Głównym celem niniejszej pracy była identyfikacja i charakterystyka krótkich ncRNA zaangażowanych w regenerację *S. mediterranea*, ze szczególnym uwzględnieniem tzw. fragmentów RNA – cząsteczek powstających z dojrzałych konstytutywnych ncRNA. Aby to osiągnąć, badania koncentrowały się na opracowaniu strategii zaburzenia puli ncRNA podczas regeneracji i ocenie skutków tego zaburzenia na kilku poziomach fizjologicznych. W związku z tym, u wypławków reprezentujących bezpłciowy szczep *S. mediterranea* wyciszono ekspresję genu kodującego rybonukleazę Smed Elac2, biorącą udział w metabolizmie ncRNA. Następnie efekty tego wyciszenia zostały zbadane na poziomie fenotypowym, anatomicznym, komórkowym, ekspresji genów i krótkich ncRNA.

W wyniku wyciszenia ekspresji genu *Smed ELAC2*, na poziomie fenotypowym i anatomicznym zaobserwowano, odpowiednio, opóźnienie w regeneracji fotoreceptorów i nieprawidłowy rozwój pni nerwowych. Analiza na poziomie komórkowym doprowadziła do odkrycia u wypławków komórek wielojądrzastych. Podczas gdy w warunkach wyciszenia *Smed ELAC2* podstawowe populacje komórek niezróżnicowanych pozostały nienaruszone w trakcie regeneracji, w komórkach wielojądrzastych zaobserwowano wzrost liczby jąder. Szczegółowa charakterystyka tych komórek przy użyciu cytometrii przepływowej z obrazowaniem i sortowania aktywowanego fluorescencją ujawniła, że są to duże komórki występujące w warunkach homeostazy i prawdopodobnie mają charakter progenitorów epidermalnych. Analizy ekspresji genów i ich ontologii pozwoliły zidentyfikować kluczowe procesy, które zostały ograniczone w wyniku wyciszenia *Smed ELAC2*. Były to: proliferacja komórek, funkcjonowanie komórkowych szlaków migracyjnych, procesy rozwojowe i sygnalizacja synaptyczna - kluczowe elementy w

kontekście regeneracji. W wyniku przeprowadzonych badań, zidentyfikowano także krótki ncRNA niezbędny do prawidłowego przebiegu regeneracji: połówkę 5′ tRNA Gly-GCC (ang. *5′ tRNA half Gly-GCC*, 5’ tRNAh Gly-GCC). Poziom akumulacji tej cząsteczki wyraźnie obniżał się podczas niedoboru rybonukleazy Smed Elac2, co wskazywało, że enzym ten bierze udział w biogenezie 5’ tRNAh Gly-GCC. Wyniki badań funkcjonalnych *in vivo* ujawniły że 5’ tRNAh Gly-GCC pełni rolę regulatorową i wycisza gen kodujący receptorową białkową fosfatazę tyrozynową. Podwyższona ekspresja tego genu w warunkach wyciszenia *Smed ELAC2* wydaje się być związana z wzrostem liczby jąder komórek wielojądrzastych i ograniczeniem funkcjonowania szlaków migracji komórek.

Podsumowując, przedstawione w tej pracy dane na temat: (i) udziału Smed Elac2 w biogenezie 5’ tRNAh Gly-GCC, (ii) znaczenia funkcjonalnego tego ncRNA oraz (iii) komórek wielojądrzastych, poszerzają wiedzę na temat regeneracji wypławków i otwierają perspektywy dalszych badań zachowawczej ewolucyjnie roli ncRNA w różnych kontekstach biologicznych.

Abbreviations

ncRNA	Non-coding RNA
dsRNA	Double stranded RNA
sncRNA	Small non-coding RNA
KD	knockdown
IEG	Immediate early genes
dpa	Days post amputation
hpa	Hours post amputation
CDK	Cyclin-dependent kinases
MuNs	Multinucleated cells
MoNs	Mononucleated cells
FACS	Fluorescence-Activated Cell Sorting
IS	ImageStream
EdU	Ethynyl-2'-deoxyuridine
BrdU	bromodeoxyuridine
hESC	Human embryonic stem cell
mESC	Mouse embryonic stem cell
miRNA	Micro RNA
piRNA	Piwi protein associated RNA
tRF	tRNA-derived fragments
cNeoblasts	Clonogenic neoblasts
SPG	Subperineurial glia
PC2	Proprotein convertase
COLL	Collagen
PORCN	Porcupine
Egr	Early growth response
TERC	Telomerase RNA component
lncRNA	Long non-coding RNA
circRNA	Circular RNA
snRNA	Small nuclear RNA
vtRNA	Vault RNA
HST	Heterokaryon-to-synkaryon
DSB	Double stranded breaks

CNS	Central nervous system
AP	Anterior posterior
DV	Dorsoventral
PCG	Position control genes
RCF	Relative Centrifugal Force
PCR	Polymerase chain reaction
qRT-PCR	Quantitative real time - polymerase chain reaction
FISH	Fluorescence *in situ* hybridization
BF	Brightfield
NGS	Next generation sequencing
MTS	Mitochondrial target sequence
NTD	N-terminal domain
CTD	C-terminal domain
DEG	Differentially expressed genes
GO	Gene Ontology
ROCK	Rho Kinase
CDS	Coding sequence
UTR	Untranslated region
COXPD-17	Combined oxidative phosphorylation deficiency-17

Table of Contents

1. Introduction

Regeneration restores damaged or missing cells, tissues, organs, or body parts to full functionality, aiding in the maintenance or replacement of lost physiological structures (Bely and Nyberg, 2010; Tanaka and Reddien, 2011). Unlike cell turnover, regeneration is typically triggered by nonspecific pathological factors that lead to acute damage and affect multiple tissue types (Pellettieri and Alvarado, 2007). Known since ancient times, this process is evolutionarily conserved to varying degrees across species and even life stages (adult or early development), raising a key question: why can some organisms regenerate certain structures while others cannot? Principally, regeneration is triggered primarily for structures that are not immediately essential for survival but are vital for the broader maintenance of a healthy, fully functioning organism (Reichman, 1984). An added complexity is that compensatory replacement of missing structures induced by the partial loss of physiologically crucial organs like heart or liver, only takes place if the injury repair is energetically feasible for the organism – if not the organism perishes (Alvarado, 2000). Hence for centuries, researchers have sought to understand the diversity and intricacies of this fundamental process.

Understanding the molecular basis of regeneration is crucial for advancing regenerative medicine. Research in this field operates on two levels: one explores mammalian stem cells and organoids to replicate human-like structures *in vitro* and uncover molecular pathways, while the other uses non-mammalian models to study *in vivo* regeneration processes, such as wound healing and differentiation (Sandoval-Guzmán and Currie, 2018). While both approaches provide valuable insights, focusing solely on one can lead to a biased and incomplete understanding of regenerative processes (Sandoval-Guzmán and Currie, 2018). Therefore, the recommended mode of study involves the use of both approaches in a complementary fashion, whenever possible.

1.1. The metazoan regenerative pathway

All multicellular organisms must replace cells, tissues, or even entire organs as part of routine homeostasis or recovery from disease and injury. Thus, a certain degree of basic regenerative potential is vital for their survival and overall health. The varying regenerative abilities across species present a significant challenge to study this process extensively in widely used model systems. Most of the available cellular and molecular insights come from a few well-studied invertebrate models (e.g., cnidarians, acoels and flatworms) and vertebrates, primarily salamanders (Srivastava, 2021). Interestingly, despite the diversity in

regenerative strategies among organisms, many underlying mechanisms are conserved. For example, Wnt signalling plays a crucial role in coordinating regenerative polarity vital in both full-body regenerating organisms, like *Hydra* (Tursch and Holstein, 2023), acoels (Srivastava et al., 2014) and flatworms (planarians) (De Robertis, 2010), and in organisms with limited regenerative capacity, such as zebrafish and salamanders (Lovely et al., 2022; Wehner et al., 2014). The section below aims to highlight the similarities in regeneration across phyla, emphasizing its evolutionary significance. Wnt signalling is used as a representative example to illustrate key aspects of regeneration in this context.

The discovery of parallels in the molecular mechanisms underlying the otherwise diverse process of regeneration across species, highlights the fundamental principles of this phenomenon. In line with this, researchers have developed a general and step-wise scheme for regenerative processes. First, an injury quickly triggers molecular changes in the cells at the wound site, which then signal other tissues to initiate a coordinated regeneration process. The next step usually (not always) involves the production of new cells, providing the necessary building blocks for new tissue formation. Finally, newly generated cells must interpret patterning cues to adopt the appropriate cell identities and integrate both with one another and with existing tissues to reconstruct a fully functional organ or organism. Each step is underlain by complex interactions between processes like cell proliferation, migration, differentiation and death (Tiozzo and Copley, 2015).

Similarities in the foundational principles governing regeneration, along with the involvement of common molecular players—such as the Wnt protein and its partners—highlight a coordinated orchestration of specific steps during the regenerative process. Such strong parallels further suggest that the underlying homology might extend to fundamental cell types driving the process, creating a possibility for the existence of regenerative cell types having similar molecular identity across phyla. Cellular identity is controlled by a sophisticated interplay of specific transcription factors and their downstream effector genes, collectively forming a cell type-identity network that enables cell-specific functions (Arendt et al., 2016; Srivastava, 2021). The networks in different organisms show notable similarities. As a proof of fact, many highly regenerative invertebrate species—such as sponges, cnidarians, acoels, and planarians—harbor pluripotent stem cells defined by a conserved set of homologous genes, such as the Piwi family genes regulating similar pathways during regeneration (Lai and Aboobaker, 2018; Srivastava, 2021; van Wolfswinkel, 2014). Similarly, among vertebrates with exceptional regenerative abilities, such as salamanders, Piwi protein production is highly enriched in the undifferentiated

regenerative tissue masses formed after injury (Zhu et al., 2012). The unifying molecular homology established by the well-studied Wnt signalling pathway can be further extended to critical stages of regeneration, such as patterning and wound healing. These processes in turn play a pivotal role in shaping of proper morphological features of an organism or organ. Following an injury, multiple signalling pathways are activated to initiate a primary wound-healing response (Arenas Gómez et al., 2020). While the Wnt signalling pathway does not directly regulate the wound-healing process, certain conserved immediate early genes (IEGs), triggered as part of the initial healing response, may serve as direct or indirect effectors of Wnt signalling activation required during subsequent patterning processes. Initially identified in mammals, IEGs were recognized as the earliest transcriptional responders in processes such as growth stimulation and injury repair. These genes encode transcription factors that exhibit low expression levels prior to an activating stimulus. However, their transcription is rapidly and robustly induced within minutes of activation, occurring independently of new protein synthesis. For example, homologs of certain mammalian IEGs, including early growth response (*Egr*), *Jun*, *Fos*, and *Creb*, are activated upon wounding in distantly related invertebrates (Cary et al., 2019; Cazet and Juliano, 2020; Gehrke et al., 2019; Wenemoser et al., 2012). Concurrently, following transverse amputation wounds, Wnt ligands are expressed in and around the injury sites as part of the primary wound-healing response. This phenomenon is observed in the same group of highly regenerative invertebrates such as acoels, *Hydra*, and planarians. This localized Wnt signalling response, regulated by the Wnt-independent wound-healing pathway, initiates a patterning response that establishes the proper polarity of either the entire organism or the specifically missing body structures (Cazet and Juliano, 2020; Gurley et al., 2010; Petersen and Reddien, 2009; Ramirez et al., 2020; Vogg et al., 2019).

Severe wounds that damage entire organs or significantly impair an organism require robust regenerative responses. A crucial aspect of this process involves organizing cells and tissues in a precise spatial and temporal manner to restore the original structure and function of the tissue or organism—a process known as patterning. Several functional and genetic studies, especially in invertebrates like acoels, planarians and cnidarians, have revealed it to rely heavily on Wnt signalling gradients distributed throughout the body (Chen et al., 2020; Gehrke et al., 2019; Gurley et al., 2010; Lengfeld et al., 2009; Ramirez et al., 2020). The patterning homology governed by Wnt signalling is not exclusive to whole-body regenerating invertebrates; it is also observed in vertebrates like zebrafish (fin regeneration)

and salamanders (limb regeneration) (Lovely et al., 2022; Walczyńska et al., 2023; Wehner et al., 2014).

Overall, while the processes of regeneration seem highly diverse across different phyla, several fundamental parallels emerge at the levels of molecules, cells, and mechanisms. The presence, variation, or complete absence of these foundational elements could hold the key to understanding why regeneration potential varies so widely across the phylogenetic tree.

1.2. Comparison of embryonic development and adult regeneration

For the last centuries, regeneration has often been seen as an adult developmental process resembling embryonic development, particularly in forming an undifferentiated tissue mass composed of pluripotent and multipotent cells, which later proliferate and differentiate into required cell types – called a blastema (Holland, 2021). Even recent studies show similarities in morphological and proliferative features, as well as plasticity between regenerative blastema cells and embryonic cells (Aztekin, 2024).

Stem cells are typically pluripotent, possessing the ability to self-renew and differentiate into multiple lineages, making them essential for the formation of new structures during both development and regeneration (Aztekin, 2024; Poliwoda et al., 2022). However, as stem cells advance toward producing fully differentiated cell types, they transition through an intermediate stage, characterized by reduced potency and more restricted lineage potential. These intermediate cells known as progenitor cells (sometimes referred to as precursor cells), ultimately differentiate into fully functional differentiated cell types, demonstrating exceptional capacity for tissue formation (Ffrench et al., 2015). Potencies of fate restricted progenitor cells serve as key reference points in comparing the processes of development and regeneration. Early lineage-tracing studies suggest that these cells generally display less plasticity during development compared to regeneration. For example, during organ development such as lung, lung specific progenitors can only form cells constituting the lungs and not any other differentiated cell types (Aztekin, 2024). In contrast, during axolotl tail regeneration neural precursors or progenitor cells harboured in the spinal cords, could transdifferentiate into regenerating muscle and cartilage cell types (Aztekin, 2024; Echeverri and Tanaka, 2002). This example is particularly striking, because it relates to the neural tissue, which has been perceived as one of the least plastic ones. Recent research employing *in situ* lineage tracing and single-cell RNA sequencing (scRNA-seq) across various vertebrate models has reinforced the view that stem cell progenitors involved in regeneration can exhibit greater potency than during development. However,

these studies also have made it clear that this enhanced plasticity does not extend to pluripotency (Aztekin et al., 2019; Gerber et al., 2018; Johnson et al., 2020; Tu and Johnson, 2011).

Cell proliferation plays a key role in both early development and regeneration. Early development in many species begins with rapid, synchronous mitotic divisions that slow down as the embryo approaches gastrulation (O'Farrell, 2015). During this period, the cell cycle oscillates between DNA synthesis and mitosis, without gap phases (Farrell and O'Farrell, 2014). Prior to gastrulation, metazoans shift from rapid, synchronous cell divisions to patterned divisions, often coinciding with the onset of cell fate specification (Arora and Nüsslein-Volhard, 1992; Kane et al., 1992; Murakami et al., 2004). In case of limited regeneration in vertebrates like axolotls (limb) and zebrafish (fin) (McCusker et al., 2015), and whole-body regeneration in invertebrates like Hydra (Fan and Bergmann, 2008) and planaria (King and Newmark, 2012), the onset of regenerative process also involves a burst of proliferative response.

Another common cellular response in both development and regeneration is apoptosis, a programmed cell death. Insights into the involvement of programmed cell death during development largely come from studies on *Caenorhabditis elegans*, Drosophila, and mice. While apoptosis is not essential for development in C. elegans, it is crucial and more finely regulated in Drosophila and mice (Fuchs and Steller, 2011). In regeneration however, apoptosis plays a more critical role, occurring in all organisms and organs undergoing the process. Its importance lies in reorganizing existing cells and tissues to compensate for the loss before the new structure becomes functional (King and Newmark, 2012; Mescher et al., 2000; Pellettieri et al., 2010).

Despite the parallels between regeneration and development highlighted above, these processes exhibit significant differences. A major difference lies in gene expression patterns. Developmental genes may be completely inactive during regeneration (as observed for *Xenopus laevis* tail regeneration (Sugiura et al., 2004), or the same genes may be expressed, but at different levels such as in *Hydra* (Burton and Finnerty, 2009). Another dissimilarity lies at the cellular level: the stem cells involved in regeneration may have different origin than those that give rise to the same tissues during embryonic development. For instance, regenerative muscle stem cells in *Xenopus laevis* and mice have a distinct origin from that of embryonic myoblasts (Daughters et al., 2011). The final difference relates to anatomical structure: while regeneration restores functional integrity, the newly formed structures can sometimes differ anatomically from the embryonically formed ones, as seen for regenerated

amphibian tails (Aztekin, 2024; Vervoort, 2011). Nonetheless, the existing parallels are important and, in some cases, enough for providing valuable insights regarding the developmental program of organisms while studying regeneration.

For studying mammalian congenital defects that perturb the normal developmental route, focussing solely on *in vivo* models is inefficient for pinpointing the specific developmental stage at which phenotypic alterations first appear. Owing to their early onset nature, these defects often affect multiple organs simultaneously, adding significant complexity to the disorders. These factors limit the potential for developing treatment strategies that directly target early changes. Instead, addressing such disorders requires a combined approach using *in vivo* (model organisms) and *in vitro* (induced pluripotent stem cells, iPSCs, and stem cell-based organoids) methods (Wang et al., 2023; Dutta et al., 2025). Over the past two decades, advancements in stem cell research, *in vitro* organ generation, and tissue engineering have provided promising solutions for a wide range of organ and tissue losses, primarily in adults. These investigations essentially arose from foundational research comparing developmental and regenerative pathways, as previously mentioned, to uncover potential similarities and differences in their cellular and molecular mechanisms (Saxena, 2010).

1.3. Types of metazoan regeneration

Regeneration in metazoans can be classified into two types: (i) one that occurs in the absence of active cell proliferation and (ii) one that requires extensive cell proliferation. The first type is termed as morphallaxis and involves replacing missing body parts by re-modelling of the existing tissues and cells, while avoiding the generation of new raw structures. *Hydra* provides the best example of such a form of regeneration (Agata et al., 2007). The other, more advanced, type requiring cell proliferation and differentiation is epimorphosis, which is further subdivided into non-blastemal and blastemal regeneration. Non-blastemal regeneration is mediated by: (i) transdifferentiation of existing tissue(s) into the missing tissue type, (ii) proliferation and dedifferentiation of the remaining cells within the affected structure and (iii) proliferation and differentiation of pluripotent cells to form the missing part. Such a route of regeneration is adopted for example by mammalian organs like liver, and amphibian eye lens (Alvarado, 2000). Blastemal regeneration, on the other hand, is mediated by the formation of a dedicated cell mass, called blastema, at the wound site. This mode of regeneration is more common and is observed in organisms like mollusks and echinoderms, as well as in case of vertebrate limbs and (Agata et al., 2007; Alvarado,

2000). Different modes of regeneration have been represented in **Figure 1**. In general, when considering the animal kingdom, epimorphosis is the most prevalent form of regeneration.

Regardless of the specific mechanism, the production of new cell types is a fundamental prerequisite for regeneration. Organisms leverage the diverse differentiation potential of various cell populations through multiple strategies to generate new cells. First, required or missing cell types can be generated by pluripotent stem cells, which possess the ability to both self-renew and differentiate into cells of multiple lineages (Weissman et al., 2001). Elsewhere, via de-differentiation, differentiated cells lose their specialized identity and revert to a progenitor-like state, enabling them to contribute to the formation of new cell types (Jopling et al., 2011). Finally, through transdifferentiation, differentiated cells convert into another specialized cell type, with or without passing through an intermediate progenitor phase. Notably, transdifferentiation can occur without cell division (Jopling et al., 2011). In practice, the regeneration of complex tissues often involves a combination of these pathways to ensure the efficient production of new cells. Interestingly, in certain organisms like freshwater planarians or starfish, the regeneration process falls in the gray area between these two traditional mechanisms, morphallaxis and epimorphosis (Peter W. Reddien, 2018).

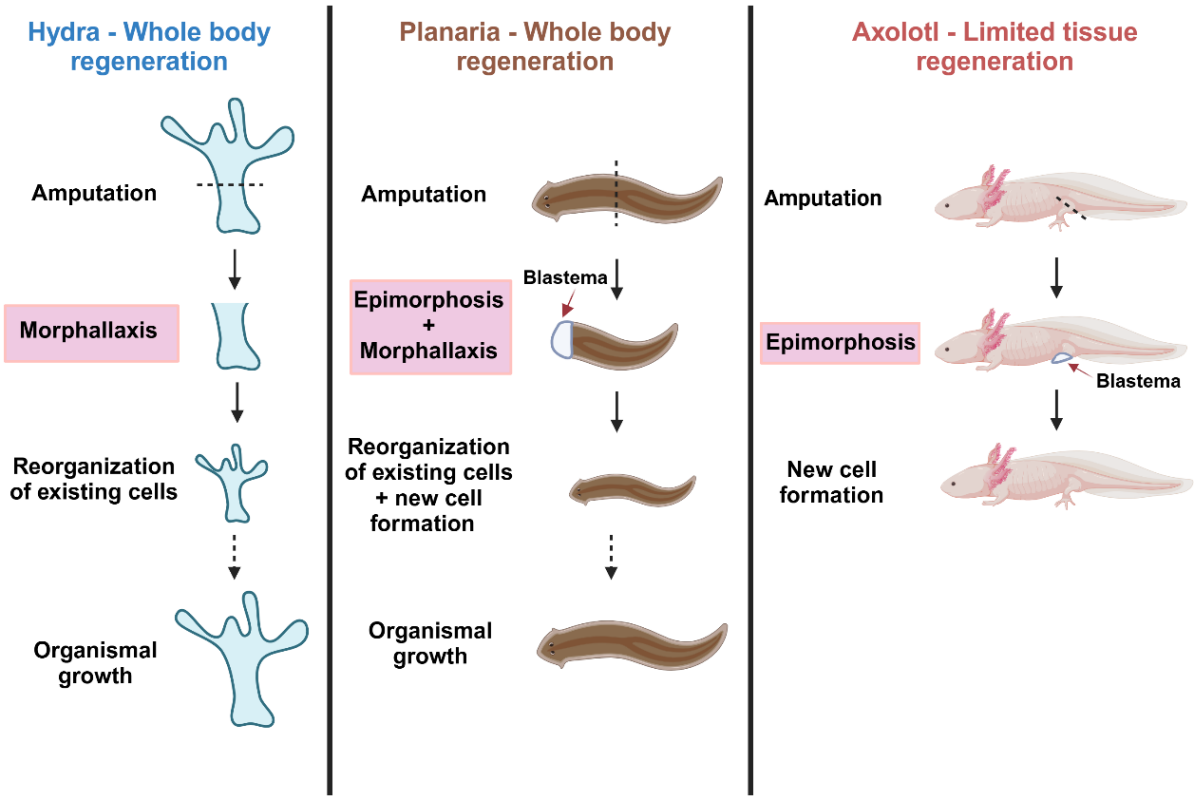

Figure 1. Major types of regeneration observed across exemplar regenerative models - Hydra, planarians and axolotl. Detailed discussion of these processes has been provided in the text.

1.4. Polyploid cells as crucial players in regeneration and repair

Cellular polyploidy is a widespread phenomenon observed across metazoans. It refers to particular cells in diploid organisms that contain multiple sets of chromosomes in the nucleus or are multinucleated (Peterson and Fox, 2021)extensively linked to pathological conditions, such as cancer, foreign body responses, and resilience to genotoxic insults (Moein et al., 2023). However, it is also crucial for developmental and regenerative processes. For example, in mammals, polyploid cells play essential roles in early embryonic development, as well as in regeneration of heart, liver, eye, kidney and bladder (Anatskaya and Vinogradov, 2022; Lazzeri et al., 2018; Wilkinson et al., 2019). Similarly, other organisms representing evolutionary distant phyla, like zebrafish and *Drosophila*, have adopted comparable strategies using polyploid cells for tissue maintenance and restoration (Anatskaya and Vinogradov, 2022; Cao et al., 2017).

Multinucleated cells can form through both cell cycle-dependent and independent pathways (**Figure 2**). In the latter, cells fuse to create a syncytium, a process involving priming, chemotaxis, adhesion, membrane fusion, and post-fusion stabilization (Zhou and Platt, 2011). Priming transitions cells into a pro-fusogenic state, followed by close interaction through chemotaxis or adhesion, enabling membrane merging (Aguilar et al., 2013; Zhou and Platt, 2011). Proteins like cytokines, chemokines, and adhesion molecules and those involved in actin cytoskeleton remodelling regulate these processes (Aguilar et al., 2013; Zhou and Platt, 2011). For instance, myoblast fusion in Drosophila larvae and mice, crucial for muscle development, occurs via a conserved strategy involving two phases: initial fusion forming multinucleated cells and subsequent fusion increasing nuclearity to create myofibers (Richardson et al., 2008). Similarly, osteoclasts, derived from hematopoietic progenitors, fuse to maintain bone mineralization and contribute to bone formation (Kodama and Kaito, 2020).

Most often polyploid cells are formed via endoreplication, which can be further divided into endocycle and endomitosis. During endocycle, the cell bypasses the mitosis (M) phase, resulting in the formation of a polyploid mononucleated cell with replicated DNA and an enlarged nucleus (Cohen et al., 2018). This process shares regulators like cyclin-dependent kinases (CDKs) and E2F transcription factors with normal mitosis but is distinguished by inhibited mitotic entry due to reduced mitotic cyclin activity(Shu et al., 2018). During the endocycle, cells alternate between S and G phases through cyclic accumulation and degradation of cyclin E-Cdk2, crucial for DNA synthesis (Hong et al., 2007; Swanson et al., 2015). In contrast, endomitosis involves mitosis followed by failed

cytokinesis, hence increasing cellular ploidy by the formation of multinucleated cells. Cytokinesis can be perturbed by inhibiting furrow formation or chromosomal segregation. This process occurs in liver, heart, and bladder cells during development, repair, and regeneration (Donne et al., 2020; González-Rosa et al., 2018; Wang et al., 2018). Notably, endocycle and endomitosis often do not operate in isolation; they can occur simultaneously or in a sequential manner (Bailey et al., 2021).

Cell fusion events have two major outcomes: retention as bi- or multinucleated cells, or nascent ploidy reduction in a process known as heterokaryon-to-synkaryon transition (HST). If this process is symmetric, characterized by the formation of a typical bipolar mitotic spindle, it results in the generation of diploid cells. In asymmetric HST, multipolar spindle is formed, leading to aneuploidy or genomic instability in the progeny cells. Alternatively, ploidy reduction can be associated with mitotic errors leading to micronuclei in aneuploid cells (Dörnen et al., 2020). Similar cellular outcomes can arise from endoreplication events as well (Fox and Duronio, 2013), however specific terminologies like HST have not yet been used in the endoreplication context. Aneuploidy, although often linked to tumorigenesis and malignancy (Holland and Cleveland, 2009), can also play adaptive roles. For instance, multinucleated polyploid hepatocytes reduce ploidy to form aneuploid cells capable of repolyploidization (Matsumoto et al., 2020). Aneuploidy in hepatocytes facilitates stress adaptation, aiding resistance to liver injury (Duncan et al., 2012). Here it should be noticed that polyploid cells have been shown to serve as reservoirs of diploid cells, which has a particular significance in stress conditions (discussed later in this chapter).

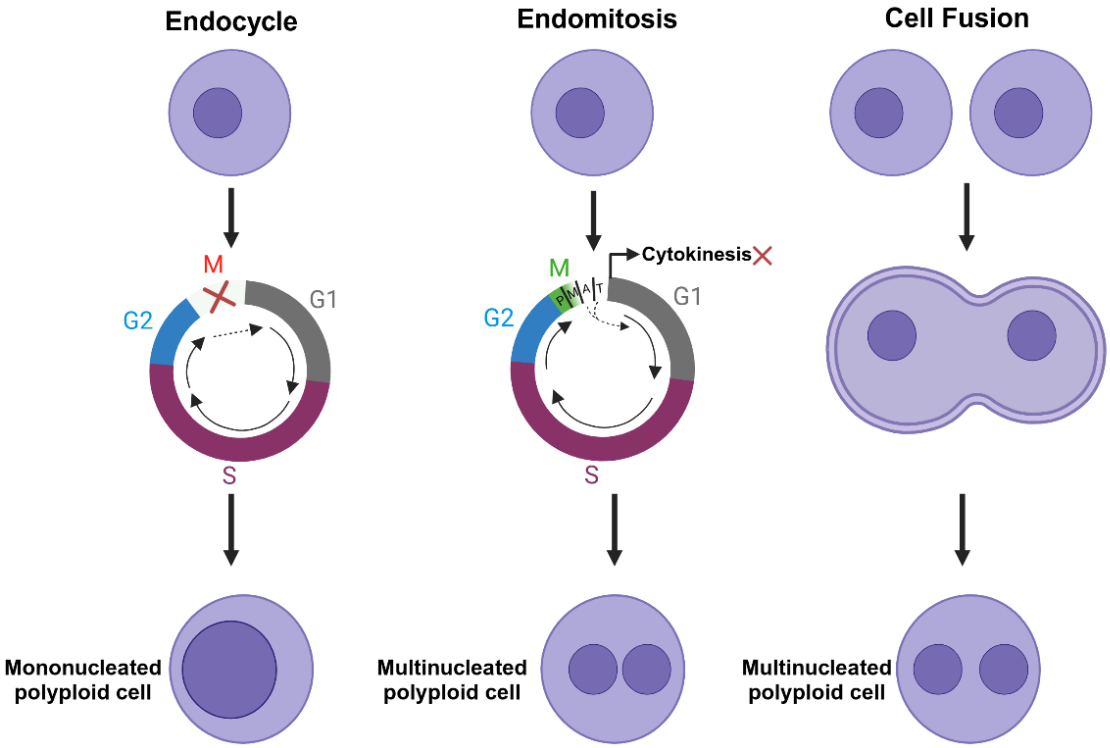

Figure 2. Mechanisms of formation of mononucleated/multinucleated polyploid cells. Detailed discussion of these processes has been provided in the text.

In this context, a question arises whether mononucleated polyploid cells and multinucleated cells are functionally equivalent. The answer depends on the context. For example, in mouse megakaryocytes, both forms are functionally equivalent. Inhibition of multinucleation via perturbation of endomitosis, leads to a switch to the endocycle mediated mononucleated cell polyploidy, without any functional loss (Trakala et al., 2015). However, *Drosophila* subperineurial glia (SPG) glial cells forming the blood-brain barrier require both forms; blocking either of them causes dysfunction (Von Stetina et al., 2018). It is therefore clear that this subject is complex, with no universal principles. Ongoing research is focused on the regulation of gene expression in polyploid cells and its effects on the transcriptome, as well as on epigenetic factors. It is anticipated that these studies will provide deeper insights into why some cells exhibit polyploid nuclei, while others are multinucleated (Schoenfelder and Fox, 2015).

In terms of physiological functions, polyploid cells are often involved in organ size regulation or in organismal stress mitigation, both of which are of utmost importance in the context of regeneration. Organ size and mass are regulated not only through cell proliferation (increasing cell numbers), but also through multinucleation, which results in increased cell size. Large polyploid or multinucleated cells form to replace lost tissue mass and maintain the original total tissue ploidy. This phenomenon can be observed in multiple instances,

including mouse liver hepatocytes (Wilkinson et al., 2019) and kidney tubule epithelial cells (Lazzeri et al., 2018), as well as zebrafish heart epicardial cells (Cao et al., 2017). Cell polyploidization and the resultant growth are particularly important regenerative mechanisms when cell divisions are not feasible due to the characteristics of a specific tissue, or when proliferation may pose a risk of malignancy (Bailey et al., 2021).

Cells face genotoxic stress from endogenous (e.g., DNA replication errors, reactive oxygen species) and exogenous (e.g., irradiation, mutagens) sources, causing DNA double-strand breaks (DSBs), cell cycle arrest, or apoptosis. Regeneration is intrinsically linked to stress and the associated effects. Polyploid cells play a crucial role in managing such stresses, as their increased genomic content enhances their capacity for repair and survival under adverse conditions. Examples of polyploid cell formation as part of the stress response are evolutionary ancient and widespread across organisms. In the protozoan parasite *Entamoeba* multinucleated giant cells provide genetic redundancy to survive DNA damage and mutations (Krishnan and Ghosh, 2018). In Drosophila, endocycling cells, regardless of tissue type, are resistant to DNA damage associated cell death, due to the silencing of pro-apoptotic promoters (Mehrotra et al., 2008). Finally, in mammals large multinucleated bone marrow cells, involved in regeneration, are resistant to irradiation stress (Moein et al., 2023).

Although polyploid cells are commonly found and play a key role in regeneration across a wide range of organisms, some aspects of their biology are not well understood. For instance, in highly regenerative organisms like planarians, these cells have not been observed under either wild-type or regenerating conditions. Additionally, while these cells are intricately involved in tissue formation during regeneration, few studies have explored their differentiative potential. These knowledge gaps highlight the need for further exploratory research to provide new insights into the role and potential of these wide-spread cell types.

1.5. Non-coding RNAs (ncRNAs) and their roles in regeneration

Non-coding RNAs (ncRNAs) are classified into two main groups: (i) constitutive (housekeeping) and (ii) regulatory (Kaikkonen et al., 2011). Constitutive ncRNAs are encoded by genes that are continuously and stably expressed. These molecules are essential for cell function due to their involvement in basic processes, related mainly to protein biosynthesis and the maturation of primary transcripts. This group involves: rRNA, tRNA, snoRNA, snRNA, TERC (telomerase RNA component), vtRNA and YRNA (Zhang et al., 2019). The regulatory RNA group includes molecules whose expression varies in response to cellular conditions and states (Samarfard et al., 2022). Among these, small regulatory

RNAs such as miRNAs, piRNAs, and siRNAs are the most extensively studied ones (Riedmann and Schwentner, 2010; Zhang et al., 2019). Meanwhile, regulatory RNA classes of greater lengths, including long non-coding RNAs (lncRNAs) and circular RNAs (circRNAs), are also gaining increasing attention for their potential cellular roles (Ma et al., 2023). The newest class composed of fragments derived from mature constitutive ncRNAs belonging to various classes, remains among the least studied subsets within the regulatory RNA category. Once considered non-functional by-products of RNA degradation, these ubiquitous molecules have been increasingly recognized for their broad functional significance within the cell, over recent decades. While the most recognized examples are those that are generated from tRNAs (Yu et al., 2020) and snoRNAs (Wajahat et al., 2021), functional fragments can also be generated from other RNA molecules (Tuck and Tollervey, 2011). Regulatory ncRNAs modulate crucial cellular processes like cell proliferation, apoptosis, migration and differentiation (Di Leva and Croce, 2010; Fu et al., 2023; Huang et al., 2022; Yu et al., 2019) via diverse molecular mechanisms. All the ncRNA classes have summarized in **Figure 3**. The sections below focus on the small regulatory RNA classes that are known to be involved in cell differentiative and tissue regenerative processes.

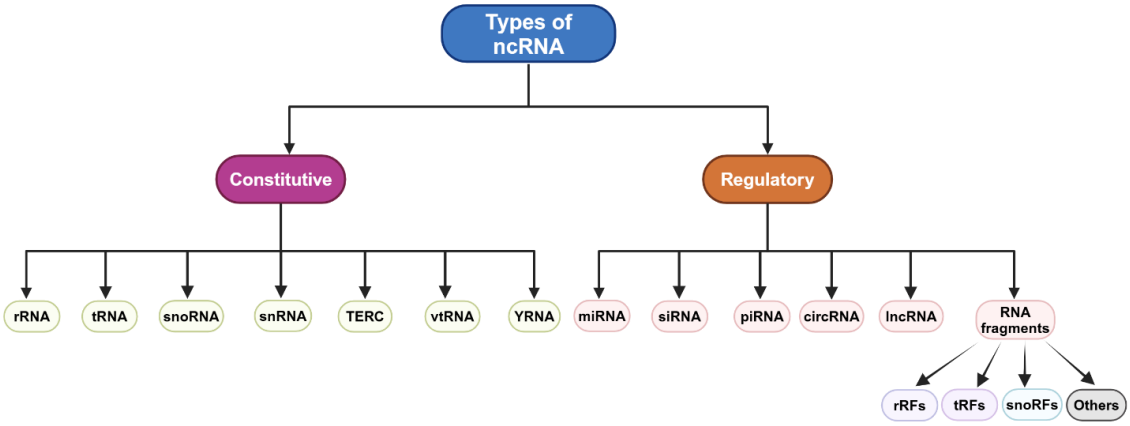

Figure 3. Classification of constitutive and regulatory ncRNAs. Flowchart depicting types of constitutive and regulatory RNAs.

1.5.1. Micro RNA (miRNA)

Mature miRNAs are small RNA molecules, 20-23 nucleotides in length, initially transcribed as pri-miRNAs by RNA polymerase II. These are processed into pre-miRNAs by the Drosha complex in the nucleus and further cleaved by Dicer in the cytoplasm. The resulting mature miRNAs are incorporated into the RISC complex, which includes Ago2 proteins and other components, to mediate post-transcriptional silencing of target transcripts

(Ong et al., 2015). A diverse array of miRNAs has been identified in humans, many of which are evolutionarily conserved across a broad range of organisms, from closely related species such as mice to more distantly related ones like planarians (Bartel, 2018). However, silencing mechanisms differ between organisms. In certain basal metazoans, miRNAs exhibit perfect complementarity with their target mRNAs, resulting in transcript degradation. By contrast, in bilaterian animals, miRNAs primarily use partial "seed"-based pairing with mRNAs, leading to translational inhibition and downregulation of target protein production (Bartel, 2018; Mauri et al., 2017).

miRNA activity differs between germline and somatic cells, with variations in the composition of the RISC complex influencing the regulatory roles of these molecules, as observed in *C. elegans* (Dallaire et al., 2018). Additionally, in organisms such as *Drosophila*, zebrafish, and mice, miRNA function is completely abolished in germline cells due to minimal or absent expression of miRNA molecules (Dexheimer and Cochella, 2020). In contrast, miRNAs are crucial regulators of gene expression in embryonic development. Disruption of the miRNA biogenesis pathway causes impaired embryogenesis or lethality in organisms like planarians, *C. elegans*, *Drosophila*, zebrafish, and mice (Dexheimer and Cochella, 2020; Li et al., 2011). Their spatiotemporal expression patterns, specific to cell types and developmental stages, underscore their importance in forming body structures (Brosnan et al., 2021) and regulating distinct life stages (Chen et al., 2005; Huang et al., 2017; Nahar et al., 2024; Todorov et al., 2024).

Given the numerous parallels between development and regeneration, miRNA expression during the latter process also exhibits a distinct spatiotemporal pattern. This includes variations in the types and levels of specific miRNAs at different stages of regeneration and within specific cell types. Such patterns have been characterized in regenerative models like Hydra, planarians, and zebrafish (Krishna et al., 2013; Ribeiro et al., 2022; Sasidharan et al., 2013). Notably, in stem cells, a limited set of miRNAs are initially expressed, with their expression increasing as differentiation progresses. Across different phyla, specific miRNAs are involved in maintaining pluripotency, while others are responsible for sustaining the differentiated state and repressing the activity of stem cells (Thatcher and Patton, 2010). In this way, miRNAs regulate critical processes such as cell proliferation and differentiation, guide the formation of fully differentiated cell types and participate in the organization of the regenerating tissue or organ (Aránega et al., 2021; Nakasa et al., 2015; Ouyang and Wei, 2021).

The functional conservation of specific miRNA families in regeneration across organisms can be exemplified by two notable ones: miR-21 and miR-29. The expression of miR-29 family molecules is often modulated during wound healing, response-associated extracellular matrix remodelling and cell death processes in mammalian organs, such as the heart, kidney, liver, and lungs (Sen and Ghatak, 2015). Additionally, it plays a critical role in post-injury regeneration of the central nervous system (CNS) in zebrafish (Fuller-Carter et al., 2015) and in blastema formation during axolotl limb regeneration (King and Yin, 2016). miR-21 family is associated with stem cell differentiation processes in mammalian embryonic stem cells (Gangaraju and Lin, 2009) and injury-induced liver regeneration (Dippold et al., 2012), newt limb regeneration (Zhang and Lu, 2024) and zebrafish fin and heart regeneration (Ribeiro et al., 2022; Wu et al., 2017). Given the high conservation of miRNA sequences and targets across distantly related organisms, further cross-species studies on these molecules shall potentially provide necessary explanations regarding the skewness of robust regenerative potentials in invertebrates.

1.5.2. PIWI protein-associated RNA (piRNA)

piRNAs are small non-coding RNAs (26–31 nts) derived from sense and/or antisense strands of genomic piRNA cluster regions via two pathways: primary and Ping-Pong amplification. In the primary pathway, precursor piRNA transcripts are processed in the cytoplasm, with 5'-ends bound by Piwi proteins and 3'-ends trimmed and methylated, to finally form mature piRNA/Piwi complexes (Chen et al., 2021). The Ping-Pong pathway involves sense and antisense piRNAs, respectively forming complexes with two different proteins (e.g., piRNA/Ago3 and piRNA/AUB in Drosophila) that cleave precursors to generate additional mature piRNAs (Saito and Siomi, 2010; Wu et al., 2020). piRNA biogenesis generally occurs in perinuclear structures like nuage in metazoans (Al-Mukhtar and Webb, 1971; Eddy, 1974; Mahowald, 1968). The piRNA-Piwi complexes play a crucial role in transposon silencing by repressing retrotransposon expression at either the transcriptional or post-transcriptional level. During transcriptional silencing, the binding of piRNA-Piwi conjugates to nascent transposon transcripts facilitates the recruitment of chromatin-modifying factors, promoting a repressive chromatin state at transposon-associated genetic regions. In contrast, during post-transcriptional silencing, piRNA-Piwi complexes bind to complementary sequences within transposon transcripts, leading to target cleavage through the slicer activity of Piwi proteins (Wang and Lin, 2021).

piRNAs and their associated Piwi proteins play essential roles in embryonic and sexual development across various organisms. During embryogenesis, they ensure mitotic

integrity (Mani et al., 2014) and facilitate epigenetic programming (Akkouche et al., 2013; Gu and Elgin, 2013), as well as regulate stability and localization of maternally deposited mRNAs (Lau et al., 2009; Rodriguez et al., 2005; Rouget et al., 2010). Beyond embryogenesis, piRNAs maintain genome stability by suppressing transposable elements, a function essential for germ cell survival and sexual development in metazoans (Lim and Kai, 2015). While most germline piRNAs map to transposons, a smaller subset map to the 3'-UTRs or coding regions of genes, as observed in human and mouse testes, zebrafish gonads, Drosophila ovaries, and Xenopus oocytes (Aravin et al., 2007; Ha et al., 2014; Houwing et al., 2008; Lau et al., 2009; Li et al., 2013; Robine et al., 2009).

Somatic PIWI proteins are closely associated with stem cells. Interestingly, the expression of genes encoding piRNA pathway proteins show similarities between bilaterian germline cells and adult pluripotent, multipotent, or lineage-restricted stem cells, crucial for regeneration (Lim and Kai, 2015). This suggests that classical germline genes, including piRNA pathway components, may confer "stemness" also to somatic stem cells (Juliano and Wessel, 2010; Juliano et al., 2010), potentially linking the piRNA pathway to regenerative abilities. Complyingly, PIWI protein production has been observed in stem and progenitor cells of sponges (Funayama et al., 2010), Hydra (Lim et al., 2014), acoels (Srivastava et al., 2014), planarians (Palakodeti et al., 2008), and annelids (Janssen et al., 2010). In vertebrates, PIWI protein production is limited, appearing mainly in hematopoietic and mesenchymal stem cells (Lim and Kai, 2015), blastemal progenitors in regenerating species like axolotl (Zhu et al., 2012), and embryonic or pluripotent stem cells in mice (Cheng et al., 2014). The pronounced difference in Piwi protein production suggests a significant disparity in the activity levels of the piRNA/Piwi pathway between invertebrates and vertebrates. Thus, piRNA pathway components likely play a crucial role in the enhanced regenerative potential of invertebrates compared to vertebrates.

1.5.3. tRNA-derived fragments (tRFs)

tRFs are processed from mature or pre-tRNAs, and range in lengths between 15 and 50 nt. These molecules are conserved throughout the phylogenetic tree, from bacteria to mammals (Thompson and Parker, 2009). Based on the origin and location of cleavage sites, they are classified into the following types: tRF-1, tRF-3/5, tRNA halves (5’/3’ tiRNA or tRH), and i-tRF. Although the biogenesis of tRFs is not yet fully understood, several enzymes involved in this process have already been identified. tRF-1 (16-48 nt) result from cleavage of the 3’ trailer sequence of pre-tRNA by Elac2 (tRNase Z) and its homologs (Zhu et al., 2020). tRF-3 (22nt) are generated by cleavage near the TΨC loop of mature tRNAs

by enzymes like Dicer, Angiogenin and members of RNase A family. tRF-5 on the other hand are produced when Dicer cleaves mature tRNAs at the D loop. Both these types are ~22 nt in length. Internal tRFs (i-tRF; ~36 nt) are derived from the region between D and T loops and are formed by cleavage by Dicer or Angiogenin. tRNA halves (30-50 nt) have been long perceived as being generated in response to stressors like oxidative damage, infection, or cancer, by Angiogenin cleavage at the anticodon loop (Kumar et al., 2016; Sarais et al., 2022; Wen et al., 2021). However, it has become increasingly clear that they are also formed under physiological conditions (Dhahbi et al., 2013; Peng et al., 2012). Further, other enzymes than Angiogenin have been found to be able to produce specific tRNA halves, especially 5' tRNA halves (Sarais et al., 2022).

Although these molecules have been systematically studied for just over a decade (Lee et al., 2009), researchers have already uncovered a wide range of their functional roles, including their involvement in several fundamental molecular and cellular processes (Krishna et al., 2021), including sperm maturation, embryonic development, stem cell differentiation and regeneration. For instance, specific tRF molecules, such as the 5' tRNA half Gly-GCC, have been shown to influence organismal development from the earliest stages, including sperm maturation and the formation of preimplantation embryos, by suppressing the expression of genes associated with endogenous retroelements (Sharma et al., 2016). Later in development, sperm-specific tRNA halves can regulate metabolic gene expression from embryogenesis to adulthood, with disruptions in this transgenerational inheritance leading to altered phenotypes in first-generation offspring (Chen et al., 2016). Furthermore, studies on mouse and human embryonic stem cells (mESCs and hESCs) have revealed additional roles of tRFs in embryogenesis, underscoring their importance in developmental processes. Certain tRFs regulate cellular differentiation and lineage commitment by inhibiting the translation of key proteins during early development (Guzzi et al., 2018; Krishna et al., 2019; Weidensdorfer et al., 2009). Thus, tRFs might play crucial roles in regulating "stemness" of specific cell populations in mammals. Coherently, differential accumulation of several tRFs have been also recently observed in various developmental stages of zebrafish (Wei et al., 2012) and Drosophila (Shi et al., 2023). However, further cross-species research is needed to confirm the universal role of tRFs in developmental programs and provide more insight into the phylogenetic aspects of regulation mediated by these molecules.

Evidence regarding roles of tRFs in regeneration is relatively limited, with most available insights derived from master regenerators, planarians. Further details on this topic

are presented in a dedicated chapter later in section **1.6.5**. The few other existing evidence on the roles of tRFs in this process comes from tissue-specific regeneration in mammals. For instance, during skeletal muscle regeneration, the upregulation of 5' tRNA half Gly-GCC inhibits cell proliferation and promotes differentiation by modulating the expression of a gene within the TGF-β pathway – involved in processes like inflammation, cell proliferation, and differentiation (Shen et al., 2023). In skin regeneration, while the molecular mechanisms remain unclear, specific tRF molecules, often derived from tRNA Gly-GCC, have been shown to yet again target proliferation-related pathways such as TGF-β and Wnt signalling (Fang et al., 2021; Zhang et al., 2023). These findings suggest that cell proliferation might be one of the primary pathways targeted by tRF molecules during regeneration.

Overall, tRFs, represent a burgeoning field of research. Insights gained from just two decades of functional studies highlight their significance as promising candidates for future exploration. To better understand the disparities in regenerative potential across the phylogenetic tree, it is imperative to thoroughly investigate these molecules, much like the extensive studies conducted on miRNAs and piRNAs.

1.6. *Schmidtea mediterranea* as a model organism for regeneration studies

1.6.1. Classification of planarians

Planarians are classified within the phylum *Platyhelminthes*, class *Turbellaria*, and the order *Tricladida*, commonly referred to as triclads. Various species of planarians exist with each of them having either sexual or asexual or both types of strain. Sexual strains produce gametes to generate offspring, while retaining the ability to regenerate. In contrast, asexual worms rely solely on regeneration for both reproduction and injury repair. Planarian diversity can be approached from various perspectives, such as: habitat/ecology, morphology/anatomy, and phylogeny/taxonomy, and the currently established classification criteria are most often combinations of these three categories. Initially there were three taxonomic groups of triclads based on their habitats – marine (*Maricola)*, fresh-water (*Plaudicola*), and terrestrial (*Terricola*) (Hallez, 1894). Later, results from phylogenetic analyses based on 18s rRNA sequences of the groups *Terricola* and *Plaudicola* showed the former to be a part of the latter and hence these groups were merged to form *Continenticola* (Álvarez-Presas et al., 2008; Carranza et al., 1998). The *Continenticola* group is further divided into two main superfamilies: *Planarioidea* (comprising of families *Planariidae*,

Dendrocoelidae, and *Kenkiidae*) and the *Geoplanoidea* (*Dugesiidae* and *Geoplanidae* (Rink, 2018). Freshwater planarians, particularly those from the superfamilies *Planarioidea* (Sluys and Kawakatsu, 2006) and *Geoplanoidea* (Sluys et al., 2009), are the most extensively studied among all existing groups. Notably, various planarians from the family *Dugesiidae* (within the superfamily *Geoplanoidea***)** are widely used as modern models for studying regeneration and have been thoroughly characterized. Key genera in this family include *Girardia*, *Dugesia*, and *Schmidtea* (Rink, 2018). Although planarians are not considered popular model organisms today, they have been established as models in the research of regeneration already in 19th century (Morgan, 1898). At present, *S. mediterranea* has been one of the most extensively studied.

1.6.2. Planarians as regenerative models

Many freshwater planarian species display remarkable ability to regenerate entire organisms, including the nervous system, from small body fragments. This capability is attributed to a heterogeneous population of adult stem cells, called neoblasts. In an intact worm, neoblasts continuously replace aged tissue via the cell turnover process. Consequently, all cell lineages, from progenitors to differentiated cells, are constantly present in an adult organism. This unique feature makes planarians, including *S. mediterranea*, excellent *in vivo* models to study regeneration and differentiation. Researchers seeking alternatives to vertebrate models with limited adult tissue turnover and narrow regenerative capabilities, have turned to planarians. These flatworms, despite evolutionary distance from vertebrates, share many cellular and molecular pathways (Oviedo et al., 2008b). In a developmental context, planarians exhibit most of the major signaling pathways, cell types, and molecules necessary for maintaining a bilateral body structure, similar to those in higher animals. This evolutionary conservation is particularly evident when studying the small non-codng RNA (sncRNA) landscape during regeneration and development; for example, certain miRNA molecules are involved in similar developmental processes across species, from worms to humans. Despite having a smaller genome (1–2 Gb) (Grohme et al., 2018) than vertebrates like salamanders (Sclavi and Herrick, 2019; Sun et al., 2012), humans and mouse (Mullins and Mullins, 2004; Piovesan et al., 2019), planarians have comparable number of genes (~30,000). Other than that, highly regenerative planarians like *S. mediterranea* and *Dugesia japonica* are very easy and cheap to maintain under laboratory conditions with very minimal culture requirements. Their remarkable regenerative abilities, which allow them to develop into fully functional new organisms from tissue fragments, facilitate simple and efficient population propagation

methods (Dean and Duncan, 2020; Merryman et al., 2018). Decades of studies on these worms have not only advanced the use of molecular tools for their study but have also driven significant developments at the level of genome and transcriptome characterization and annotation. Established protocols for methods such as dsRNA mediated RNAi, whole body colorimetric and fluorescent *in situ* hybridization protocols, flow cytometry, stem cell ablation methods, single-cell sequencing methods, bromodeoxyuridine (BrdU) and 5-ethynyl-2'-deoxyuridine- (EdU) staining for cell cycle measurements, as well as chromatin immunoprecipitation (ChIP), are currently available (Ivankovic et al., 2019). However, the community faces a significant challenge in establishing robust transgenesis protocols, which are essential for the development of effective live-imaging strategies. Also, significant challenges persist at the level of complete and accurate genome annotation. The genome's high degree of repetition leads to frequent annotation errors, which are evident even in the most recent versions of the genome and transcriptome. Nevertheless, the latest genome versions released by two scientific groups have made exhaustive attempts to overcome many of these challenges (Guo et al., 2022; Ivanković et al., 2024). Finally, studying planarians provides the rare opportunity to study embryo-like pluripotent stem cells in adult tissues at homoeostasis and in regenerative processes. **Figure 4** visually represents various techniques and tools, some of which are already standardized in planarians, while others are not yet implemented. Therefore, understanding the behavior and function of adult tissue-resident stem cells in full-body regeneration could uncover crucial insights into why higher organisms possess limited regenerative abilities (Oviedo et al., 2008a; Sánchez Alvarado, 2012). Further, investigations on underexplored sncRNA classes in regeneration could enhance our understanding of their functions, potentially providing valuable insights into the molecular mechanisms of human regenerative processes and developmental diseases.

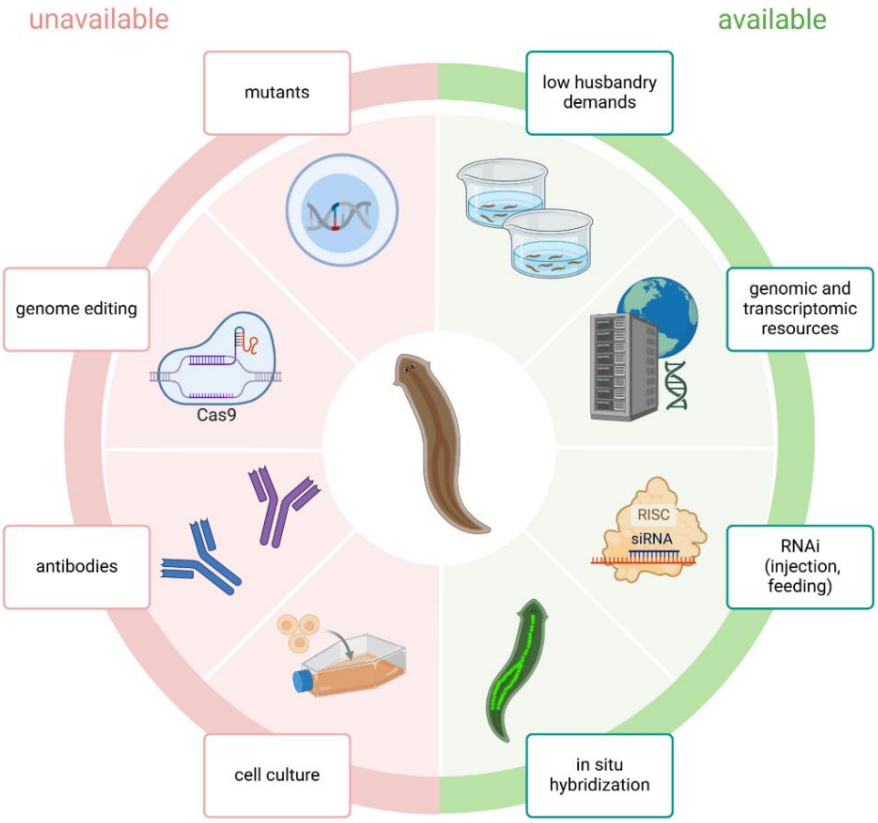

Figure 4. A visual representation of molecular tools categorized by their successful application and standardization, or lack thereof, in planarian studies. The available and unavailable categories respectively indicate experimental techniques that are either frequently applied to planarians or have not yet been standardized in this model system, respectively.

1.6.3. Anatomy

The typical planarian anatomy includes a brain, eyes (photoreceptors), muscles, intestine, pharynx, protonephridia, and epidermis. The musculature extends throughout the body, consisting of several fiber types: longitudinal, transverse, circular, and diagonal. The head features two eyespots made up of photoreceptor cells. The central nervous system comprises a bilobed brain, or cerebral ganglia, two ventral nerve cords running longitudinally, and a complex network of neurons and glial cells. The alimentary system consists of the gut and pharynx. The gut branches extensively throughout the body and connects to the pharynx—a multifunctional tube serving as both the mouth and a waste disposal system. During feeding, pharyngeal muscle contractions thrust the pharynx outward, allowing it to insert into prey or food particles to ingest fluids and small tissue fragments. The epidermis produces mucus and is densely covered with cilia, facilitating locomotion. The protonephridia function as the primary excretory and osmoregulatory system. Lastly, most sexually reproducing planarians are hermaphroditic, containing both male and female reproductive organs within a single individual. Testes are distinct follicular

structures, and their location and distribution within the body serve as essential taxonomic markers. Additionally, planarians have a pair of ovaries situated in the anterior region of the body (Orii et al., 2002; Peter W Reddien, 2018; Sluys and Riutort, 2018).

1.6.4. Cell types

For decades, flow cytometry has been the preferred method for studying and isolating various planarian cell populations. Accordingly, a landmark study described a fluorescence-activated cell sorting (FACS) method utilizing X-ray sensitivity and triple fluorescent staining— propidium iodide (PI) for dead cell exclusion, Hoechst 33342 for nuclear staining, and calcein AM for cytoplasmic staining— to distinguish planarian cell populations with varied differentiative potentials, viz., X1 (X-ray sensitive neoblasts or stem cells), X2 (X-ray sensitive progenitor cells), and Xins (X-ray insensitive differentiated cells) (Hayashi et al., 2006). Since then, this has become the gold-standard method for studying these cell populations and has been widely used in advanced studies, including the generation of the first planarian cell-type atlas via single-cell transcriptomics (Plass et al., 2018). Furthermore, using this approach, researchers attributed the remarkable whole-body (including the nervous system) regenerative ability of planarians such as *S. mediterranea* (Karami et al., 2015) to the pluripotent X1 neoblasts, interchangeably called adult stem cells (Karami et al., 2015). A more profound insight into planarian cell types, along with their differentiation trajectories, has emerged through single-cell transcriptomics analyses, beginning with detailed atlases of the whole organism (Fincher et al., 2018; Plass et al., 2018). The text below presents a brief overview of the main planarian cell types, including: neoblasts, epidermis, intestine, pharynx, muscle, protonephridia, parenchymal and nervous system cells.

Neoblasts are commonly described as mitotically active cells, characterized by a high nucleus-to-cytoplasm ratio. As a general population they were found to be marked by the high expression of *piwi-1* (*SMEDWI-1*) (Alvarado et al., 2002), however now it is clear that neoblasts form a heterogenous collection of cell subtypes. A series of single neoblast transplantation experiments on lethally irradiated worms demonstrated that within the pool of *SMEDWI-1+* neoblasts, there is a small group of cells called clonogenic neoblasts (cNeoblasts), which when transplanted into the neoblast-ablated worms, could rescue them. The rescue is mediated by means of clonal expansion of cNeoblasts to repopulate the lethally irradiated worms. Neoblasts other than these were not as potent (Wagner et al., 2011). Later, four subclasses of neoblasts were identified based on gene expression profiles and functional assays: σ(sigma), γ(gamma), ζ(zeta), ν(nu) (Molina and Cebrià, 2021). Amongst these, σ are

the most important ones for regeneration as they have broad lineage specification capacity, are highly proliferative and give rise to other neoblast populations, like ζ. Thus, it has been suggested that cNeoblasts could in fact be within the σ subclass (van Wolfswinkel et al., 2014). Molecularly, other than being *SMEDWI-1*^{high}, cNeoblasts were found to be *Tetraspanin-1+* (*tspan-1+*) (Zeng et al., 2018). The other subclasses, γ, ζ and ν represent specialised neoblasts that give rise to lineage-restricted progenitors. Accordingly, γ neoblasts are involved in generating the intestine, ζ are specialized towards epidermal lineage and ν give rise to neural cells (Scimone et al., 2014; van Wolfswinkel et al., 2014). Specialized neoblasts are characterized by the expression of *SMEDWI-1* and lineage-specific genes. These marker genes are summarized in **Table 1.**

Table 1. Major planarian specialized neoblast types with associated marker genes

Specialised neoblast type	Molecular marker	Source
Eye	*ovo, otxA, six1/2, eya,dlx, sp6-9*	(Chen, 2025; King et al., 2024)
Protonephridia	*POU2/3, six1/2-2, eya, sall, osr*	
Epidermis	*zfp-1, egr-1, p53, prog-1*	
Muscle	*ston-2, coe, Pitx, lhx1/5*	
Pharynx	*FoxA, meis*	
Pigment	*foxF-1, ets-1*	
Intestine	*hnf4, gata4/5/6 -1*	
CNS	*ston-2, coe, Pitx, lhx1/5*	
Parenchymal	*foxA, NKX2-4*	

The planarian epidermis consists of ciliated and non-ciliated cells, as well as cells located at the dorsal-ventral boundary. The epidermal lineage is well characterized, with cells revealing continuous transitions from ζ neoblasts to differentiated cells, identified by specific gene expression patterns. The intestine contains three distinct cell populations: an inner intestine layer with absorptive enterocytes, goblet cells population and an outer intestine layer. The pharynx has progenitors that reside outside this organ and generate cells of the pharyngeal cavity epithelium and pharyngeal muscles. Planarian muscle cells, constituting distinct populations, are present in the body wall, pharynx and around the intestine. The protonephridia are composed of flame cells, tubule cells and a collecting duct. The parenchyma, which surrounds the planarian organs, is highly heterogeneous and remains the least studied tissue. Single-cell transcriptomics has revealed distinct parenchymal populations, including gland cells (dorsal, lateral, and ventral), fixed parenchymal cells (likely phagocytic), and several precursor subclusters. While the precise functions of parenchymal cells are not well understood, they are thought to support the

planarian's internal structure and provide pathways for other cell types. The nervous system contains an extensive diversity of cell types, including both ciliated and non-ciliated neurons, as well as the rare ones constituting the photoreceptors. Furthermore, the planarian cell type landscape is made even more complex by the presence of a population called cathepsin+ cells, comprising glial and pigment cells (Fincher et al., 2018). Importantly, marker genes were identified for both the progenitors and differentiated cells of the major lineages (**Table 2** and **Table 3**). In several major tissue types, including the intestine, pharynx, muscle, protonephridia and cathepsin+ cells, single-cell transcriptomics revealed transition states. They represent intermediate stages in differentiation, where cells express markers overlapping between precursor and differentiated populations, indicating ongoing lineage specification (Fincher et al., 2018).

Table 2. Major planarian progenitor cell types with associated marker genes

Progenitor	Molecular marker	Source
Eye	*ovo, six1/2*	(King et al., 2024; Molina and Cebrià, 2021)
Protonephridia	*POU2/3, six1/2-2, eya*	
Epidermis	*prog-1, agat-1, egr-5, zpuf6, nb.21.11e*	
Muscle	*Myo-D, nkx1-1, foxF-1*	
Pharynx	*FoxA*	
Pigment	*ets-1, albino*	
Intestine	*hnf4, gata4/5/6*	
CNS	*soxB-2, nkx2.2, klf*	
Parenchymal	*fer3l-1, fer3l-2, ptf1, IRX1,GCM2, ascl-2+*	

Table 3. Major planarian differentiated cell types with associated marker genes

Differentiated cell	Molecular marker	Source
Eye	*Egfr-1*	(Fincher et al., 2018; King et al., 2024; Molina and Cebrià, 2021; Wurtzel et al., 2017)
Protonephridia	*POU2/3*	
Epidermis	*laminB*	
Muscle	*COL4A6A*	
Pharynx	*FoxA*	
Pigment	*ets-1, foxF-1*	
Intestine	*gli1, rreb2*	
CNS	*ChAT, PC2*	
Parenchymal	*Rreb1, rreb2*	

1.6.5. Regeneration process

The regeneration process in these worms is remarkably plastic, enabling them to regenerate any type of missing tissue following regular or irregular amputations at various defined (transverse and medial-lateral) or undefined anatomical planes. Plasticity comes from the use of both blastemal and morphallactic routes of regeneration simultaneously.

Immediately after any injury, simultaneous short waves of mitotic (at ~6 hours post amputation or hpa) and apoptotic (at ~4 hpa) responses occur at the injury site and proximal to the injury site, respectively. These responses are generic wound-healing mechanisms triggered by any type of injury. However, for severe injuries like amputations, these initial responses alone are insufficient to restore the missing structures. To address this, a second, more sustained wave of proliferation (~48 hpa) occurs at the wound site, resulting in blastema formation, alongside elevated apoptosis (~48–72 hpa) in the surrounding tissue, supporting morphallaxis. This second phase, known as the "missing tissue" or "regenerative" response, is essential for reconstructing the lost structures (Peter W Reddien, 2018; Wenemoser and Reddien, 2010). In terms of gene expression, there also exist regeneration time point specific waves. The first wave of expression (W1) starts from 30 min post-injury and extends up to 6 h post-injury. Most of these genes are homologous to mammalian IEGs that are upregulated in response to various stimuli, as explained previously. The W2 and W3 genes are expressed between 6 h and 12 h post-injury and many of them encode for secreted proteins and matrix-remodelling factors. While W2 genes are exclusively expressed at subepidermal regions of the wound site, W3 gene expression extends to the epidermis and further beyond the wound area. Finally, the W4 consists of the expression neoblast-specific genes encoding for transcription factors, chromatin remodelling proteins, cell cycle factors, and histone methyltransferases (Wenemoser et al., 2012). For regenerated tissues and organs to be optimally functional, their positioning with respect to other structures within the worm's body is of particular relevance. Positional information is also crucial context for conserving the planarian's anatomical polarity. Hence to regenerate proper missing body parts, planarians have multiple position control genes (PCGs) for polarity maintenance at the anterior-posterior AP axis (*wnt1; notum*), dorso-ventral DV axis (*bmp*) and medial-lateral ML axis (*wnt5; slit*). It was observed that most of the PCG genes are regionally expressed throughout the musculature and are induced as a part of wound signaling (Fincher et al., 2018; Scimone et al., 2011). Wound signaling is composed of the induction of two gene categories consecutively: 1) stress response genes expressed in most tissues, 2) genes upregulated in tissues like muscle, epidermis and neoblasts - most PCGs fall in this category

(Wurtzel et al., 2017). The specific expression profile of muscle inherent PCGs spatially influences the fates of neoblasts and progenitors (Wurtzel et al., 2017).

At the level of sncRNAs, the expression is also very dynamic. Planarian regeneration is tightly regulated by specific miRNA, coordinating various events at crucial regenerative time points (Cao et al., 2020; Friedländer et al., 2009; Sasidharan et al., 2013). Researchers identified three miRNA categories in regenerating planarians. Category 1 miRNAs are consistently upregulated or downregulated in both anterior and posterior regions across regeneration stages - the upregulated ones likely being involved in processes like healing and differentiation and the downregulated ones in homeostatic processes. Category 2 miRNAs peak between 3 and 24 hpa in both anterior and posterior tissues (overlapping the expression pattern of W1 genes), and are involved in wound healing, neoblast migration and initial proliferation. Category 3 miRNAs are expressed in the anterior region starting from 3 days post-amputation and several of them are miR-124 family members, important for CNS regeneration. No posterior-specific miRNA expression suggests miRNAs may play a minimal role in posterior regeneration (Sasidharan et al., 2013). Further, there have been studies that identified planarian miRNA molecules (sme-miRs) with specific FACS population enrichment and associated functions (**Table 4**).

Table* 4.** ***Planarian miRNA molecules in undifferentiated X1 and X2 populations

Cell type	miRNA	Enriched in specific time point	Potential function	Source
Enriched in X1	sme-miR-7b sme-miR-71c	No information	• proliferation and differentiation of neoblasts; • development of head ganglia	(Palakodeti et al., 2006; Sasidharan et al., 2013)
	sme-miR-125a	Upregulated between 3-24 hpa	• initial stages of wound healing; • proliferation of neoblasts	
	sme-miR-31a	No information	• proliferation and differentiation of neoblasts; • re-patterning of the blastema	
Enriched in X2	sme-miR-13	Upregulated at all regenerating time points	• wound healing; • proliferation and differentiation of neoblasts; • re-patterning of the blastema	
	sme-miR-2b-3p	No information	• development of digestive system and pharynx	
	sme-miR-2d-3p	Upregulated between 3-7 dpa	• development of CNS tissues, medial parenchyma and brain ganglia	
	sme-miR-2173	No information	• wound healing	
	sme-let-7a sme-let-7b sme-let-7c sme-let-7d	No information	• homeostasis; • control proliferation and differentiation of neoblasts; • development of organs such as the brain ganglia	
	sme-miR-756	No information	• organ development	
Enriched in both X1 and X2	sme-miR-2a sme-miR-36b sme-miR-36c	No information	• proliferation and differentiation of neoblasts	
	sme-miR-71a	No information	• organ development	
	sme-lin-4-5p	Upregulated between 3-24 hpa	• germ line development and homeostasis maintenance	

Unlike miRNAs, the piRNA pathway operates exclusively in germline and somatic stem cells. Consequently, research on piRNAs often focuses on determining whether the piRNA pathway is active in a specific cell or tissue type. The expression of key protein components associated with the piRNA pathway is typically considered a clear indicator of an active piRNA-mediated regulatory process within that tissue or cell type. Consistently,

in the asexual *S. mediterranea*, the piRNA pathway is most active in neoblasts, making it critical for regeneration (Kim et al., 2020). Among all components of the piRNA pathway, the piRNA-binding PIWI proteins have been the most extensively studied in the context of planarian regeneration. For example, Smedwi-3/piRNA complexes regulate neoblast mRNA turnover (Kim et al., 2019), while the knockdown of *SMEDWI-2* and *SMEDWI-3* disrupts both regeneration and homeostasis (Palakodeti et al., 2008). Additionally, Smedwi-1/piRNA complexes ensure neoblast functionality by removing defective transcripts and converting them into functional piRNAs (Allikka Parambil et al., 2024). Beyond these well-studied Piwi proteins (Smedwi-1/2/3), several other components of the piRNA pathway contribute to orchestrating a fully functional piRNA network in neoblasts, further highlighting its essential role in maintaining regeneration and cellular integrity. The prominent piRNA pathway components in *S. mediterranea* are presented in **Table 5**.

Table 5. Prominent piRNA pathway components in S. mediterranea

piRNA pathway components	Function in the pathway	Disruption-associated phenotype	Source
Smedwi-1	Cytoplasmic mRNA/Transposable element surveillance	no prominent phenotype	(Kim et al., 2020)
Smedwi-2	Transcriptional gene silencing	fatal	
Smedwi-3	Cytoplasmic mRNA/Transposable element surveillance	fatal	
Smed-DNAJA1	Binding smedwi1/2	fatal	
Smed-UAP56	Nuclear export of piRNA precursors	no information	
Smed-PLD6	Primary piRNA biogenesis pathway	no information	
Smed-PNLDC1	Trimming of pre-mature piRNAs	no information	
Smed-MOV10L1	Loading/unloading PIWI proteins	no information	
Smed-Gasz	Primary piRNA biogenesis pathway	no information	
Smed-Mino	Primary piRNA biogenesis pathway	no information	
Smed-TDRKH	Pre-piRNA 3' trimming	no information	
Smed-FKBP2	Guide loading to PIWI	no information	
Smed-Hsp83	Guide loading to PIWI	no information	
Smed-Hen1	3' methylation of piRNAs	no information	
Smed-TDRD12	Ping pong pathway	no information	
Smed-vasa-1	Ping pong pathway	fatal	

Finally, similar to miRNAs, tRFs of various types exhibit distinct spatiotemporal accumulation patterns during planarian regeneration. These patterns are tightly regulated across multiple levels, including: (i) differences between anterior and posterior regeneration, (ii) cell type-specific occurrence, and (iii) timing-specific accumulation during key regenerative stages. Notably, 5′ tRNA halves, tRF-5s, and i-tRFs have been identified as the most tightly regulated tRF types during regeneration (Lakshmanan et al., 2021). For example, 5' tRNA half Gly-GCC appears as the most abundant 5' tRNA half in amputated planarians (~50%) and its expression is most enriched in pre- and post-pharyngeal regions with lower expression in head and tail. **Table 6** summarizes these aspects of tRF accumulation during planarian regeneration. Although research on the functional roles of tRFs in planarian regeneration is still in its early stages, emerging studies already suggest that the precise regulation of tRF production is essential for the normal progression of regeneration. **Figure 5** summarizes the involvement of various planarian proteins and sncRNA classes along a regeneration time course.

Table 6. Counts of differentially accumulated tRF molecules at 3, 6, 12, 24,72, 120, 168 hpa

Body regions					**Source**
Posterior	**5' tRNA halves**	**Body regions**	**tRF-5s**	**i-tRFs**	(Lakshmanan et al., 2021)
Anterior	49	Pharynx enriched	9	11	
Others	62	Head enriched	12	8	

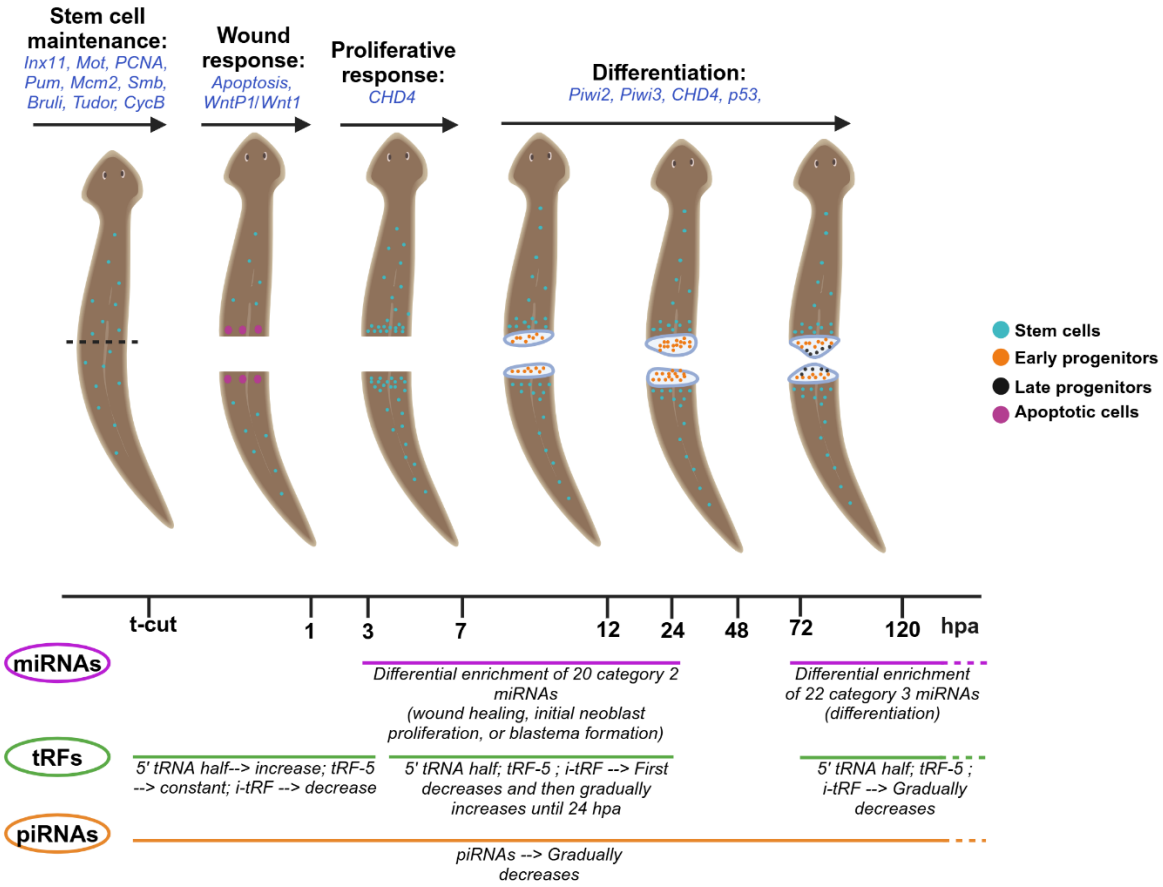

Figure 5. Major gene expression and sncRNA enrichment patterns during planarian regeneration time course. The regenerative time frame (not to scale) shows enrichment of genes and small ncRNAs during crucial processes such as wound healing, proliferative and differentiative responses.

Building on the detailed discussion above, it is evident that while certain sncRNA classes, such as miRNAs, have been extensively studied, others, like tRFs, are only beginning to be explored. Moreover, what remains largely missing across these studies is functional information on specific differentially regulated sncRNA molecules. Even in the case of miRNAs, where research is most advanced, only a limited number of studies have focused on validating the functional roles of crucial smed-miRs. This highlights a significant gap in our understanding, emphasizing the need for current research to prioritize the functional characterization of specific sncRNAs in planarian regeneration.

2. Aims and Objectives

Regeneration is a critical biological process, and gaining a deeper understanding of its mechanisms remains one of the central challenges in biomedical research. *S. mediterranea* presents an excellent model organism for studying regeneration in a whole-organism context, as all cell lineages are consistently present in an adult individual. Additionally, *S. mediterranea* shares homologous genes with humans, including those that are associated with Mendelian diseases when disrupted. sncRNAs have been extensively investigated in the context of regeneration and differentiation; however, numerous questions persist, particularly regarding the role of RNA fragments. Investigating the functions of these molecules in regeneration of *S. mediterranea* is important for advancing our understanding of the molecular mechanisms underlying human diseases.

The aim of this dissertation was to identify and characterize sncRNAs involved in *S. mediterranea* regeneration, with particular focus on the RNA fragments. Achieving this goal required the completion of the following specific tasks:

(i) Development of a research strategy to investigate the impact of sncRNA pool alterations on the regeneration process in *S. mediterranea*,

(ii) Determination of the effects of sncRNA pool disruptions on the regeneration process in *S. mediterranea* at the following levels:

- Morphology and anatomy
- Cell populations
- Transcriptome (including gene expression and sncRNA profiles)

(iii) Identification and functional characterization of selected sncRNA involved in regeneration.

3. Materials

3.1. Basic buffers and solutions

Table 7. 1.6 mM NaCl

Ingredients	Volume/Amount
NaCl	46.72 mg
Ultrapure water	up to 500 mL

Table 8. 1.0 mM $CaCl_2$

Ingredients	Volume/Amount
$CaCl_2$	88.8 mg
Ultrapure water	up to 500 mL

Table 9. 1.0 mM $MgSO_4$

Ingredients	Volume/Amount
$MgSO_4$	96.3 mg
Ultrapure water	up to 500 mL

Table 10. 0.1 mM $MgCl_2$

Ingredients	Volume/Amount
$MgCl_2$	4.8 mg
Ultrapure water	up to 500 mL

Table 11. 0.1 mM KCl

Ingredients	Volume/Amount
KCl	3.8 mg
Ultrapure water	up to 500 mL

Table 12. 1.2 mM $NaHCO_3$

Ingredients	Volume/Amount
$NaHCO_3$	84 mg
Ultrapure water	up to 500 mL

Table 13. 3M Sodium Acetate

Ingredients	Volume/Amount
CH_3COONa	123.1 mg
Ultrapure water	up to 500 mL

Table 14. 7.5% NAC

Ingredients	Amount/Volume
1x PBS	up to 10 mL
NAC	7.5 g

Table 15. PBSTx

Ingredients	Amount/Volume
1x PBS	498.5 mL
Triton X-100	1.5 mL

Table 16. 20X SSC

Ingredients	Amount/Volume
3M NaCl	175.3 g
0.3M sodium citrate	88.2 g
Filled up to 1L ultrapure water and pH was set to 7.	

Table 17. 2X SSC

Ingredients	Amount/Volume
20X SSC	25 mL
Ultrapure water	225 mL

Table 18. 0.2X SSC

Ingredients	Amount/Volume
20X SSC	200 µL
Ultrapure water	249.8 mL

Table 19. TNTx

Ingredients	Amount/Volume
Tris pH: 7.5	6.057 g
NaCl	4.383 g
Triton X-100	0.3 %
Ultrapure water	Up to 500 mL

Table 20. TSA buffer

Ingredients	Amount/Volume
NaCl	11.7 g
Boric acid	0.618 g
Ultrapure water	Up to 100 mL
pH 8.5, Keep in 4°C	

Table 21. Tyramide solution

Ingredients	Amount/Volume
Fluor-tyramine	2 µL
IPBA dissolved in DMF	5 µL
H_2O_2	0.015 µL
TSA buffer	493 µL
Kept at -20°C	

Table 22. Blocking solution

Ingredients	Amount/Volume
Horse serum	500 µL
Western blocking reagent	50 µL
TNTx	9.45 mL

Table 23. Antibody solution

Ingredients	Amount/Volume
Blocking solution	1999 µL
Antibody	1 µL

Table 24. Hybridisation

Ingredients	Amount/Volume
Prehyb	up to 50 mL
Dextran sulfate	2.5 g
Store in -20°C	

Table 25. Pre-hybridisation solution

Ingredients	Amount/Volume
Deionized formamide	25 mL
Yeast RNA	0.1 mL
20x SSC	12.5 mL
Tween 20	5 mL
Ultrapure water	up to 50 mL
Store in -20°C	

Table 26. Riboprobe mix

Ingredients	Amount/Volume
Hyb	300 µL
Probe	400 ng

Table 27. Fixative solution

Ingredients	Amount/Volume
Formaldehyde	1 mL
PBSTx	8 mL

Table 28. Bleaching solution

Ingredients	Amount/Volume
20x SSC	250 µL
30% H_2O_2	1.5 mL
Formamide	500 µL

Table 29. Proteinase K solution

Ingredients	Amount/Volume
PBSTx	9.9 mL
SDS	100 µL
Proteinase K	5 µL

Table 30. 10X CMF

Ingredients	Amount/Volume
KCl	1.903 g
NaH_2PO_4	0.883 g
$NaHCO_3$	1.979 g
NaCl	2.087 g
Ultrapure water	up to 250 mL
pH 7.3 to 7.4; Store in room temperature	

Table 31. CMFB

Ingredients	Amount/Volume
10x CMF	5 mL
BSA	0.500 g
Ultrapure water	up to 45 mL
Kept on ice	

Table 32. PBSB

Ingredients	Amount/Volume
PBS	25 mL
BSA	up to 0.250 g
Kept on ice	

Table 33. LB broth liquid culture medium

Ingredients	Amount/Volume
LB broth	3.7 g
Ultrapure water	up to 100 mL
Ampicillin (100 µg/mL)	100 µL
10 mL of this solution was poured into 10 separate flasks each	

Table 34. LB agar plates

Ingredients	Amount/Volume
Yeast extract	5 g
Peptone	10 g
NaCl	10 g
Agar	12 g
Ultrapure water	up to 1 L
Solution was autoclaved at 121ºC for 30 min. Just before pouring, 100 µg/mL Ampicillin was added. 20 mL of this solution was poured into each petri plate, waited until solidification and stored at 4ºC.	

Table 35. Agarose gel

Ingredients	Amount/Volume
Agarose	0.400 g
1X TBE	up to 40 mL
Midori Green	4 µL
Before adding Midori Green, the ingredients were mixed by microwaving for 2 mins. The mixture was cooled to ~60ºC, before adding the required amount of Midori Green.	

3.2. Raw materials

Table 36. Reagents

Reagent	Manufacturer	Catalog number
RNaseOUT Recombinant Ribonuclease Inhibitor	ThermoFisher	10777019
Nuclease free water	ThermoFisher	4387936
1x PBS	ThermoFisher	A1286301
96% Ethanol	Merck	111727
Methanol	Merck	179337-1L
Formaldehyde	ThermoFisher	033314.AP
Random Hexamers (50 µM)	ThermoFisher	N8080127
dNTP Mix (10 mM each)	ThermoFisher	R0192
Qubit™ RNA Broad Range (BR) Assay Kit	ThermoFisher	Q10211
Qubit™ 1X dsDNA High Sensitivity (HS) Assay kit	ThermoFisher	Q33230
High Sensitivity RNA ScreenTape	Agilent	5067-5579
High Sensitivity RNA ScreenTape Ladder	Agilent	5067-5581
High Sensitivity RNA ScreenTape Sample Buffer	Agilent	5067-5580
Gentamicin solution	Sigma Aldrich	G1397-100ML
mirVana™ miRNA Isolation Kit, with phenol	ThermoFisher	AM1560
TURBO™ DNase (2 U/µL)	ThermoFisher	AM2239

SuperScript IV Reverse Transcriptase	ThermoFisher	18090010
SuperScript II Reverse Transcriptase	ThermoFisher	18064-014
High-Capacity cDNA Reverse Transcription kit with RNase Inhibitor	ThermoFisher	4374966
TRIzol™ Reagent	ThermoFisher	15596018
TruSeq® Small RNA Library Prep Kit	Illumina	RS-200-0012
Total RNA Zol-Out™	A&A Biotechnology	030-100
Herculase II Fusion DNA Polymerase	Agilent	600675
pLJM1-eGFP plasmid	Addgene	Addgene – plasmid 19319
QIAprep Spin Miniprep Kit	Qiagen	27106
AmpliScribe T7-Flash Transcription Kit	Biosearch technologies	ASF3507
Anti-Digoxigenin-POD, Fab fragments solution	Merck	11207733910
NHS-Fluorescein	ThermoFisher	46410
Tyramine hydrochloride	Sigma-Aldrich	T2879
Fluoroshield™	Sigma-Aldrich	F6182
HighYield T7 Digoxigenin RNA Labeling Kit	Jena Bioscience	RNT-101-DIGX
5x HOT FIREPol® EvaGreen® qPCR Supermix	CytoGen	08-36-000001
CellTrics® 50 μm, sterile	Sysmex	04-004-2327
T4 RNA Ligase 2, Truncated	NEB	M0242L

DRAQ5™ Fluorescent Probe Solution (5 mM)	ThermoFisher	62251
Calcein AM	ThermoFisher	65-0853-78
Hoechst 33342, Trihydrochloride	ThermoFisher	H21492
KAPA RNA HyperPrep Kit with RiboErase	Roche	8098131702
1X PBS	ThermoFisher	A1286301
N-Acetyl-L-cysteine (NAC)	Sigma-Aldrich	A7250-25G
Triton X-100	ThermoFisher	85111
4-iodphenylboronic acid (IBPA)	Sigma-Aldrich	471933-5G
N,N-Dimethylformamide (DMF)	Sigma-Aldrich	227056-100ML
Hydrogen peroxide (H_2O_2)	Merck	H1009-100ML
Horse serum	Sigma-Aldrich	H0146-5ML
Western blocking reagent	Roche	11921673001
Dextran sulfate	Merck	3730-OP
Deionized formamide	Sigma-Aldrich	S4117
Yeast RNA	ThermoFisher	AM7118
Tween 20	Sigma-Aldrich	655206
SDS	Bioshop	SDS002.500
Proteinase K	ThermoFisher	EO0491
BSA	Bioshop	ALB003.100

Ampicillin, sodium salt	Bioshop	AMP201.25
LB broth	Bioshop	LBL405.1
Agarose	Bioshop	AGA001.500
10X TBE buffer	Bioshop	TBE444.4
DirectLoad™ Wide Range DNA Marker	Sigma-Aldrich	D7058
Midori Green	Nippon Genetics	MG04
NaCl	Sigma-Aldrich	S9625
MgCl2	Sigma-Aldrich	208337
MgSO4	Sigma-Aldrich	M2643
CaCl2	Sigma-Aldrich	C5670
KCl	Sigma-Aldrich	P5405
NaHCO3	Sigma-Aldrich	S5761
CH_3COONa	Sigma-Aldrich	S8750

Table 37. Oligonucleotides

Name	**Sequence (5'-3')**
Hot-start PCR primers for genes	
H2B_forward_T7	TAATACGACTCACTATAGGGTCTGTTAAGAAGATTTCAAAGG
H2B_reverse_T7	TAATACGACTCACTATAGGGTCCTGTGTATTTTGTAACAGC
Elac2_forward_T7	TAATACGACTCACTATAGGGTTATTGAATGCCCAACTCTCG
Elac2_reverse_T7	TAATACGACTCACTATAGGGTGGAAATGAGAATTGATCCG

PARN_forward_T7	TAATACGACTCACTATAGGGTAAAAGAGCATTCGATGCCA
PARN_reverse_T7	TAATACGACTCACTATAGGGAAAAATTCGATTGTGTCTGCATT
RNase T2_forward_T7	TAATACGACTCACTATAGGGGCAATTCTGCCGCCTTTAT
RNase T2_reverse_T7	TAATACGACTCACTATAGGGTGGCACAGTTAAACCGGAAT
RNase H1_forward_T7	TAATACGACTCACTATAGGGATAAACGGTCGAGAACCAGG
RNase H1_reverse_T7	TAATACGACTCACTATAGGGCCGACATTCCACGGACTATT
GFP_forward_T7	TAATACGACTCACTATAGGGGGTGGTGCCCATCCTGGTCGAG
GFP_reverse_T7	TAATACGACTCACTATAGGGGTGGTCACGAGGGTGGGCCAGG
qPCR primers for genes	
H2B_forward_qPCR	AGTTGAACGGCCCTCTTTAG
H2B_reverse_qPCR	ACGTACTTCAACGACGTTTT
Nb.21.11e_forward_qPCR	AAAGTCTCCCGCCAAATCAA
Nb.21.11e_reverse_qPCR	CGCAATCTTTGTCGAGCTTC
Smed1_forward_qPCR	AAACGTGAGCCTAGAGAACG
Smed1_reverse_qPCR	GACCACGAATCGTAATCGGT
Agat1_forward_qPCR	AGAGGAACCAGTTTTCGACG
Agat1_reverse_qPCR	AGGTGTGAAAAGTGTCGTGT
GST_forward_qPCR	AATGGCCAGAAGTGAAACCA
GST_reverse_qPCR	AACCCATGTTTTCGTGCAAC
PC2_forward_qPCR	GCATTTGTGGTGTTGGAGTG
PC2_reverse_qPCR	TCATTTCTCGGCCCATCTAC
H.55.12e_forward_qPCR	TTCCTACAGCCACTTGAGCGAC
H.55.12e_reverse_qPCR	GTCGGTGGTTATTTTGCG
Ef2_forward_qPCR	TGCTGGTGACACTTTGCTTC

Ef2_reverse_qPCR	CATCACCAAGTGTCCGTTTG
Elac2_forward_qPCR	CGATTGTTTCTCTTGCACGG
Elac2_reverse_qPCR	CACGGAAAACAGTCCTGAGT
RNApolII_phosphatase_forward_qPCR	TACCGCATTCGACCTTTTCA
RNApolII_phosphatase_reverse_qPCR	ACCCACCCATTCCAGAGATA
Tyrosine_phosphatase_forward_qPCR	TCGCTTCTACACTTGACGAC
Tyrosine_phosphatase_reverse_qPCR	GATATTCCTCCTCCCCGACT
SMESG000076350_forward_qPCR	TATCGACTCCCCTCAAACCA
SMESG000076350_reverse_qPCR	ATCAAGGGAGGGGTAAGTGT
qPCR primers for mitochondrial chimeric transcripts	
Region2_junc_forward_qPCR	TTTGGTTTCGGCCCATTTTT
Region2_cox3_forward_qPCR	TTCGTAGTAGTTGTTGGCCT
Region2_junc_reverse_qPCR	CCAAAGCAACGAAACAACCA
Region4_junc_forward_qPCR	AACGAGTATATTTAGTTTACATCTAAAAGG
Region4_ND1_forward_qPCR	TTCAGACTCGTAAGGGTCCA
Region4_junc_reverse_qPCR	ATCAGCAAAAGCAGTAGCCA
Region8_junc_forward_qPCR	AGCTCAGTTGTTGGTTTCCT
Region8_12SrRNA_forward_qPCR	AACTGGCATGCTGTTAAACG
Region8_junc_reverse_qPCR	AGCATATACCGACTCAAGCA
Region9_junc_forward_qPCR	CCAAGCTGTTAACTTGGAGA
Region9_mtlncRNA_forward_qPCR	AGGTGTTGATGGAAGTTACGTT
Region9_junc_reverse_qPCR	AACCAACGAGCAAACAATCA
Region3_junc_forward_qPCR	AGGAACTTATTGTTTCCCAG
Region3_ATP6_forward_qPCR	CTTTGTTCTTTGATCCTTGG

Region3_junc_reverse_qPCR	GGACCATAAACCAAAAGACTC
qPCR primers for small RNA targets	
5`tRNA half Gly-GCC_forward_qPCR	ACGATCGCATCGGTGGTTCA
5`tRNA half Gly-GCC_reverse_qPCR	CCGAGAATTCCAAGGCGAGC
sme-miR-8b-3p_forward_qPCR	GTCCGACGATCTAATACTGTCA
sme-miR-8b-3p_reverse_qPCR	GCACCCGAGAATTCCAAGTAT
microRNA_Ros-gga_forward_qPCR	GTCCGACGATCACCCTGTAG
microRNA_Ros-gga_revrese_qPCR	GGCACCCGAGAATTCCATTCTA
sme-miR-71a_revrese_qPCR	GTCCGACGATCTGAAAGACA
sme-miR-71a_reverse_qPCR	CACCCGAGAATTCCACTACC
Primers for RNA probe synthesis	
PC2_forward_probe	AACGCAAAACAAGTTGAAGG
PC2_reverse_probe	TAATACGACTCACTATAGGGCATCATAGCTTGCGGTTTCT
Collagen_forward_probe	TAACGGGACCACAAGGTTTA
Collagen_reverse_probe	TAATACGACTCACTATAGGGTGGACCGTAATTTCCAGGTA
Porcupine_forward_probe	TCAGCGCATTTGGTAACGTA
Porcupine_reverse_probe	TAATACGACTCACTATAGGGTCTGAGCCATCTTGTTGTGG
Synthetic RNA molecules	
5' tRNA half Gly-GCC mimic (Modifications: 2-O-Me; 5' phosphorylation)	GCAUCGGUGGUUCAGUGGUAGAAUGCUCGCCU
Scrambled (Modifications: 2-O-Me; 5' phosphorylation)	GGGUCUGCUAACGUGCUAUGUGCGCGUCAAGU

4. Methods

4.1. Maintenance of planarian cultures

4.1.1. Planarian culture

A diploid (2n) strain of the asexual planarian *Schmidtea mediterranea* was maintained in plastic containers filled with culture solution (**Table 38**) and kept in dark incubators at 20°C. The dark conditions were necessary as these worms are photophobic. They were fed with small cubes of chicken liver once or twice a week. For each feeding, 2–3 cubes were placed in each culture box and planarians were allowed to feed in the dark for approximately three hours. After feeding, the remaining liver cubes were removed, the culture solution was drained, and the container walls and bottoms were wiped clean. Fresh culture solution was then added. Additionally, the containers were cleaned in a similar manner about three times per week to remove bio-secretion and waste.

4.1.2. Maintenance of planarian colonies

Adult, fully-grown worms (~70–80 mm in length) were used to produce progeny. These worms were placed on a dry petri dish and amputated into three segments—head, trunk, and tail—along the horizontal plane, with each fragment measuring approximately 20 mm in length. After amputation, the fragments were returned to their culture boxes containing planarian culture solution. Regenerating worm fragments were not fed for up to a week post-amputation, as those lacking a feeding tube (pharynx) require time to regenerate this structure. During this period, the cultures were cleaned regularly as described in **4.1.1**.

Table 38. Planarian culture solution recipe

Final molar concentrations in planarian culture solution	Volume/Amount to be added
1.6 mM NaCl	320 µL from 5M stock
1.0 mM $CaCl_2$	1 mL from 1M stock
1.0 mM $MgSO_4$	1 mL from 1M stock
0.1 mM $MgCl_2$	100 µL from 1M stock
0.1 mM KCl	100 µL from 1M stock
1.2 mM $NaHCO_3$	0.1008 g
Ultrapure water	up to 1 L

4.1.3. Care of restoration of compromised cultures

Although technically immortal, planarian cultures occasionally experience instances of disease or infection as part of natural biological processes. These conditions can be identified by symptoms such as the spontaneous loss of the tail and the appearance of white

necrotic spots on the worms, observable under an inverted light microscope. Affected individuals display reduced motility, even when exposed to light, and tend to adhere to the bottom or walls of the culture box. When such symptoms were observed, the affected worms were promptly amputated above and below the necrotic spots to ensure the regeneration of healthy progeny from the remaining viable tissue. The original cultures showing signs of disease, as well as their immediate progeny, were maintained in culture solution supplemented with Gentamicin (50 mg/mL at a 1:1000 dilution)

for up to two weeks. This treatment aimed to prevent further infections and improve the viability of the worms.

4.2. RNA isolation

4.2.1. From frozen tissue

Worms or worm fragments were put into 1.5 mL tubes and flash frozen in liquid nitrogen. Total RNA was isolated using the mirVana™ miRNA Isolation Kit, with phenol, according to the basic manufacturer's protocol. For purposes which required further fractionation of total RNA into long (>200 nt) and small (<=80 nt) RNA fractions, the same kit and appropriate manufacturer's protocol were used.

4.2.2. From sorted cells

Approximately 50,000 cells were sorted per sample into Eppendorf® Protein LoBind 1.5 mL tubes containing 350 µl TRIzol™ Reagent for total RNA extraction. Next, the sorted samples were vigorously shaken once out of the sorter and kept on ice until the next step. Total RNA was isolated and treated with DNase using the Total RNA Zol-Out™ D and dissolved in 20 µl water. Concentrations of total RNA isolated from this process were too low to be measured using Qubit or Nanodrop. Therefore, samples were directly checked on Agilent TapeStation 4150 system using High sensitivity RNA screen tapes, to check RIN and get an estimate of the concentration.

4.3. Standard ethanol-sodium acetate precipitation method

Table 39. Ethanol-sodium acetate precipitation of nuclei acid

Ingredients	Volume
DNA/RNA	Total volume
Ice cold Ethanol	3 volumes (Eg.: 60 µL ethanol to 20 µL DNA/RNA)
3M sodium acetate (NaOAc)	0.1 volumes (Eg.: 2 µL NaOAc to 20 µL DNA/RNA)

The mix in **Table 39** was incubated at -20°C overnight or -80°C for 1 hour and then centrifuged at 18349 RCF (radius 8.4 cm) for 20 minutes in a centrifuge set at 4°C. The nucleic acid pellet was air-dried and dissolved in 20-50 µL nuclease free water.

4.4. DNase treatment

Up to 10 µg of total, long and short RNA fractions were treated with TURBO™ DNase for 30 minutes at 37°C in a thermal cycler, and DNA-free RNA samples were purified using standard ethanol-sodium acetate precipitation method (**Table 39**). **Table 40** shows the DNase treatment mix.

Table 40. DNase treatment reaction mix

Ingredients	Amount/Volume
RNA	10 µg
TURBO DNase buffer	5 µL
TURBO DNase enzyme	1 µL
RNase inhibitor	1 µL
Nuclease free water	Up to 50 µL

4.5. Standard ethanol-sodium acetate precipitation method

Table 41. Ethanol-sodium acetate precipitation of nuclei acid

Ingredients	Volume
DNA/RNA	Total volume
Ice cold Ethanol	3 volumes (Eg.: 60 µL ethanol to 20 µL DNA/RNA)
3M sodium acetate (NaOAc)	0.1 volumes (Eg.: 2 µL NaOAc to 20 µL DNA/RNA)

The mix in **Table 41** was incubated at -20°C overnight or -80°C for 1 hour and then centrifuged at 18349 RCF (radius 8.4 cm) for 20 minutes in a centrifuge set at 4°C. The nucleic acid pellet was air-dried and dissolved in 20-50 µL nuclease free water.

4.6. RNA concentration measurement and quality check

The purified RNA sample concentrations were measured on Qubit 4 Fluorometer using Qubit™ RNA Broad Range (BR) Assay Kit. Standards and sample(s) were prepared according to **Table 42**.

Table 42. Qubit™ RNA Broad Range (BR) Assay reaction mixes

Ingredients	Volume
RNA Sample	1-10 µL RNA + 199-190 µL working solution
Standard 1	10 µL RNA + 190 µL working solution
Standard 2	10 µL RNA + 190 µL working solution

Before measuring the sample concentrations, Standards 1 and 2 were sequentially measured first to generate the standard curve. The RNA samples were then measured immediately afterwards.

RNA quality profiles were checked on Agilent TapeStation 4150 system using the High sensitivity RNA screen tapes, according to respective manufacturer described protocols. Samples were prepared according to **Table 43**.

Table 43. High sensitivity RNA Assay reaction mixes

Ingredients	Volume
HS RNA Ladder/ RNA Sample (500-10000 pg/ µL)	1 µL
Loading buffer	2 µL RNA per RNA sample or ladder

Before loading, the sample strips were briefly vortexed, incubated at 72ºC for 3 minutes, immediately cooled on ice for 2 minutes, mixed again, and then placed into the tape nest of the TapeStation 4150 device. After the run, the capillary electrophoresis gels and corresponding electropherograms for each sample were analysed. For long RNA and total RNA, samples with RIN 8 or higher were used for further downstream procedures.

4.7. cDNA synthesis

4.7.1. Total or long RNA fraction isolated from tissue

cDNA was synthesised from 1µg total or long RNA samples using SuperScript™ IV Reverse Transcriptase using Random hexamer primers. The reaction mixture was made as per **Table 44** and

Table *45* and the reaction was incubated on a thermal cycler according to the PCR program in **Table 46**. The obtained cDNA was straightaway used for Hot start and/or quantitative real time PCR reactions, without further concentration measurement or purification steps.

Table 44. cDNA synthesis using SuperScript IV – Mix-A

Ingredients for Mix-A	Amount/Volume (for one cDNA sample)
RNA treated with DNase	1 µg
Random hexamers (50 µM)	1 µL
dNTPs (10 mM)	1 µL
Nuclease free water	Up to 13 µL

This mix was incubated for 5 minutes each, first at 65°C and then on ice.

Table 45. cDNA synthesis using Superscript IV – Mix-B

Ingredients for Mix-B	Volume (for one cDNA sample)
5x SSIV buffer	4 µL
DTT (100mM)	1 µL
RNase inhibitor	1 µL
Superscript IV enzyme	1 µL

Mix-B was combined with Mix-A and then the sample was incubated in a thermal cycler, using the following program.

Table 46. cDNA synthesis using Superscript IV – incubation program

Temperature	Time
23°C	10 minutes
55°C	10 minutes
80°C	10 minutes

4.7.2. Small RNA fraction

RNA molecules from the small RNA fraction required a dedicated strategy of cDNA synthesis, relying on ligation with 3' and 5' adapters that provided primer binding sites. To achieve this, the TruSeq® Small RNA Library Prep Kit was utilized, and the protocol was followed up to library amplification. The PCR program in **Table 47** was used for amplification. Illumina kit specific primers were used for reverse transcription (RT) and cDNA amplification.

Table 47. PCR program for synthesis of cDNA from small RNA fractions

Lid temperature: 100°C		
Temperature	**Time**	**No. of cycles**
98°C	30 seconds	1
98°C	10 seconds	13
60°C	30 seconds	
72°C	15 seconds	
72°C	10 minutes	
4°C	∞	1

4.7.3. Total RNA from sorted cells

10 µl of the isolated total RNA was processed for cDNA synthesis using random hexamer primers and High-Capacity cDNA Reverse Transcription kit with RNase Inhibitor (**Table 48** and **Table 49**). Final volume of synthesised cDNA was 20 µL.

Table 48. Reaction mix for cDNA synthesis from total RNA from sorted cells

Ingredients	Volume
Total RNA from sorted cells	10 µL
10x RT buffer	2 µL
25x dNTP mix (100 mM)	0.8 µL
10x RT random primers	2 µL
Multiscribe reverse transcriptase	1 µL
RNase inhibitor	1 µL
Nuclease-free water	3.2 µL
Total	**20 µL**

Table 49. cDNA synthesis from total RNA from sorted cells – incubation program

Temperature	Time
25°C	10 minutes
37°C	120 minutes
85°C	5 minutes
4°C	∞

4.8. PCR amplification

PCR amplification reactions were carried out using Herculase II Fusion DNA Polymerase (**Table 50** and **Table 51**). For optimizing primer annealing temperatures in the beginning, gradient PCR for each primer set and its associated target was carried out independently.

Table 50. Reaction mix for Hot-start PCR amplification

Ingredients	Volume
Forward primer	1 µL
Reverse primer	1 µL
dNTPs (10mM)	1.25 µL
5x Herculase II reaction buffer	10 µL
cDNA/plasmid DNA	0.5 µL cDNA or 30 ng plasmid DNA
Herculase II fusion DNA polymerase	0.5 µL
Nuclease-free water	35.25 µL
Total	**50 µL**

Table 51. PCR program for Hot-start PCR amplification

Lid temperature: 105°C		
Temperature	**Time**	**No. of cycles**
95°C	2 minutes	1
94°C	30 seconds	10
55.5°C	20 seconds	
72°C	30 seconds	
94°C	30 seconds	25
64.4°C	20 seconds	
72°C	30 seconds	
72°C	10 minutes	1
4°C	∞	1

4.9. Agarose gel electrophoresis

A 1% agarose gel was prepared following standard protocols and poured into a gel casting setup. The gel was allowed to cool and solidify before being placed in a gel tank filled with 1X TBE buffer to the maximum level. For sample preparation, 5.5 µL of each dsDNA product was combined with 1.5 µL of gel loading dye, and the DNA ladder (DirectLoad^{TM} Wide Range DNA Marker) was prepared similarly. Approximately 7 µL of each sample was loaded into individual wells, and electrophoresis was performed for ~45 minutes at ~120 V. The gel was then imaged using a Bio-Rad Gel Documentation system (GelDoc) to visualize the DNA bands.

4.10. Bacterial culture and plasmid isolation

The pLJM1-eGFP plasmid containing bacterial inoculum was used for plasmid isolation. To cultivate bacterial colonies, a small portion of the inoculum was spread onto an LB agar plate containing ampicillin (100 µg/mL) using a sterile spreading loop. The plates were incubated overnight at 37°C, and distinct colonies were observed the following day. From these, 3-5 individual bacterial colonies were selected using separate sterile pipette tips and inoculated into 15 mL culture flasks containing 10 mL of LB broth supplemented with ampicillin (100 µg/mL). The flask lids were loosely closed to allow proper oxygen exchange, and the cultures were incubated overnight at 37°C with constant shaking. Plasmid DNA was isolated using the QIAprep Spin Miniprep Kit. The isolated plasmid DNA was subsequently used to amplify the target GFP amplicon as described in section **4.8**.

4.11. dsRNA synthesis and RNAi knockdown of target transcripts

RNAi-mediated target gene knockdown (KD) experiments were performed by the introduction of artificial dsRNA synthesized using AmpliScribe T7-Flash Transcription Kit (**Table 52**), via microinjections into the worms. A total of 10-20 worms were used for each sample in such experiments. Two types of control sets were used, unless mentioned otherwise: 1) worms injected with dsRNA synthesised against an unrelated transcript, absent from planarians (RNA encoding green fluorescent protein, GFP); 2) wild type worms without any injections. Animals unfed for a week were injected with 32 nl of 2 µg/µL dsRNA, using Nanoject III™ (Drummond Scientific Company) according to the following regime: injection for 3 consecutive days, a gap of 2 days and, again injection for next 2 consecutive days, for a total of 5 days. All worms from knockdown and control groups were cut into 3 fragments – head, trunk and tail after the last injection day. Regenerating fragments were then harvested at specific days post amputation (dpa) (as when required), for downstream analyses. All experiments were performed in 3 independent biological replicates.

Table 52. Reaction mix for dsRNA synthesis

Ingredients	Volume
Nuclease-free water	Up to 20 µL
DNA template with T7 promoter	1 µg
10x reaction buffer	2 µL
100 mM ATP	1.8 µL
100 mM CTP	1.8 µL
100 mM UTP	1.8 µL
100 mM GTP	1.8 µL
100 mM DTT	2 µL
RNase inhibitor	0.5 µL
Ampliscribe T7-Flash enzyme	2 µL
Total	**20 µL**

This reaction mix was incubated for 2.5 hours at 37°C. Finally, the synthesised dsRNA was precipitated using ethanol-sodium acetate precipitation method and resuspended in 50 µL nuclease-free water.

4.12. Fluorescent in-situ hybridization (FISH)

On day 1, starved planarians were euthanized by gentle rocking in 10 mL of 7.5% NAC solution (**Table 14**) (2% NAC for regenerating fragments) in a 15 mL tube for 13 minutes (5 minutes for regenerating fragments). The solution was discarded, and the planarians were fixed by transferring them to 10 mL of 4% fixative solution (**Table 27**) and

rocking for 15 minutes (5 minutes for fragments). After discarding the fixative, the planarians were washed twice with 10 mL PBSTx solution (**Table 15**) for 5 minutes each. Dehydration was carried out by soaking and rocking the animals in 10 mL 50% methanol for 5 minutes, followed by two 5-minute washes in 10 mL 100% methanol. The planarians were then stored overnight at -20°C in 10 mL 100% methanol.

On day 2, the dehydrated animals were rehydrated by gentle rocking for 5 minutes in 10 mL 50% methanol, followed by two 5-minute washes with 10 mL PBSTx solution. They were then rinsed in 10 mL 2x SSC solution (**Table 17**) for 5 minutes. Bleaching was performed under bright light using bleaching solution (**Table 28**) on aluminium foil for 4–6 hours, or until the animals were completely depigmented and appeared white. Following bleaching, the planarians were washed once in 10 mL of 2x SSC solution for 5 minutes and twice in 10 mL PBSTx solution for 5 minutes each. The animals were then incubated in 10 mL proteinase K solution (**Table 29**) for 15 minutes (7 minutes for fragments), after which they were fixed again in 10 mL 4% fixative solution. This was followed by three washes of 10 mL PBSTx solution for 5 minutes each. The planarians were transferred to 1.5 mL tubes, incubated in 300 µl of a 1:1 Prehybridization mix (Prehyb **Table 25**)–PBSTx solution for 10 minutes, and then in 300 µl of Prehyb solution at 56°C for 2 hours. Target RNA probes (section **4.13**) were denatured at 80°C and cooled to 50°C before hybridization. The probes were hybridized in the dark by incubating the planarians in 300 µl of denatured probe solution (**Table 26**) at 56°C for approximately 16 hours with gentle shaking. From this step onward, all procedures were performed under light-protected conditions using aluminum foil.

On day 3, the hybridization solution was discarded, and the planarians were incubated at 56°C for 20 minutes in 300 µl of Wash-Hyb solution. This was followed by a series of washes: three washes in 300 µl of 2x SSCx solution at 56°C for 20 minutes each, two washes in 300 µl of 0.2x SSCx solution (**Table 18**) at 56°C for 20 minutes each, and two washes in 300 µl of TNTx solution (**Table 19**) at room temperature for 10 minutes each. The planarians were then soaked and gently rocked in 500 µl of blocking solution (**Table 22**) for 1–2 hours. After blocking, they were incubated overnight at 4°C in 500 µl of Anti-Digoxigenin-POD, Fab fragments solution (**Table 23**).

On Day 4, the antibody solution was discarded, and the planarians were washed six times in 500 µl of TNTx solution for 20 minutes each. They were then rinsed twice in 300 µl of TSA buffer (**Table 20**) for 5 minutes at room temperature. The planarians were transferred to 6-well plates and incubated in 700 µl of 1:250 NHS-Fluorescein (Ex/Em:

494/518 nm) + Tyramine hydrochloride conjugate (Tyramide solution **Table 21**) for 10 minutes, with gentle swirling every 2 minutes. Following this, they were washed six times in 500 µl of TNTx solution for 5 minutes each. The planarians were briefly examined under the Leica M205 FA fluorescence stereomicroscope, to confirm staining. To remove or minimize non-specific signals, they were soaked overnight at 4°C in 500 µl of TNTx solution.

On the following day, slides were prepared by mounting 1–2 whole planarians (or ~3 fragments) under a square coverslip with Fluoroshield™. Animals were imaged on a Nikon Eclipse Ti2 confocal system, using 20 X magnification. The fluorescent signals were excited using the FITC laser with specifications: Ex/Em: 480/535nm. Emitted signals were obtained in green fluorescence spectrum.

4.13. Probe synthesis for FISH

Total RNA was isolated (section **4.2.1**) followed by cDNA synthesis using Superscript IV protocol (section **4.7.1**) and target amplicon (~800 nt) amplification using Herculase II protocol (section **4.8**), as described earlier. A differing point from the dsRNA synthesis workflow is that while amplifying the target amplicon primers were designed in a way such that only the reverse primer (not the forward primer) has the T7 promoter sequence. This is because the DNA strand synthesised by this primer shall only be transcribed to form the probe RNA, which will further target the complementary cellular mRNA transcripts. Such RNA probes against target mRNA molecules were synthesised using HighYield T7 Digoxigenin RNA Labeling Kit (**Table 53**).

Table 53. Reaction mix for RNA probe synthesis for FISH

Ingredients	**Volume**
Nuclease-free water	Up to 20 µL
DNA template with T7 promoter	1 µg
10x reaction buffer	2 µL
10 mM ATP/GTP/CTP working solution	2 µL
10 mM UTP working solution	1.3 µL
10mM DIG-11-UTP	0.7 µL
T7 polymerase	2 µL
Total	**20 µL**
The mix was incubated at 37°C for 1.5-2 hours and the probe RNA was purified using Ethanol-sodium acetate precipitation method.	

4.14. Phenotypic documentation

The phenotypes of regenerating worms from RNAi knockdown and control samples were observed and documented at specific time points during regeneration: 0, 1, 3, 5, 7, and 14 days post-amputation (dpa), using the Nikon SMZ1270 zoom stereomicroscope. Each regenerating fragment was individually inspected and photographed. To ensure stable and clear images, the worms were placed on a moist black sheet of paper positioned on a cold metal block maintained at 4°C. The cold block minimized worm mobility during imaging. Key features assessed during phenotype documentation included motility, the pace of regeneration in the anterior and posterior blastema, eyespot regeneration, abnormal tissue masses, mispositioned tissue growth, pigmentation anomalies, necrotic spots, and overall viability of the regenerating fragments.

4.15. qRT-PCR approaches

4.15.1. qRT-PCR to assess gene expression

qRT-PCR primers were designed for target genes in a way such that the target regions for qRT-PCR amplification and for dsRNA synthesis do not overlap. The amplification reactions were performed in 3 technical replicates for each cDNA sample (section **4.7.1**) using 5x HOT FIREPol® EvaGreen® qPCR Supermix. The final volume of each sample was adjusted to 10 µl (**Table 54** and **Table 55**). Analysis was done using 2^-ΔΔCt method and normalised with respect to expression of reference gene *Smed EF2* (dd_Smed_v6_69721_0_1).

Table 54. Universal reaction mix – used for all types of qPCR in this thesis

Ingredients	Volume per technical replicate
Forward primer (10 µM)	0.5 µL
Reverse primer (10 µM)	0.5 µL
EvaGreen® qPCR Supermix	9 µL
Total	**10 µL**

Table 55. Universal qPCR program – used for all types of qPCR in this thesis

Lid temperature: 105°C		
Temperature	**Time**	**No. of cycles**
95°C	15 minutes	1
95°C	15 seconds	39
60°C	1 minute	
Plate read		
65 - 95°C	5 seconds (0.5°C/s)	N/A
Plate read		
4°C	∞	1

4.15.2. qRT-PCR to detect mitochondrial unprocessed transcripts

To detect mt-tRNA + other RNA chimeric transcripts, cDNA was synthesised from long RNA fractions of *Smed ELAC2* KD, GFP mock and WT samples (for all replicates). Two unique forward primers were designed for each unprocessed region under study: 1) forward primer complementary to a region within the tRNA sequence; 2) forward primer complementary to a region within the other RNA sequence, immediately downstream to the tRNA sequence. A universal reverse primer, complementary to a region within the downstream other RNA, was used. The amplification reactions were performed in 3 technical replicates for each cDNA sample (section **4.7.1**) using 5x HOT FIREPol® EvaGreen® qPCR Supermix. The final volume of each sample was adjusted to 10 µl. Analysis was done using 2^-ΔΔCt method and normalised with respect to expression of reference gene *Smed Ef2*. Reaction mix and qPCR program were set up according to **Table 54** and **Table 55**.

4.15.3. qRT-PCR to detect sncRNA molecules

To detect such small RNA molecules using qRT-PCR, a manoeuvre was devised where small RNA samples underwent adapter ligation at the 5' and 3' ends using the TruSeq Small RNA Library Prep Kit (section **4.7.2**). qRT-PCR primers were specifically designed in the following way: the reverse primer targeted the junction between the 3' adapter and the small RNA transcript, while the forward primer targeted the junction between the 5' adapter and the small RNA transcript. The amplification reactions were performed in 3 technical replicates for each cDNA sample using 5x HOT FIREPol® EvaGreen® qPCR Supermix. The final volume of each sample was adjusted to 10 µl. Analysis was done using

2^-ΔΔCt method and normalised with respect to the expression of a suitable reference miRNA molecule, taken from our own small RNA sequencing datasets - microRNA_ROS_GGA. Reaction mix and qPCR program were set up according to **Table 54** and **Table 55**.

4.15.4. qRT-PCR for obtaining individual marker gene expression proportions within each sorted sample

qRT-PCR primers were designed for Smed1, Agat-1 and GST genes. The amplification reactions were performed in 3 technical replicates for each cDNA sample (section **4.7.3**) using 5x HOT FIREPol® EvaGreen® qPCR Supermix. The final volume of each sample was adjusted to 10 µl. Analysis was done using 2^-ΔCt method. ΔCt values were normalised with respect to expression of reference gene *Smed H.55.12e*. The final 2^-ΔCt values were converted into percentage expression of each of the three selected markers in each sorted sample. Reaction mix and qPCR program were set up according to **Table 54** and **Table 55**.

4.16. Cell dissociation for flow cytometry

A total of 20–30 whole worms were suspended in ice-cold CMFB (Calcium Magnesium-Free Buffer with 1% BSA) and dissociated into single cells using the gentleMACS™ Octo Dissociator (Miltenyi Biotec). The spleen-1 dissociation program (55-second pulse) was run three times to achieve a homogeneous single-cell suspension with minimal debris. The resulting cells were filtered through 50 µm CellTrics™ filters and centrifuged at 4°C to collect the cell pellet, leaving 50 µL of supernatant after discarding the excess. For live-cell staining, cytoplasms were labeled with 0.4 µg/mL Calcein AM dye (Ex/Em 495/515 nm) in 500 µL CMFB solution. This was incubated for 10 minutes in the dark at room temperature, followed by a PBS wash. Nuclear staining was then performed using 10 µM DRAQ5™ (Ex/Em 646/697 nm) in 100 µL PBS solution, incubated for at least 30 minutes in the dark at room temperature. These cells were not washed post-staining and were directly processed for flow cytometry analysis. Alternatively, if nuclei were stained with Hoechst 33342 dye, the cell pellets were first incubated with 40 µL of 1 µg/mL Hoechst 33342, Trihydrochloride (Ex/Em: 350/461) in 460 µL PBSB (total volume 500 µL) for 10 minutes in the dark at room temperature. Following centrifugation, the dye solution was carefully discarded without disturbing the cell pellet. This was followed by Calcein AM staining and final resuspension of the pellet in ~100 µL PBS as described earlier. All

centrifugation steps for buffer or staining solution exchanges were performed at room temperature for 7 minutes at 855 RCF (radius 19.1 cm).

4.17. Flow cytometry analyses

4.17.1. Classical flow cytometry

For each dissociated cell sample, a small portion of it was kept as unstained and most of it was stained with Calcein AM and Hoechst 33342 as described before. Cell samples (stained or unstained) were diluted with PBS in a way such that the cells samples that the total volume was 200 µL for each sample. Guava easyCyte 12HT flow cytometer specific specifications were – Lasers (FSC – gain 19.9; SSC – gain 1.68; BLU-V – gain 19.9; GRN-B – gain 2.95; Threshold – FSC 1000); Flow rate – medium. Plate templates were designed on the Guava® InCyte software to indicate the order and identity of each sample in each well and accordingly cells were pipetted into wells of a 96-welled plate. Data were analysed using the FlowJo software package.

4.17.2. Imaging flow cytometry

Imaging flow cytometry was performed using the Cytek® Amnis® ImageStream®X Mk II cytometer equipped with two CCD camera detectors (Cytek Biosciences, USA). INSPIRE software (Cytek Biosciences) was used for data acquisition. Cell samples were diluted with PBS to a final volume of 200 µL. The images were captured using a 40x objective at a low fluidics speed. Brightfield images were obtained in channels 1 and 9, side scatter (SSC) images were obtained in channel 6 (745-785 nm filter), using a 785 nm laser with power of 3.75 mW, Calcein AM was detected in channel 2 (480-560 nm filter) using a 488 nm laser with power of 4 mW, Draq5 was detected in channel 11 (642-745 nm filter) using a 642 nm laser with power of 30 mW and Hoechst 33342 was detected in channel 7 (435-505 nm filter) using a 405 nm laser with power 20 mW. From each unsorted sample, at least 60,000 events were acquired. From each sorted sample, at least 2,000 events were acquired. IDEAS v6.2 software (Cytek Biosciences) was used for data analysis. For the measurement of cell and nuclear diameters, approximately 170 to 200 cells from each category, multinucleated and mononucleated cells, were analysed.

4.17.3. Fluorescence activated-cell sorting (FACS)

FACS was performed with a high-speed flow cytometer BD FACSAria™ Fusion (Becton Dickinson). Calcein AM was excited with 488 nm laser and detected in FITC channel (BP 530/30). Draq5 was illuminated using 640 nm laser and detected in APC

channel (BP 670/30). The cells were sorted using 100 µm nozzle and 4-way purity sorting mode. Approximately 50,000 cells were sorted per sample into Eppendorf® Protein LoBind 1.5 mL tubes, containing 300 µl PBS with 1% BSA for downstream imaging flow cytometry, or 350 µl TRIzol™ Reagent for total RNA extraction. The former was processed immediately, and the latter were vigorously shaken once out of the sorter and kept on ice until the next step. Data were analysed using FACSDiva 9.0.1 software (Becton Dickinson).

4.18. Next generation sequencing library preparation

As suggested from phenotypic observation and qPCR validations, 3 and 5dpa time points were selected for further sequencing analyses. Both long and small RNA libraries were prepared for 3 biological replicates of *Smed ELAC2* KD, GFP mock and WT worms, where each sample comprised of n=10 worms. Libraries from long RNA molecules >200 nt were prepared from 1 µg long RNA samples (in 10 µL), using the manufacturer's protocol of KAPA RNA HyperPrep Kit with RiboErase (HMR). Small RNA <=80 nt libraries were prepared from 50 ng small RNA samples (in 5 µL), using TruSeq Small RNA Library Prep Kit -Set A. The small RNA libraries were enriched for all molecules of length between ~140-200 bp (length with adapters) to majorly select for molecules like miRNA, piRNAs, RNA fragments or other sncRNA classes within similar size range. NGS analyses were performed at the Laboratory of Genomics IBCH PAS.

4.19. 5' tRNA half Gly-GCC mimic experiment

For each experimental condition (e.g., *Smed ELAC2* KD), three soaking treatments were applied: 5' tiRNA Gly-GCC mimic, scrambled RNA, and culture solution only (no RNA). A total of 4 worms were used per sample, with up to two worms placed in each well of a 24-well plate. Each sample was thus divided across two wells. For a single replicate of *Smed ELAC2* KD, 12 worms were required (4 worms × 3 soaking conditions). All experiments were conducted in triplicate, meaning a total of 36 worms were required for *Smed ELAC2* KD across three replicates (12 worms × 3 replicates). Including all experimental conditions (*Smed ELAC2* KD, GFP mock, and WT), the total number of worms used in the study was 108 (36 worms × 3 conditions). Solutions of both synthetic RNAs were prepared at a concentration of 5 µM by diluting the required volumes of RNA stocks in culture solution. Following the usual protocol, *Smed ELAC2* KD, GFP mock, and WT worms were cut into three fragments each, and the regenerating pieces were placed into designated wells. A maximum of six regenerating pieces (equivalent to two whole worms) were placed in each well. On the first day of soaking (0 dpa), worm fragments in each well

were first washed with 100 µL of the designated soaking solution before being soaked in 400–500 µL of the same solution. On 2 and 4 dpa, soaking solutions were discarded, wells were carefully cleaned, and fresh volumes (400–500 µL) of the corresponding solutions were added to each well. On 5 dpa, the worms were either processed for downstream qRT-PCR analysis or utilized for phenotypic documentation, as described previously.

4.20. Bioinformatics and statistical analysis

All bioinformatic and statistical analyses were conducted by Anastasiia Zaremba, M.Sc., from the same research group, within the scope of her doctoral dissertation.

5. Results

5.1. Development of a research strategy to investigate the impact of sncRNA pool alterations on the regeneration process in *S. mediterranea*

The first part of the study was focused on developing a stepwise strategy for identifying sncRNAs involved in the regeneration of *S. mediterranea*. The strategy aimed to disrupt the sncRNA pool by silencing a ribonuclease, then assess its impact on regeneration through initial phenotypic evaluation. Next, a comparative analysis of sncRNAs from both RNase-knockdown and wild-type worms was expected to allow the identification of sncRNAs implicated in regeneration. However, RNases have not been extensively studied in planarians, making the selection of a suitable candidate RNase for this purpose particularly challenging. To facilitate this choice and simultaneously place the study in a broader context, the following criteria were adopted for an RNase: (i) its human homolog should be implicated in Mendelian disease, (ii) it should be directly involved in the metabolism of sncRNAs, (iii) it should be upregulated in neoblasts.

To identify the RNases implicated in Mendelian diseases, a search of Online Mendelian Inheritance in Man catalog of human genes and genetic disorders (https://omim.org/) was performed, yielding 15 RNase genes listed in **Table 56**. These genes encoded 13 RNase enzymes that are conserved across representative organisms of various phyla, with 11 being identified also in planarians (Dutta et al., 2025). Detailed analyses revealed that most of these conserved proteins (12 out of 13) were in fact involved in processing and maturation of various classes of ncRNAs. Pathways regulated by these selected proteins have been comprehensively depicted in **Figure 6**.

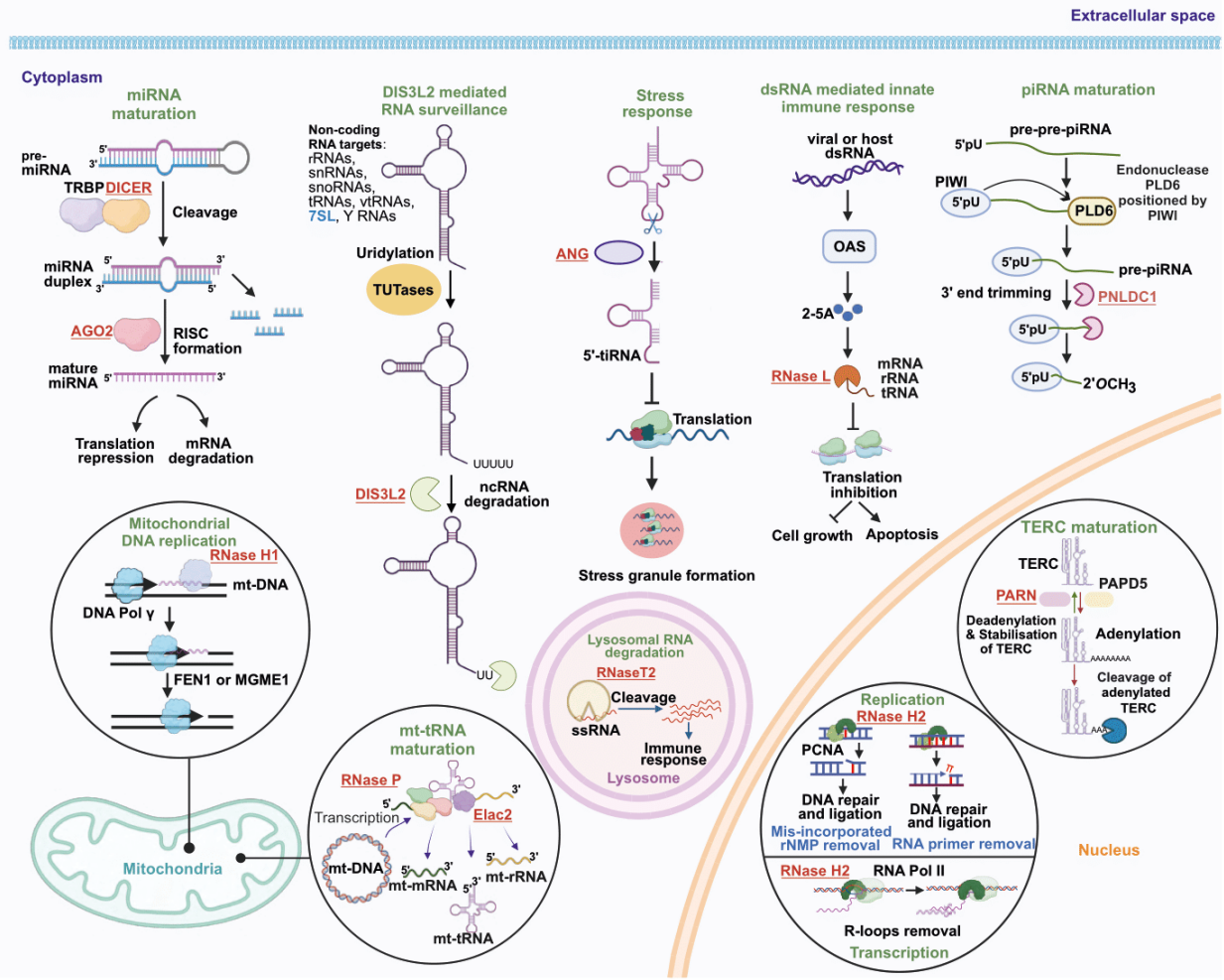

Figure 6. Non-coding RNA metabolism pathways disrupted upon mutations of the selected RNases implicated in Mendelian diseases. 12 out 13 conserved RNases depicted here are active against ncRNA classes – Elac2, PARN, Plndc1, RNase T2, RNase P, Dicer, Ago2 and Angiogenin or, against a small stretch of mis-incorporated ribonucleotides into DNA – like RNase H1 and H2.

Table 56. Conserved human ribonuclease genes associated with Mendelian disorders

Gene name	Protein name	RNase family	Substrate	Cellular localization	OMIM ID	Disease name	Disease type	Disease onset	Disease mechanism - current view
RNASEH 2A	Ribonuclease H2 subunit A (RNase H2A)	RNase H family/ Retrovirus Integrase Superfamily (RISF)	RNA:DNA hybrids	Nucleus	610333	Aicardi-Goutières syndrome 4	neurological	early	Mutations causing loss of its function lead to chronic DNA damage and replication stress. This triggers severe immunogenic response in the neuronal tissue causing Aicardi-Goutières syndrome (AGS). Chronic DNA damage affects the CNS so adversely because the bulk of the tissue is comprised of long-living neurons formed for which genome maintenance is of utmost importance.
RNASEH 2B	Ribonuclease H2 subunit B (RNase H2B)			Nucleus	610181	Aicardi-Goutières syndrome 2	neurological	early	
RNASEH 2C	Ribonuclease H2 subunit C (RNase H2C)			Nucleus	610329	Aicardi-Goutières syndrome 3	neurological	early	
RNASE5	Angiogenin	RNase A family	mature tRNA; snRNAs at specific sites; miRNA	Nucleus; Cytoplasm	611895	Amyotrophic lateral sclerosis 9	neurological	adulthood	Angiogenin curbs stress by generating stress induced tRNA fragments called 5'- tiRNA that reprogram global protein translation thereby promoting cell survival. In this disease, mutation of the gene causes progressive motor neuron death, where it is also highly expressed. The effect is specific to motor neurons as they are very long and highly active cells, for which localised stress protection by angiogenin via decentralised translation control is crucial.
AGO2	Protein argonaute-2 (Ago-2)	RNase H family/ Retrovirus Integrase Superfamily (RISF)	miRNA/siRNA: target RNA hybrids	Nucleus; Cytoplasm	619149	Lessel-Kreienkamp syndrome	neurological	early	Disease causing AGO2 mutations result from the prolonged binding of the protein onto target mRNAs in the course of the RNA silencing pathway. This leads to sequestration of Argonaute-2 protein in dendritic P-bodies and hampered RNA-silencing mediated translational regulation in neurons. Its function is especially important in neurons as much of their dynamic functions rely on compartmentalized translation.

RNASET2	Ribonuclease T2 (RNase T2)	RNase T2 family	rRNA, mRNA	Lysosomes; Mitochondria; Vacuoles; P-bodies	612951	Leukoencephalopathy, cystic, without megalencephaly	neurological	early	The lysosomal enzyme is active against single stranded RNA (ssRNA), especially rRNA. As the gene is highly expressed in the brain, deficiency of the enzyme causes an overt immune response in the brain similar to that of congenital cytomegalovirus infection or AGS in the CNS. This immune reaction is due to the accumulation of undigested ssRNAs in the lysosome and their transport to cytosol where they bind to RNA-recognising immune receptors.
DICER1	Endoribonuclease Dicer (Dicer)	RNase III family	premature miRNAs (pri-miRNA)	Nucleus; Cytoplasm	618272; 138800; 601200; 180295	GLOW syndrome, somatic mosaic; Goiter, multinodular 1, with or without Sertoli-Leydig cell tumors; Pleuropulmonary blastoma; Rhabdomyosarcoma, embryonal, 2	growth-related	early	The enzyme is involved in the generation of 3p and 5p-miRNAs. Molecularly, DICER1 mutations in a specific region result in the diminishing of 5p-miRNAs and accumulation of 3p-miRNAs. Most of the aberrantly accumulated 3p-miRNA molecules negatively regulate inhibitors and positively regulate activators of the central PI3K-AKT-mTOR growth signalling pathway. This results in the manifestation overgrowth or abnormal growth of multiple organs.
DIS3L2	DIS3-like exonuclease 2 (Dis3l2)	RNase II family (Component of RNA exosome complex)	rRNAs, snRNAs, snoRNAs, tRNAs, vault, 7SL, Y RNAs, mRNAs, lncRNAs, and transcripts from pseudogenes	Cytoplasm	267000	Perlman syndrome	growth-related	early	Dis3l2-mediated decay is a surveillance pathway for a number of coding and non-coding RNAs. Disease-causing mutations in *DIS3L2* causes the accumulation of aberrant 3' uridylated 7SL ncRNA component of signal recognition particle (SRP). Disturbed quality control of 7SL ncRNA harms ER-associated translation and disturbs cellular calcium homeostasis by ER calcium leakage.

ELAC2	Zinc phosphodiesterase ELAC protein 2 (Elac2)	RNase Z family/ MBL superfamily	tRNA precursors (pre-tRNA); miRNA; piRNA; snRNA; snoRNA	Nucleus; Mitochondria	615440 ; 614731	Combined oxidative phosphorylation deficiency 17; Susceptibility to Prostate cancer, hereditary, 2,	growth-related; prostate cancer	early	Elac2 is involved in the 3' end processing of mt-pre-tRNAs. Deficiency of the functional enzyme leads to the accumulation of unprocessed mt-tRNA transcripts and disruption of mitochondrial protein translation, especially of the mitochondrially encoded OXPHOS proteins. This leads to a mitochondrial disorder with deficiency in ATP production, affecting multiple organs.
PRORP	Mitochondrial ribonuclease P catalytic subunit (MRPP3)	Components of RNase P riboprotein complex	tRNA precursors (pre-tRNA); mRNA with modified 3' external guide sequence	Nucleus; Mitochondria	619737	Combined oxidative phosphorylation deficiency 54	growth-related	early	This protein is the catalytic subunit of mitochondrial RNase P which processes 5' ends of pre-tRNA molecules in the maturation pathway of functional tRNA. Loss of function of this subunit leads to the deficit of mature mt-tRNAs inhibiting translation of mitochondrial proteins, like several OXPHOS pathway components. This finally causes mitochondrial dysfunction affecting multiple organs.
PARN	Poly(A)-specific ribonuclease PARN (PARN)	CAF family	rRNA; snoRNA; scaRNA; mRNA; TERC	Shuffles between nucleus and cytoplasm	616353 ; 616371	Dyskeratosis congenita, autosomal recessive 6; Pulmonary fibrosis and/or bone marrow failure, telomere-related, 4	blood-related	early	The enzyme is involved in the biogenesis of TERC (telomerase RNA component). It stabilises TERC by removing 3' poly-A tails that serve as RNA degradation signals and mutation of the gene destabilises this process. Maintenance of telomere lengths by telomerase is crucial for the survival of various stem and progenitor cell populations like haematopoietic stem cells. Hence, the bone marrow is susceptible to telomeropathies.
SLFN14	Protein SLFN14 (SLFN14)	Schlafen family	rRNA	Nucleus	616913	Bleeding disorder, platelet-type, 20	blood-related	early	Platelets and erythrocytes have minimal RNA load. The protein is highly expressed in immature platelets and erythrocytes called megakaryocytes and reticulocytes, respectively. It associates with ribosomes and degrades rRNA to clear RNA during blood cell maturation process. Therefore, loss of SLFN14 function could hamper the blood cell maturation process causing bleeding disorder.

RNASEH1	Ribonuclease H1 (RNase H1)	RNase H family/ Retrovirus Integrase Superfamily (RISF)	RNA:DNA hybrids	Nucleus; Mitochondria	616479	Progressive external ophthalmoplegia with mitochondrial DNA deletions, autosomal recessive 2	muscular	adulthood	The enzyme removes RNA primers forming RNA:DNA hybrids in mtDNA replication. Loss of RNase H1 function stalls mtDNA replication fork causing mtDNA depletions and deletions and resultant mitochondrial dysfunction. The major tissue system affected are muscles as they are known to have high energy requirements.
RNASEL	2-5A-dependent ribonuclease (RNase L)	Ribonuclease 2-5 A or RNase L family	microbial rRNA, mRNA	Nucleus; Cytoplasm; Mitochondria	601518	Prostate cancer 1	prostate cancer	adulthood	RNase L is activated by cleavage product of an IFN-induced enzyme called 2′-5′ oligoadenylate synthetase (OAS). Activated RNase L cleaves 28S and 18S rRNA causing cellular apoptosis. This pro-apoptotic activity is both anti-viral and anti-tumorigenic (apoptosis of prostate cancer cells). Prostate cancer is especially implicated in RNase L mutations because the gene maps to hereditary-prostate-cancer (HPC)–predisposition locus (*HPC1*).
PNLDC1	Poly(A)-specific ribonuclease (Pnldc1)	CAF family	mRNA; pre-piRNA	Cytoplasm	619528	Spermatogenic failure 57	reproductive failure	adulthood	The protein trims 3' ends of pre-piRNAs required as a step for piRNA biogenesis. Mature piRNAs are essential in the context of transposon silencing and regulation of spermatogenesis. Therefore, dysfunction of the enzyme leads to accumulation of 3' -untrimmed piRNAs and de-repression of transposons in the testes causing failure of sperm production.

In the next step, all the 11 identified planarian homologs of RNases implicated in Mendelian diseases and involved in sncRNA metabolism were examined for their presence in neoblasts. To this end, RNase gene expression enrichment data were retrieved from PlanMine database (https://planmine.mpibpc.mpg.de/). It revealed that homologs of *RNASEH1*, *RNASEH2A*, *RNASEH2B*, *PARN* and *ELAC2* were upregulated in neoblasts. Based on the established criteria, these 5 RNase genes were eventually selected for initial experimental analyses with the aim of silencing them individually and assessing the impact of this silencing on regeneration. Additionally, a particular RNase predominantly expressed in differentiated cells - homolog of *RNASET2* - was also examined, which served as a control in the phenotypic profiling. Of these six genes, target amplicons of Smed *RNASEH2A* and *RNASEH2B* could not be amplified and hence were not studied further. Three RNase genes enriched in neoblasts (encoded by *Smed RNASEH1*, *Smed PARN* and *Smed ELAC2*) and one enriched in differentiated cells (encoded by *Smed RNASET2*) were finally chosen for gene silencing studies.

Gene silencing was carried out via RNAi by injecting planarians with dsRNA specific to the target gene. To generate the required dsRNA, *in vitro* transcription was performed as described in (section **4.11**). To that end, primers specific to the selected RNase genes were designed, incorporating T7 promoter sequences at both ends. Total RNA was isolated from the planarians, followed by cDNA synthesis and DNA amplification using these primers (section **4.7.1**). The reaction products were analysed by agarose gel electrophoresis (section **4.9**, **Figure 7**). The resulting templates were used for *in vitro* transcription to produce dsRNA (section **4.11**).

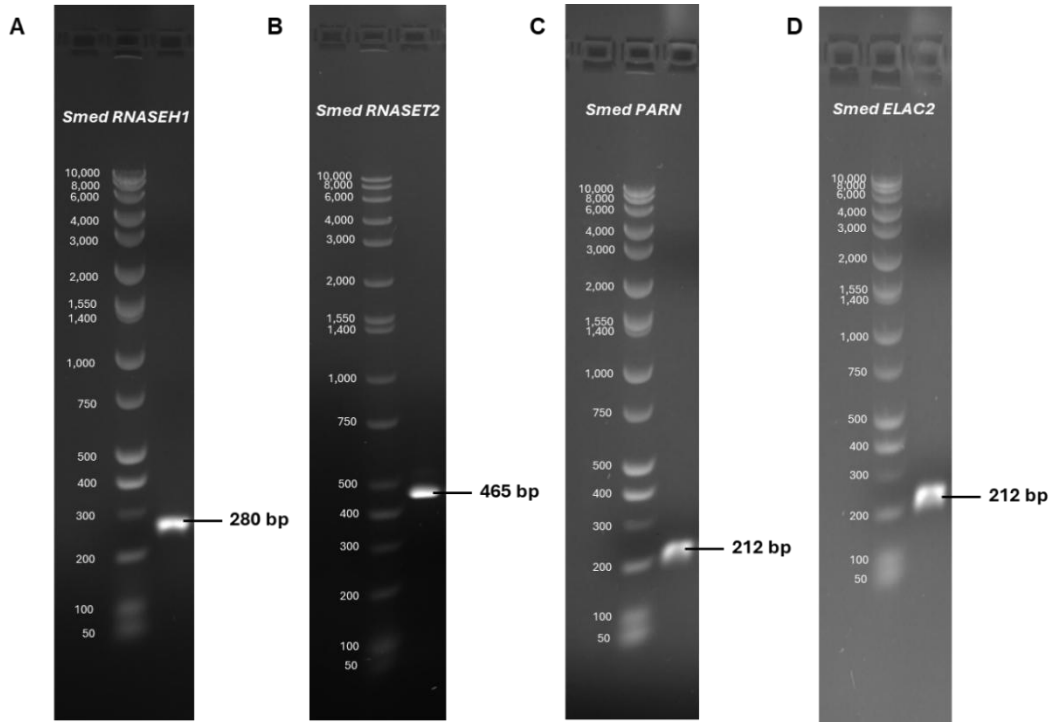

Figure 7. Gel images showing target amplicons derived from S. mediterranea homologs of the selected RNase genes. A) *Smed RNASEH1*, B) *Smed RNASET2*, C) *Smed PARN*, D) *Smed ELAC2*. All sizes mentioned are in base pairs (bp) units.

Targeted dsRNA microinjections were performed to induce RNAi-mediated knockdown according to the regime explained in Methods in section **4.11**. This was followed by amputation into head, trunk, and tail fragments to assess the effects on regeneration. The worms were examined over a period of 10 days, with phenotypic evaluation conducted visually based on general morphological characteristics, including body shape changes, photoreceptor malformations, and movement impairments. A relative scoring scale was arbitrarily adopted to evaluate the severity and overall consistency of these changes, categorized as follows: lethal (+++), strong (++), mild (+), or absent (-). The results of the phenotypic evaluation are presented in **Table 57**.

Table 57. Screening of candidate RNases based on knockdown-associated impacts on regeneration

Gene name	Phenotypic impact
Smed ELAC2	++
Smed PARN	+
Smed RNASEH1	--
Smed RNASET2	--

Based on these initial observations, *Smed ELAC2* and *Smed PARN* knockdowns were externally manifested as observable phenotypic traits. Both enzymes encoded by these genes have homologs in other organisms and are known to target a wide range of ncRNA molecules. Exoribonuclease PARN, a 3′-poly(A) tail deadenylase, acts on both coding mRNAs and non-coding RNAs, including hTR, rRNA, Y RNAs, H/ACA box snoRNAs, and scaRNAs. Endoribonuclease Elac2 is a Zn-dependent metallo-β-lactamase that predominantly processes pre-tRNAs, miRNAs, snoRNAs, and long non-coding RNAs (lncRNAs), is a dually targeted enzyme either to the nucleus or mitochondria (Siira et al., 2018). The changes observed in the case of *Smed ELAC2* silencing were more consistent and robust with respect to those observed for *Smed PARN* knockdown conditions. Also, *Smed RNASEH1* and *Smed RNASET2* knockdown apparently did not seem to affect the normal course of regeneration. Therefore, based on these observations showing that *Smed ELAC2* knockdown had the most pronounced effect on regeneration, and previously described targets of Elac2 homologs in other organisms, Smed Elac2 was selected as the final target ribonuclease used in this study. Next, the efficiency of *Smed ELAC2* knockdown was examined by qPCR at several time points post-amputation—0, 3, 5, 7, 14 dpa. It was observed that the *Smed ELAC2* transcript was stably downregulated until two weeks post amputation (**Figure 8**). Overall, the current knockdown regime could successfully downregulate the expression of the *Smed ELAC2* for an extended period.

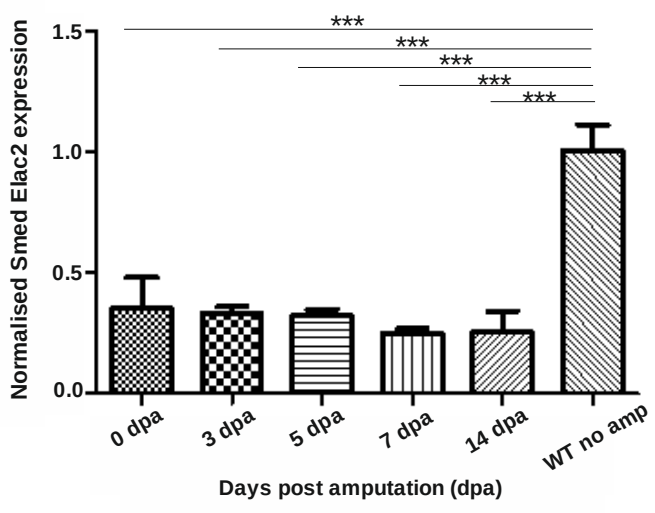

Figure 8. dsRNA mediated knockdown of Smed ELAC2. qPCR plot showing stable downregulation of *Smed ELAC2* transcript between 0 and 14 dpa. Statistical analyses were performed using one-way ANOVA followed by Tukey post-hoc method (*p-value: 0.05*). Median values from 3 replicates are presented.

In summary, to enable the identification of the sncRNAs involved in regeneration, a strategy was adopted that entailed disrupting the sncRNA pool by silencing the expression of *Smed ELAC2* that in turn enabled the comparative profiling of this pool in knockdown worms relative to the control group. Additionally, the strategy also enabled the identification and characterization of a so-far unstudied planarian homolog of a crucial sncRNA processing RNase, Elac2.

5.2. Impact of sncRNA pool disruption on the regeneration process in *S. mediterranea*

5.2.1. Phenotypical impact of *Smed ELAC2* silencing

The strategy developed as described above was subsequently employed to identify the sncRNAs involved in the regeneration process. The first phase of the process involved a comprehensive analysis of the phenotypic changes triggered by the silencing of *Smed ELAC2*. To this end, the regeneration of *Smed ELAC2* KD worms was monitored for up to two weeks following amputation, with phenotypes documented at specific regeneration time points: 0, 3, 5, 7, 10, and 14 days post-amputation (dpa). Two controls were evaluated in parallel: GFP mock (injected with dsRNA specific to green fluorescent protein gene) and wild-type (WT) untreated worms. These controls were used throughout the rest of the study. Notably, around 5 dpa, a significant eye regeneration abnormality was observed in *Smed ELAC2* KD worms, with approximately 70% of the regenerating tail fragments displaying either an eyeless or cyclopean (one-eyed) phenotype (**Figure 9C**). Eye abnormalities in trunk fragments were inconsistent and not statistically significant. In contrast, regeneration proceeded normally in both WT and GFP mock controls, with bilateral eyespot development occurring as expected at 5 dpa in all regenerating fragments devoid of the anterior half. Head fragments, on the other hand, regenerated normally for all experimental groups. Coherent with previous observations, *Smed ELAC2* gene expression was consistently downregulated at both 3 dpa (a time point representing a stage with no visible morphological differences between groups) and 5 dpa (a time point representing a stage where clear phenotypic differences start to appear) in these samples as well (**Figure 9A**). Interestingly, eye regeneration in *Smed ELAC2* KD worms eventually normalized by 8–10 dpa, leading to the characterization of the observed effect as a regeneration delay rather than a defect (**Figure 9B**). Based on the observed trend of

delayed regeneration in *Smed ELAC2* KD worms, two time points—3 dpa and 5 dpa—were selected for all molecular analyses performed later in the research. These time points were chosen so as to molecularly distinguish the changes occurring during and/or prior to the onset of visible morphological differences.

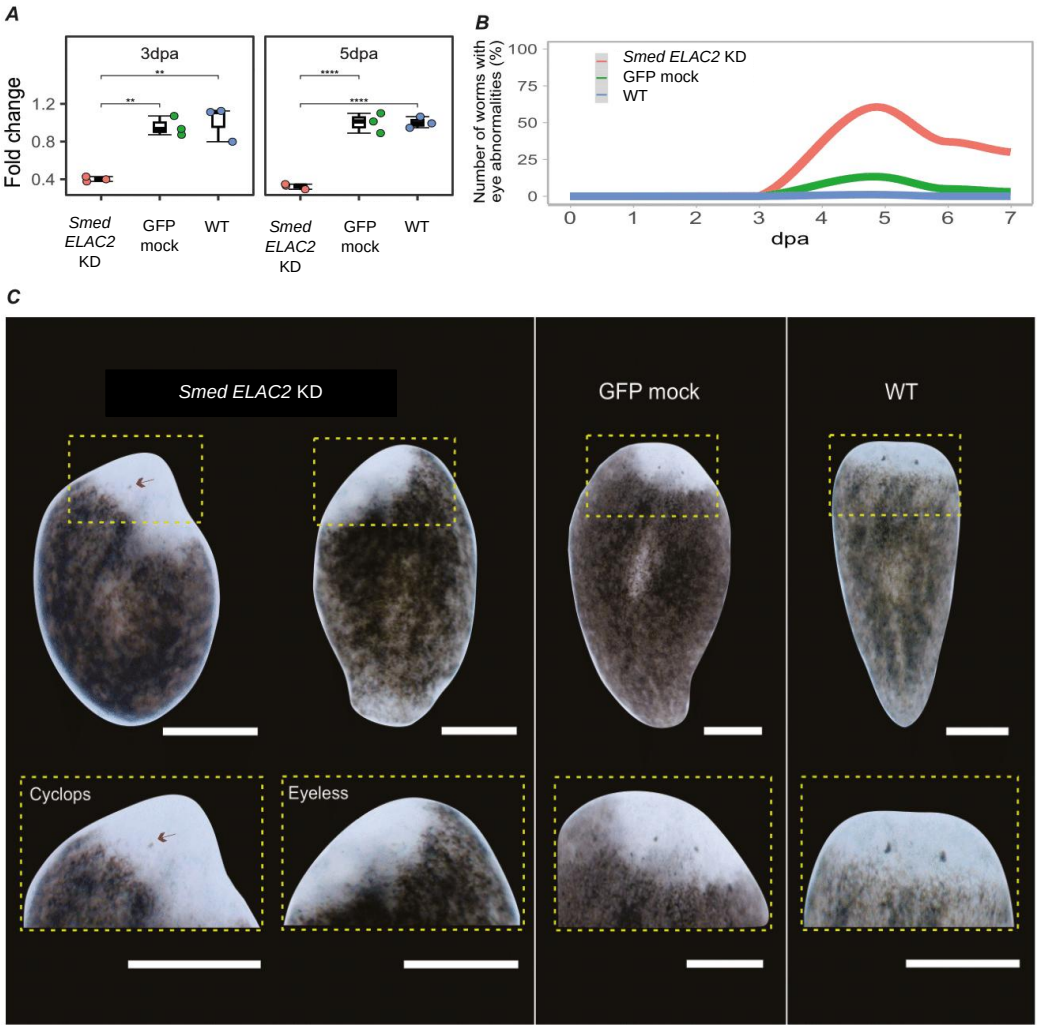

Figure 9. Phenotypic analysis of Smed ELAC2* KD *regenerating fragments. A) Validation of *Smed ELAC2* knockdown at 3 and 5 dpa. Statistical analyses were performed using one-way Anova followed by Tukey post hoc method (*p-value <0.05*). B) Almost 70% of worms regenerating from *Smed ELAC2* KD tail fragments were either eyeless or cyclops until ~7dpa. (C) Pictorial representation of eyeless and cyclops phenotype in *Smed ELAC2* KD tail regenerating worms with respect to control conditions - GFP mock and WT amputated. Scale: 300 µm.

5.2.2. Anatomical impact of *Smed ELAC2* silencing

The observed phenotypic changes pointed to the occurrence of an underlying phenomenon. Nevertheless, these alterations were limited solely to the eyes, with no other apparent effects. To gain a more comprehensive understanding of the *Smed ELAC2*

silencing impact, the focus was shifted to investigating its influence on the regeneration of specific tissue systems. Consequently, FISH was used to observe the tissue-wide expression patterns of three marker genes across all experimental groups: the nervous system marked by proprotein convertase-2 (*PC2*), the gut branches by porcupine (*PORCN*), and the muscles by collagen (*COLL*) (**Figure 10B**). While the expression patterns of *PORCN* and *COLL* appeared indistinguishable across regenerating fragments in all groups, the expression of the nervous system marker *PC2* showed clear differences between *Smed ELAC2* KD and control samples. Specifically, fluorescence intensity for *PC2* was lower in all regenerating fragments of *Smed ELAC2* KD worms compared to controls (**Figure 10C**), as measured using FIJI software (**Figure 10A**). Notably, also in head fragments that regenerated posterior parts, *PC2* intensity was lower upon *Smed ELAC*2 knockdown, suggesting that even the previously developed structures can be affected. The most prominent changes occurred in the tail-derived regenerating worms in the knockdown group, which exhibited severe underdevelopment of nerve cords. This coincided with the observed delay in eye development around the same time, suggesting a possible link between the two phenomena. Taken together, these results showed that the knockdown of *Smed ELAC2* induced a regeneration delay observable around 5 dpa localized in the newly regenerating anterior regions. This further suggested that there might be some specific cellular and molecular changes taking place around this time.

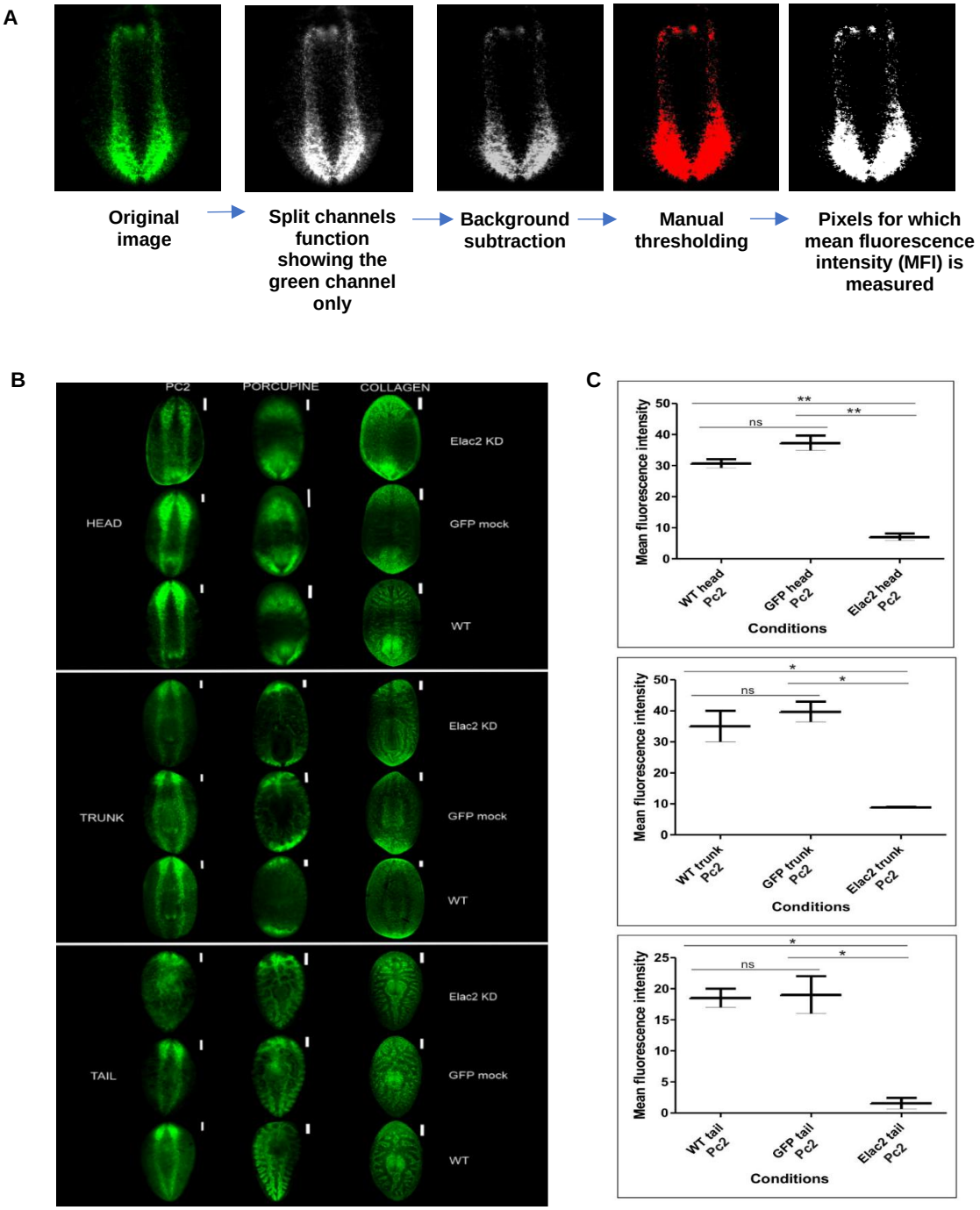

Figure 10. FISH for various tissue markers in Smed ELAC2* KD *and control regenerating worms. A) Stepwise scheme representing the method adopted for mean fluorescence intensity (MFI) measurements using FIJI software with a regenerating head fragment as an example. B) Representative FISH images of head, trunk and tail regenerating worms in *Smed ELAC2* KD, GFP mock and WT conditions at 5 dpa for nervous system marker proprotein convertase-2 (*PC2*); gut marker porcupine (*PORCN*) and muscle marker collagen (*COLL*), Scale: 200 µm. C) MFI values for *Smed ELAC2* KD head, trunk and tail fragments with respective GFP mock and WT controls. Statistical analyses were performed using one-way ANOVA followed by Tukey's post hoc method (*p-value: 0.05*). Median values of 2 technical replicates are presented.

5.2.3. Impact of *Smed ELAC2* silencing at the cellular level

The morphological and anatomical changes outlined above were prominent and were linked to a delay in the regenerative process; however, proper regeneration of the *Smed ELAC2* KD worms ultimately occurred. Previously, it was demonstrated that the regeneration delay seen in *Smed-mex3-1* knockdown worms was linked to fewer X2 (progenitor) cells accompanied by a corresponding increase in X1 (neoblast) cells (Zhu et al., 2015), which reflected disruption of cell differentiation pathways. Therefore, it was hypothesized that the regeneration delay observed in the case of *Smed ELAC2* KD could also be attributed to the same mechanism, manifested as the perturbation of one of these established cell populations. Accordingly, classical flow cytometry was used to determine whether the distribution of X1, X2 and Xins (differentiated cells) differed between knockdown and control samples. To this end, *Smed ELAC2 KD*, GFP mock and WT worms were dissociated to yield single-cell suspensions, stained with Hoechst 33342 (nuclear stain) and Calcein AM (live cell cytoplasm stain), and subsequently analysed using Guava easyCyte 12HT flow cytometer (**Figure 12A**). Cells were first gated to exclude debris, followed by doublet discrimination. Next, Calcein AM- and Hoechst 33342-positive cells were identified, and the double-positive cells were subsequently plotted on a Calcein AM versus Hoechst 33342 fluorescence area plot (**Figure 11**).

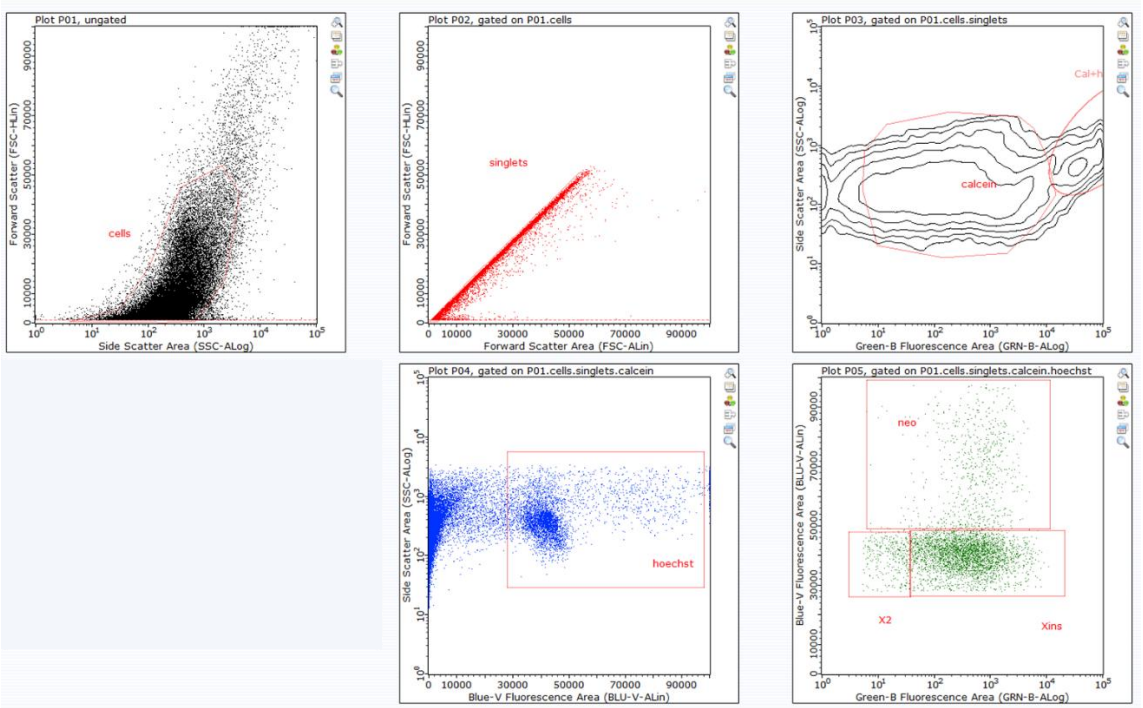

Figure 11. Identification of X1 neoblast, X2 and Xins cell populations using Guava easyCyte 12HT classical flow cytometer. Stepwise strategy adopted in the InCyte software to gate all three planarian cell populations.

The analysis revealed no significant differences in the percentage distribution of these three populations across all samples, suggesting that the overall ratio of neoblasts, progenitors, and differentiated cells remained unchanged (**Figure 12B**). This indicated that the abnormalities observed may be due to disruptions in one or more specific cell lineages, rather than a broad alteration in cell population balance.

Taking advantage of the access to the imaging flow cytometry platform, Cytek® Amnis® ImageStream®X Mk II (IS), an effort was made to analyse the morphological characteristics of individual cells within the previously described cell populations in *Smed ELAC2* KD regenerating worms compared to GFP mock and WT controls. While the preliminary screening did not reveal any significant morphological differences in cells representing X1, X2 and Xins populations between *Smed ELAC2* KD, GFP mock, and WT controls, the analysis revealed, for the first time, the presence of multinucleated planarian cells. Intriguingly, these cells were present in all kinds of samples, treated or not. Based on this finding, the distribution and fate of multinucleated cells were explored in further detail in *Smed ELAC2* KD versus control samples. These cells were analysed at 0, 1, 3, and 5 dpa. The nuclearity of planarian multinucleated cells (no. of nuclei) ranged from 2 to 8 nuclei per cell (**Figure 12C**). Accordingly, these cells were broadly grouped into two

categories: 2-nucleated (2nuc) and >2-nucleated (>2nuc). Although the total number of multinucleated cells did not significantly differ between conditions, a shift was noted in the ratio of 2-nucleated versus >2-nucleated cells. Over time, within the multinucleated cell population, a trend of increased percentage of >2-nucleated cells accompanied by a decrease in the percentage of 2-nucleated cells was observed. This shift became statistically significant at 5 dpa, the same time point at which regeneration abnormality was first observed (**Figure 12D**). Overall, the distribution of the commonly studied cell populations, X1, X2 and Xins remained largely unaffected by *Smed ELAC2* KD. However, the observed increase in the percentage of multinucleated cells with more than 2 nuclei suggests that their multinuclear state may be sensitive to the knockdown-induced molecular changes.

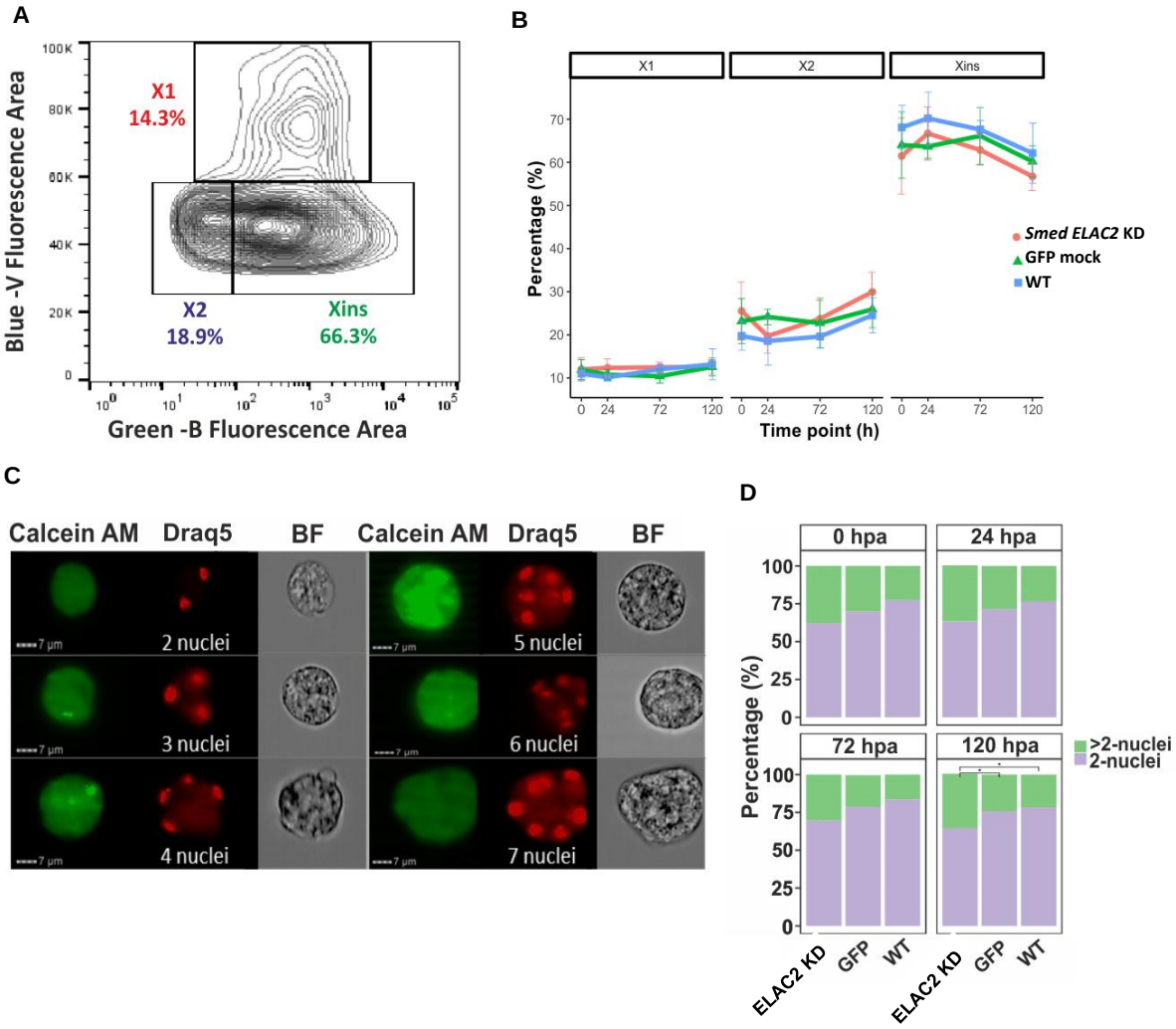

Figure 12. Distribution of various cell populations in Smed ELAC2* KD *conditions. A) X1, X2 and Xins cells identified in Calcein AM (Green-B) vs Hoechst 33342 (Blue-V) classical flow cytometry plot. (B) Distribution of the three cell populations over 4 time points during regeneration - 0-, 1, 3- and 5-days post-amputation (hpa) in *Smed ELAC2* KD and controls. (C) Imaging flow cytometry gallery representing varied nuclearities of multinucleated cells. (D) The percentage of >2-nucleated and 2-nucleated cells in the total pool of multinucleated cells, in *Smed ELAC2* KD and controls, across regeneration time points. Median values from 3 replicates are presented.

The use of imaging flow cytometry to analyse planarian cells (WT and *Smed ELAC2* KD) led to the discovery of multinucleated cells and revealed that they are affected upon regeneration impairment, caused by *Smed ELAC2* knockdown. Driven by scientific curiosity and considering the current understanding of polyploid cells and their significance in regenerative processes, investigations were initiated to provide a preliminary characterization of these cells, which is presented in the following sections.

The observations about MuNs that are presented below have been submitted as a separate research article: Dutta et al. – under revision.

5.2.3.1. Systematic identification of true planarian multinucleated cells using flow cytometry

The first step was to develop a systematic stepwise gating strategy identify true multinucleated planarian cells (called MuNs) using the IS system. To achieve this, a more robust nuclear staining method in comparison to the originally used Hoechst 33342 staining, needed to be implemented. This is because the resolution of several cell populations—including the one containing MuNs — was insufficient when analysing the Calcein AM versus Hoechst 33342 intensity plot.

Hence, in the new approach, while the cell cytoplasm continued to be stained with Calcein AM, the nuclear stain Hoechst 33342 was replaced with Draq5. The following section provides the detailed description of the process for identification of MuNs using Calcein AM and Draq5 staining.

Nuclei-containing viable Calcein AM and Draq5 double positive cells were sequentially gated using an unstained sample as control (**Figure 13A**, Steps 1-3). Next, these double positive cells were visualized on Calcein AM vs Draq5 intensity plot, which allowed to identify six distinct populations, denoted A'-F', hereafter referred to as IS populations (**Figure 13A**, Step 4). A preliminary visual assessment of cell images on the Draq5 channel revealed the existence of MuNs. Most of them were found in population E′, with only a few (~3–4) present in the adjacent population D′. Characterized by large cells with high intensities of both Calcein AM and Draq5 (**Figure 13A**, pink dots on the dot plot from Step 4), population E′ primarily consisted of large mononucleated cells (MoNs) and a small fraction of MoN clumps. To accurately distinguish true multinucleated cells (MuNs) from these other objects, a detailed visual inspection of all objects within gates D′ and E′ was performed, identifying the rare true MuNs, at a frequency of ~2% in E′ population. This analysis compared images from two channels, Calcein AM and Draq5. While both MuNs and MoN clumps in the Draq5 channel displayed multiple nuclear spots, images from the Calcein AM channel distinguished true MuNs from MoNs clustered together (**Figure 13B**).

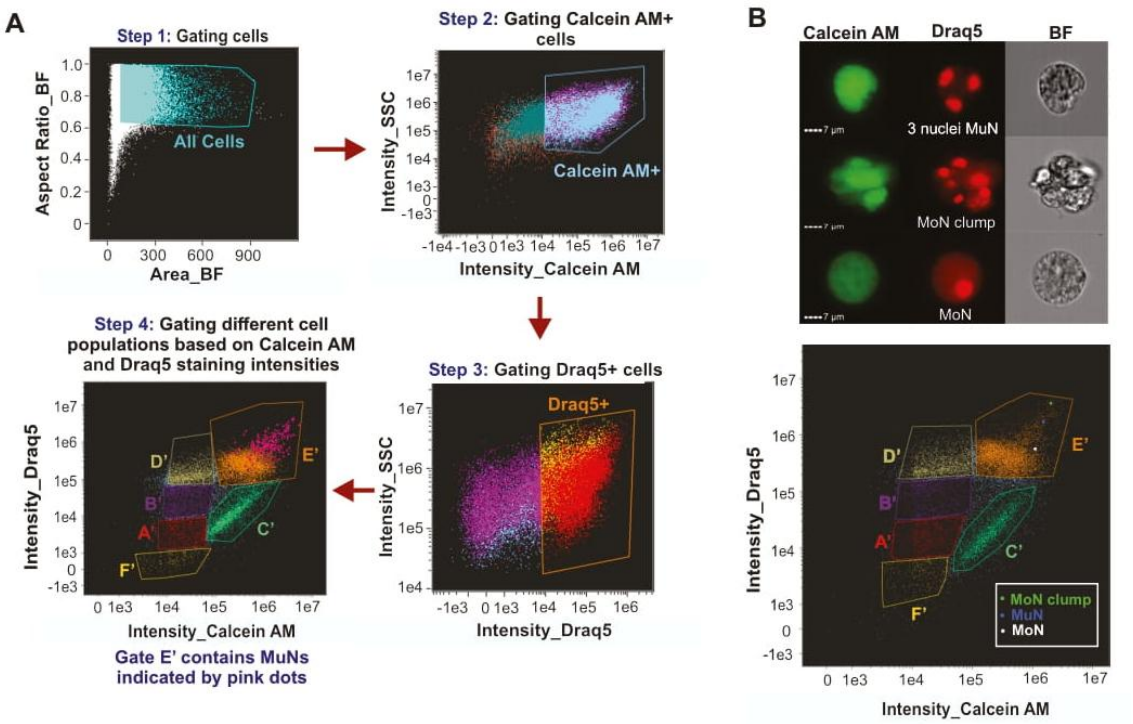

Figure 13. Identification of multinucleated cells using Calcein AM versus Draq5 staining method on IS. A) Detailed scheme for identifying true multinucleated cells on the IS system using IDEAS® data analysis software. B) Images depicting selected MuN, MoN and MoN clumps followed by a plot showing the localization of these specific cells within MuNs containing population E'.

Overall, the new staining method gave better output in terms of resolution of cell population on the cytoplasmic stain versus nuclear stain intensity plot. Consequently, all subsequent studies were conducted using Calcein AM and Draq5 staining for greater clarity and accuracy.

5.2.3.2. Morphological characterization of the MuNs using imaging flow cytometry

According to the literature data, the sizes of multinucleated cells vary widely amongst organisms and formation scenarios (Brodbeck and Anderson, 2009; Vorobjev et al., 2023). Therefore, morphological characterization of MuNs was a necessary step to start understanding their physiological functions. To that end, the cell images of planarian MuNs were analysed based on criteria such as cell and nuclear diameters, in addition to nuclearity. Accordingly, while most MuNs had 2 nuclei (~67%), a stable percentage was >2 nucleated (~33%), ranging from 3 to 8 nuclei per cell (**Figure 14A**).

Further, to measure the cellular and nuclear diameters of MoNs and MuNs, custom brightfield (BF) and Draq5 image masks were created to optimally cover the cell and nuclear surface areas, respectively. To obtain cell diameter values, the BF mask was

adjusted using the erode function, in a way so that it correctly fits the BF channel cell images. The nuclear diameters of individual nuclei of each multinucleated cell were measured using the combination of three masks available in IDEAS software: LevelSet, Watershed and Component on Draq5 channel nuclear image. For setting the optimal nuclear mask, three main aspects were considered: (i) to cover a particular nuclear spot area adequately, (ii) to ignore stain halos extending beyond the actual spot area and (iii) to differentiate between two closely placed spots as two different nuclei. Component masks are capable of identifying user-defined objects (in this case, individual nuclei stained with Draq5) one at a time. When combined, the three masks (Component, LevelSet and Watershed) enable the accurate and separate analysis of one or more nuclei within a cell, distinguishing both diffusely stained and distinctly stained nuclei as separate nuclear entities within MuNs. To achieve optimal nuclear identification, individual Component masks (defining nuclear identity) were paired with user-defined constant values for LevelSet and Watershed masks (ensuring accurate nuclear coverage). This approach was designed to accommodate the maximum number of nuclei observed in a planarian MuN, which in this case was 8. Images depicting example masks correctly covering cell and nuclear areas are shown in **Figure 14B**. The images displaying nuclear masks include 5 Component masks (combined with LevelSet and Watershed masks), each corresponding to individual nuclei within MuNs containing 2–5 nuclei. In cells with more than 5 nuclei, such as a 2-nucleated MuN – specific nuclear diameter values were recorded for nuclei 1 and 2, while the values from component masks 3, 4, and 5 were zero. This demonstrated the accuracy of the mask development approach. Next, this approach was applied to determine the cellular and nuclear diameters of the studied cells. Accordingly, it was found that although MuNs had significantly bigger diameters than MoNs, ~16 µm vs ~10 µm, respectively (**Figure 14C**), the nuclear diameters for all cells were constant at ~3 µm (**Figure 14D**). These parameters, cell and nuclear diameters, are indirect measurements for their respective sizes. Overall, MuNs could be described as larger cells containing 2-8 nuclei per cell and having comparable nuclear sizes as that of MoNs.

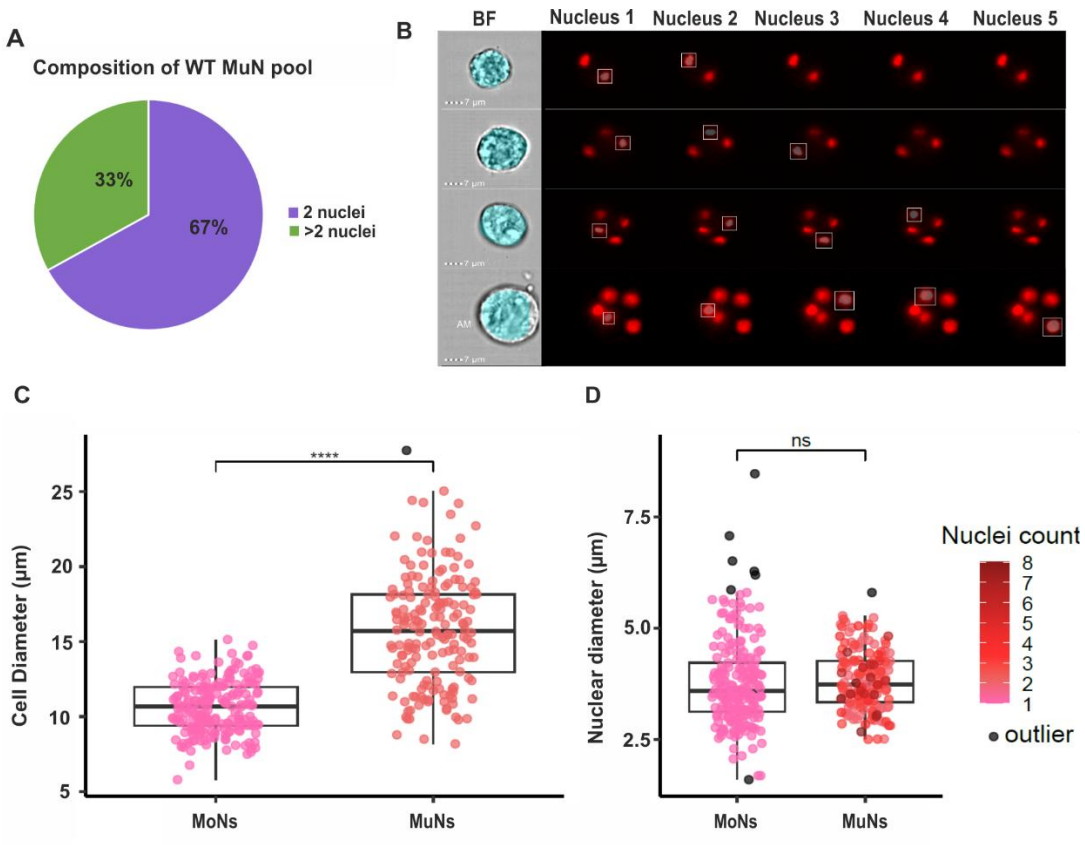

Figure 14. Analysis of cellular and nuclear sizes of MuNs and MoNs. A) Chart showing the general composition of planarian MuN cell pool, with respect to the number of nuclei. B) Images from IDEAS® software showing custom BF and Draq5 channel masks created to optimally cover the BF cell image and Draq5 nuclear images. C) Comparison of MuN sizes based on cell diameters. Statistical analyses were performed using one-way ANOVA followed by Tukey's post hoc method (p-value: 0.05). D) Comparison of nuclear sizes based on nuclear diameters. The color gradient represents the number of nuclei in a particular cell. Statistical analyses were performed using one-way ANOVA followed by Tukey's post hoc method (p-value: 0.05).

5.2.3.3. Marker gene expression profiling of sorted cell populations

It was evident by now that MuNs are distinct cell types, with certain morphological aspects clearly different from MoNs. Therefore, it was hypothesised that these MuNs might display signature expression of molecular marker genes characteristic of specific planarian cell populations (as described in the Introduction). This information shall lead to a preliminary understanding of the differentiative potential of these cells. Accordingly, the next objective was to isolate the cell population containing MuNs for molecular characterization. For this, Calcein AM and Draq5 stained cells were analysed using FACSAria™ Fusion cell sorter and FACSDiva™ 9.0.1 software as follows. Cells were gated out from the debris, followed by doublet discrimination (**Figure 15A**, Steps 1 and

2). After identifying the Calcein AM- and Draq5-positive cells (**Figure 15A**, Steps 3-4), the double positive cells were plotted on a Calcein AM vs Draq5 intensity plot (**Figure 15A**, Step 5). Clearly, due to the intrinsic instrument-related differences, the obtained dot plot presented the acquired events in a distinct way than previously seen in the case of the imaging cytometer. Accordingly, five cell populations were gated, denoted A-E, hereafter referred to as FACS populations (**Figure 15A**, Step 5). Based on the high staining intensities of both dyes, population E was postulated to contain the MuNs.

To verify this assumption, the cells from each of the FACS gates were visualized. To this end, ~50,000 cells from each population were sorted and immediately visualized separately on IS. Other than MoNs, multiple MuNs were found within population E, as expected (**Figure 15B**). The proportion of MuNs to MoNs in population E was also similar to those observed for non-sorted IS samples, i.e., ~2%. This result confirmed the hypothesis that population E contains MuNs and that cell sorting does not alter their distribution within population E.

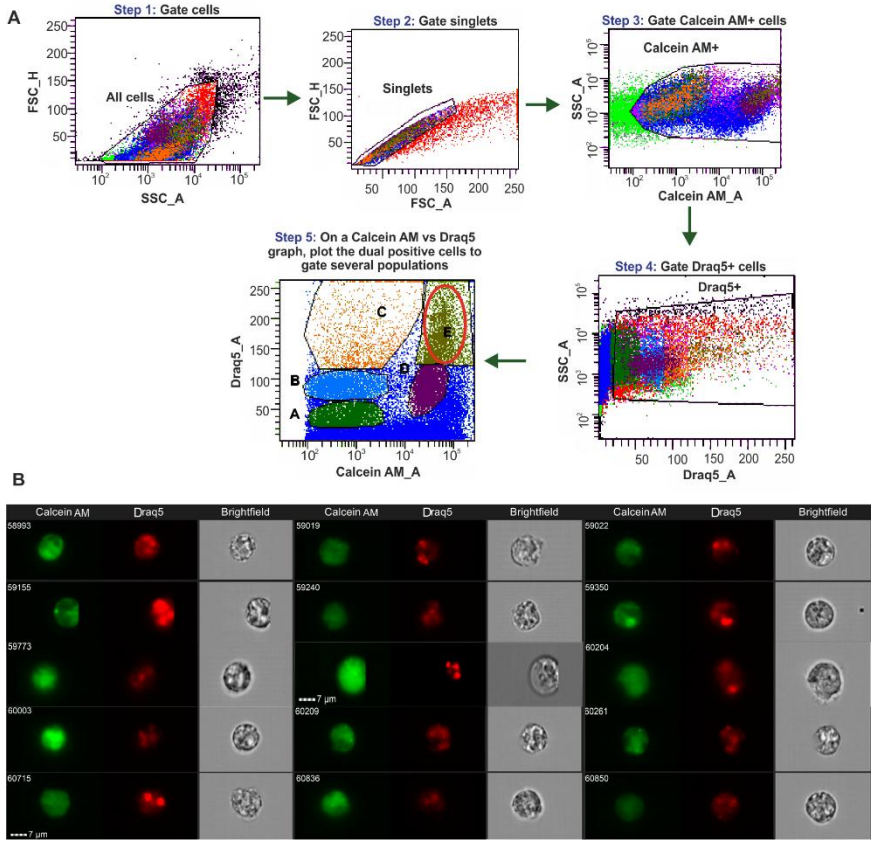

Figure 15. Identification of MuNs-containing cell population on FACS. (A) Specific population gating strategy for FACS sorting of dissociated planarian cells. (B) Picture gallery for sorted cells from population E containing MuNs. Scale: 7 µm; magnification: 40 X.

Other sorted cell populations—namely A, B, C, and D—underwent similar downstream processing to analyse their morphological characteristics. Individual inspection of these populations using IS confirmed that they consisted of MoNs of varying sizes, displaying different staining intensities for Calcein AM and Draq5 (**Figure 16**). Notably, no MuNs were detected in any population except for E. This indicated that population E identified by FACS corresponded directly to IS population E', comprising the same cell types.

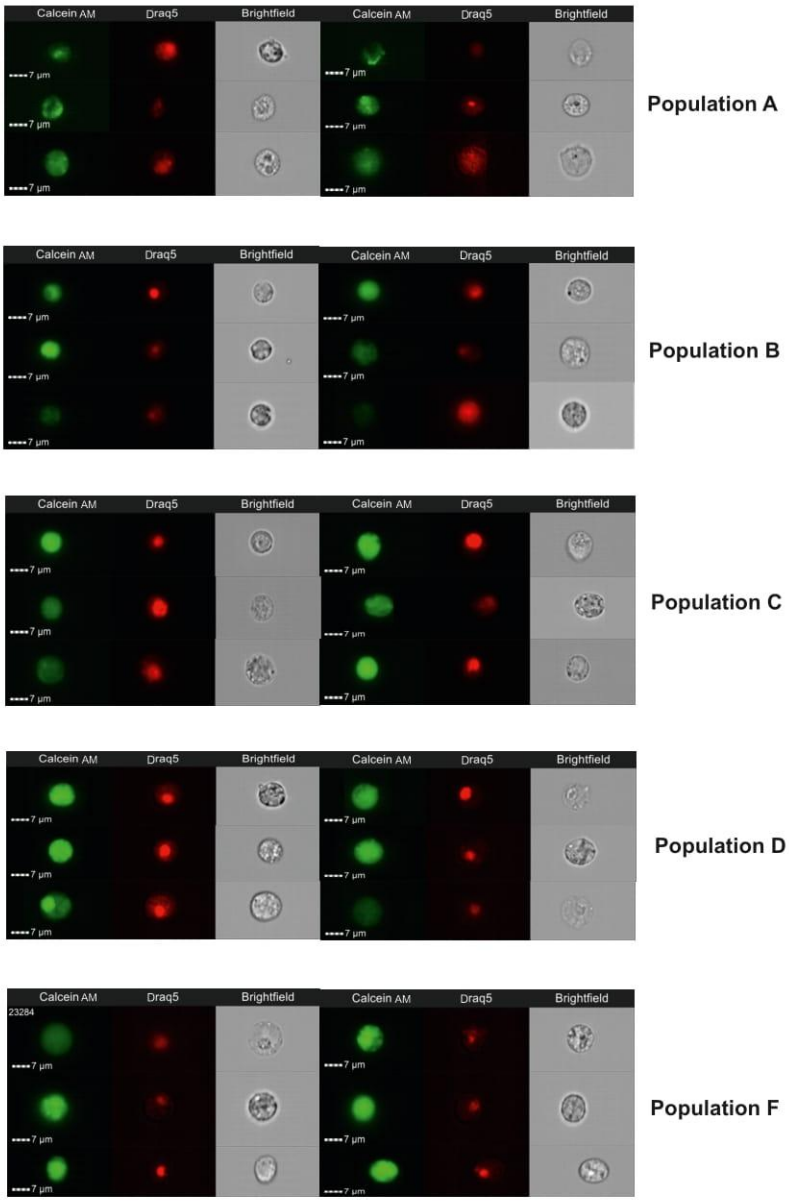

Figure 16. IS image galleries of FACS sorted populations. A, B, C, D and F. *Scale: 7 µm*; *magnification: 40 X*.

Lastly, it was necessary to ensure that MuNs, which are larger than MoNs, were not being excluded by the singlet gate, originally set to remove larger entities such as

doublets and/or clumps. Accordingly, the step of gating singlets was skipped while preserving all the downstream steps to eventually obtain double positive cells (**Figure 17A**, Steps 1-3). The new population E was named as E1, whose position on the Calcein AM vs Draq5 dot plot was identical to that of the original population E (**Figure 17A**, Step 4). Using IS, it was observed that sorted population E1 also contained a similar number of MuNs with respect to other cells in the population. Indeed, few MuNs were larger, but most of them were similar in size and morphology to those obtained from population E (**Figure 17B**).

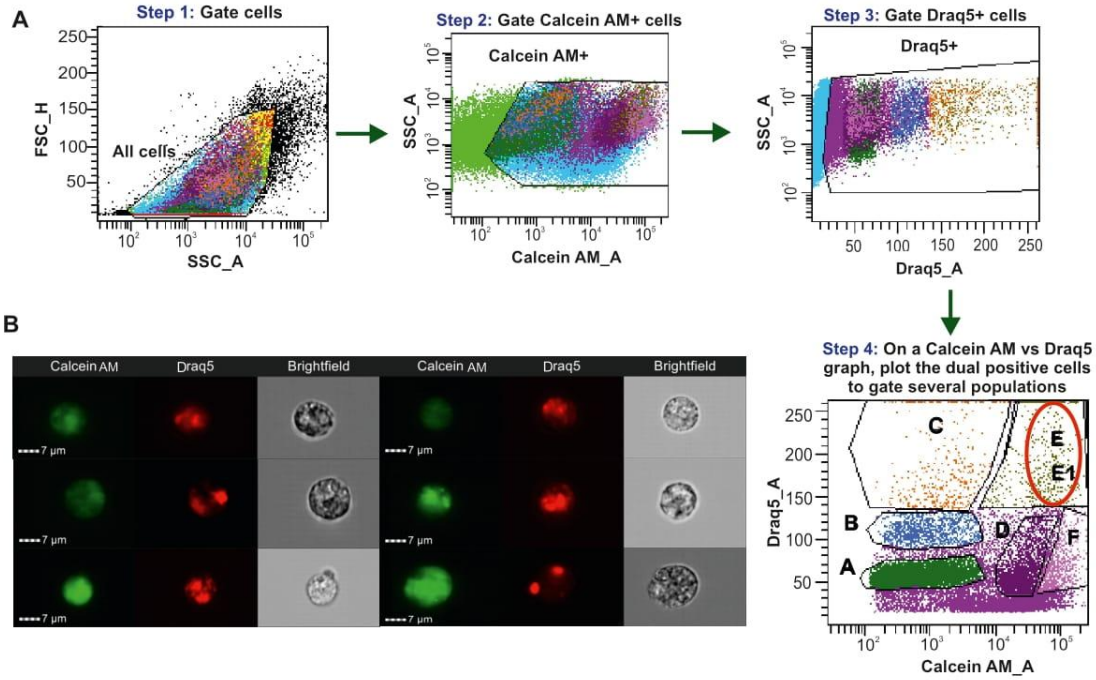

Figure 17. Analysis of the MuNs-containing FACS population without the singlets gating step. A) Specific population gating strategy skipping the singlets gating step for FACS sorting, to capture larger objects. Encircled region in the plot corresponding to Step 4 shows the co-localization of population E1 (strategy skipping singlets gating) and population E (strategy including singlets gating). B) IS image gallery of exemplar MuNs from FACS sorted population E1. Scale: 7 µm; magnification: 40 X.

To molecularly characterize all the five FACS populations, cells were sorted again, and qPCR was performed for marker gene expression profiling according to section **4.15.4**. A sorted sample of singlets, containing a mix of cells from all targeted populations and untargeted regions of the dot plot, was used as a proxy for a suspension of all cell types. The selected marker genes represented three classes of cells at various stages of differentiation – *SMEDWI-1* (neoblast), *AGAT1* (progenitor) and *Glutathione S*

transferase-1 (*GST*; differentiated phagocyte - dd_Smed_v6_20_0_1). As none of the sorted samples were homogeneous in composition, the percentage expression of each marker in a particular sample reflected the approximate proportion of the corresponding cell type within that population. The singlets sample revealed the percentage distribution of marker gene expression that reflected the proportions of specific cell types in the studied planarians. In this sample, neoblasts and progenitor cells were distributed similarly, together accounting for about 30%, while the majority (~70%) of cells expressed the marker for differentiated cells. Populations A, B, and C predominantly consisted of differentiated cells, with over 50% expressing the differentiated cell marker. Population D likely represented neoblasts, inferred from the highest proportion of the neoblast marker (~50%). Population E exhibited the highest proportion of the late progenitor marker compared to all other populations, suggesting a predominance of progenitor cell states. Additionally, populations D and E showed the lowest expression of the differentiated cell marker, further supporting their classification as undifferentiated cell types (**Figure 18**).

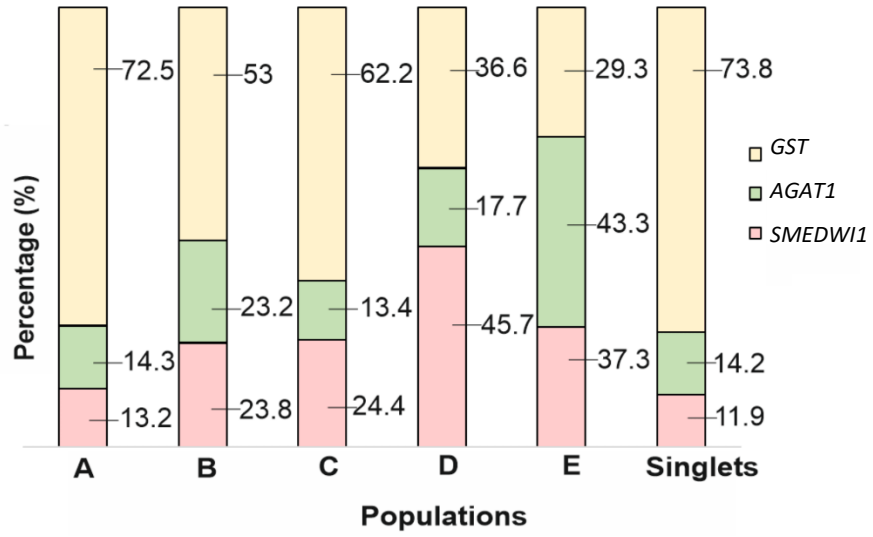

Figure 18. Marker gene expression profiling of FACS populations. Percentage expression of selected marker genes within each sorted sample as obtained from qPCR analyses. Median values from 3 replicates are presented.

Altogether, despite the heterogeneity within each population, ~70% cells with undifferentiated marker expression signatures suggested that the MuN-containing population E was likely undifferentiated – neoblast or progenitor subtypes.

5.2.3.4. Examination of MuNs along a regeneration time course

As previously discussed, undifferentiated stem and progenitor cells play a crucial role in orchestrating regeneration in planarians. Therefore, given the possible undifferentiated state of MuNs, they were next studied along a defined time frame of regeneration. This study hypothesized that MuNs are differentially regulated throughout the regenerative process and exhibit distinct patterns between regenerating and non-regenerating worms. To this end, planarians were cut, and cell dissociates were analysed using IS at 0, 24, 72 and 120 hpa (0, 1, 3 and 5 dpa). A dissociate of non-amputated worms was used as control. Unexpectedly, the percentage composition of MuNs within the total cell pool did not vary between various regenerative time points and non-amputated worms. This means that no matter the regenerative state, the total % of MuNs ranged between ~1-2% of the whole cell pool (**Figure 19A**). To analyse the MuNs further, the proportions of 2-nuc and >2-nuc cells were calculated in all the above conditions. Here, no significant difference in proportions between the samples were found (**Figure 19B**). The consistent presence of MuNs in both regenerative and non-regenerative life stages suggested that they were essential to the basal homeostatic state of planarians.

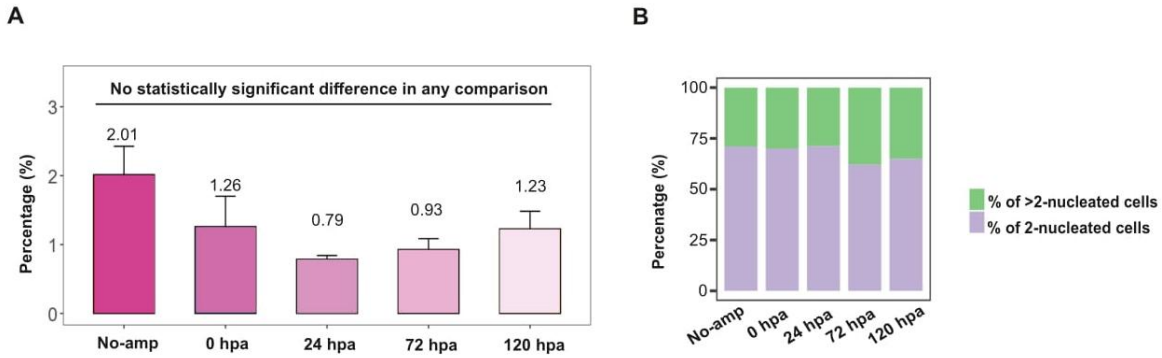

Figure 19. Study of MuNs along a regenerative time course. A) Total percentage of MuNs in the whole cell pool for worms at various regenerative time points and for non-regenerating (No-amp) worms. Statistical analyses were performed using one-way ANOVA followed by Tukey's post hoc method (*p-value: 0.05*) - median values from 3 replicates are presented. B) Distribution of 2-nuc vs >2-nuc MuNs within the MuN pool of worms at various regenerative time points and of non-regenerating (No-amp) worms. Median values from 3 are replicates presented**.**

5.2.3.5. Characterization of differentiative potential of planarian MuNs

qPCR analysis of sorted cell populations provided initial evidence suggesting that planarian MuNs may be in an undifferentiated state, potentially representing stem cell or progenitor subpopulations. To explore this further, the impact of targeted neoblast

depletion on the MuN-containing cell population was assessed. It was hypothesized that if MuNs were indeed stem cells, their numbers would be significantly reduced following neoblast ablation.

Neoblast depletion was achieved by knocking down the *Smed H2B* gene (H2B KD) using RNAi. This is a commonly used and very efficient approach for the selective removal of neoblasts (Solana et al., 2012). The RNAi was performed as described above for the silencing of the selected RNase genes (section **4.11**). At first, gene expression analyses were conducted on *H2B* KD vs WT worms, focusing on three groups of marker genes representing neoblasts, progenitors, and differentiated cells. Neoblasts and early progenitors were marked by *SMEDWI1* and *Smed NB_21.11e* (SMEST024707001.1), respectively, late progenitors by *AGAT1*, and differentiated cells by the phagocytic marker *GST* and the neural marker *PC2* (dd_Smed_v6_1566_0_1). To this end, *H2B* KD and WT worms were dissociated, and the resulting cell suspensions were analysed using FACS. Approximately 50,000 cells from the singlets gate were sorted for *H2B* KD and WT samples and used for marker gene expression profiling by qPCR. As expected, a sharp decrease in the expression of neoblast and early progenitor markers was observed. Notably, there was also a significant (~30%) reduction in the expression of the late progenitor marker. These changes were accompanied by an increase in the expression of differentiated cell markers, reflecting a compensatory enrichment in the number of differentiated cells due to the absence of neoblasts and progenitors in the constant cell pool (**Figure 20A**).

To check if *H2B* KD directly affected the MuNs, the percentage of these cells under RNAi vs WT conditions was calculated. To this end, cell dissociates for both sample types were subjected to IS analysis, which revealed that the percentage of MuNs was significantly reduced in the *H2B* KD samples (**Figure 20B**). Consequently, all the individual populations identified earlier using IS and FACS were further analysed. Based on the IS plots, 2 populations were found whose percentage contribution significantly decreased as a result of *H2B* KD. Percentage of population D' in *H2B* KD was 0.2 times of the WT value (4% in *H2B* KD and 17.8% in WT) and for E' containing MuNS, the percentage in H2B KD was 0.6 times of WT (29.2% in *H2B* KD and 51.5% in WT).

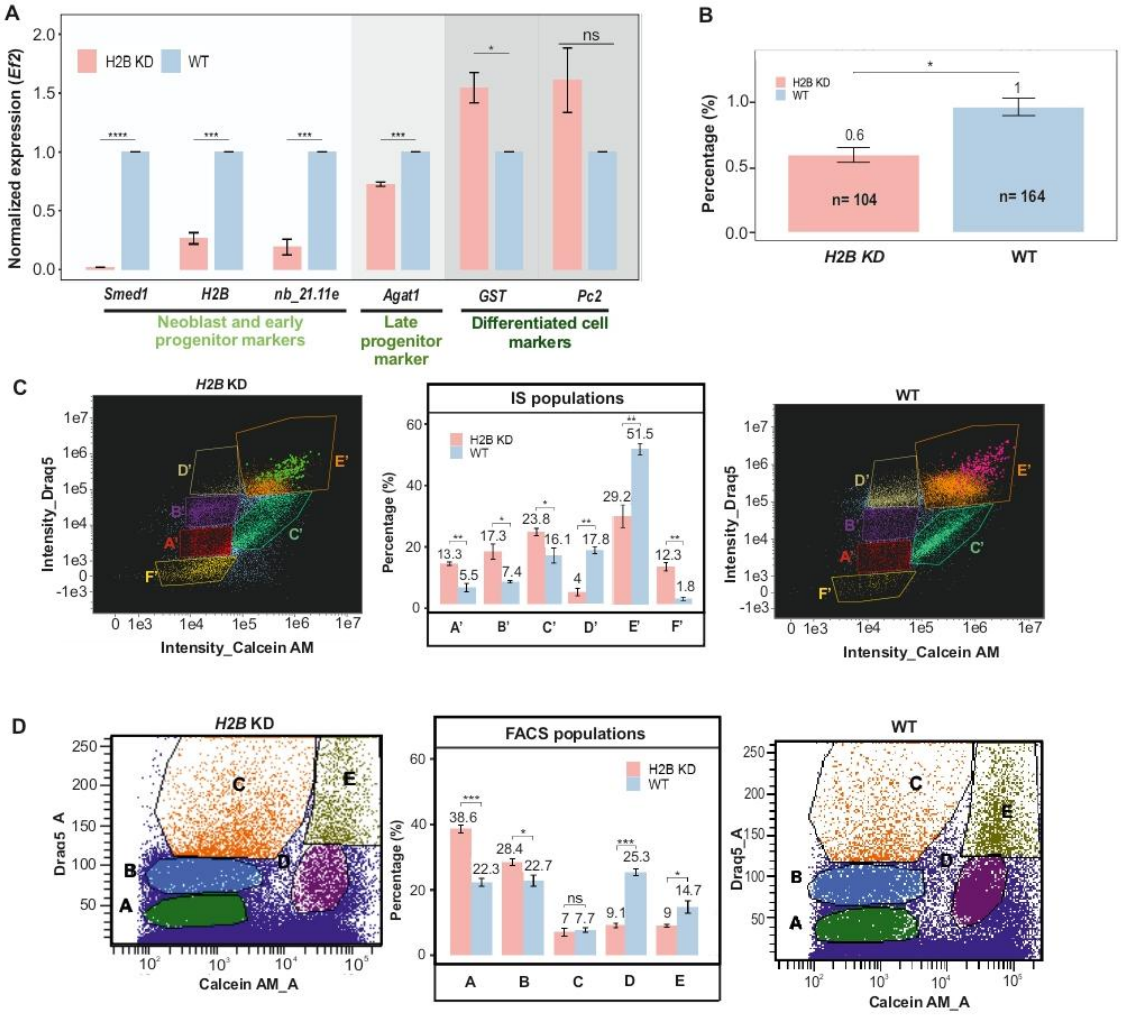

Figure 20. Characterization of the differentiative potential of MuNs based on neoblast ablation experiments. A) Marker gene expression profile comparison between *H2B* KD and WT samples. Statistical analyses were performed using one-way ANOVA followed by Tukey's post hoc method (*p-value:0.05*) - median values from 3 replicates are presented. B) The percentage of MuNs in *H2B* KD and WT samples. Statistical analyses were performed using a two-sided t-test (*p-value: 0.05*) - median values from 3 replicates are presented. C) Comparison of IS population distribution between *H2B* KD and WT samples. Green and pink dots represent manually assigned MuNs. Statistical analyses were performed using one-way ANOVA followed by Tukey's post hoc method (*p-value: 0.05*) - median values from 3 replicates are presented. D) Comparison of FACS population distribution between H2B *KD* and WT samples. Statistical analyses were performed using one-way ANOVA followed by Tukey's post hoc method (*p-value: 0.05*) - median values from 3 replicates are presented.

This led to the conclusion that these two populations contained undifferentiated cell types and based on the levels of reduction of the two, population D' contained mostly neoblasts and the lesser affected population E' was majorly comprised of progenitors at

various stages (**Figure 20C**). As for the FACS populations, again 2 populations were obtained whose percentage contribution to the total cell pool were particularly reduced. Population percentages of E (containing the MuNs) and D were 0.4 times of WT value (9.1% in *H2B* KD and 25.3 % in WT) and 0.6 times of WT (9% in *H2B* KD and 14.7 % in WT), respectively (**Figure 20D**). As the reduction in population D was much more profound than that of E, it could be concluded that D contains neoblasts and E, progenitors. This was in line with the observations presented above (**Figure 20A**) that the progenitor marker expression was reduced to a much lesser extent than the neoblast marker, and populations D and E have the highest expressions of the neoblast and progenitor markers, respectively.The characterization of MuNs presented in this chapter indicated that they are part of a population containing progenitor cells, and that they themselves likely exhibit such characteristics. The increase in the number of MuNs nuclei under *Smed ELAC2* knockdown conditions (**Figure 20B)** suggests that these cells may be involved in regenerative processes.

5.3. Impact of *Smed ELAC2* silencing on the transcriptome

Given the significant morphological, anatomical, and cellular alterations observed in *Smed ELAC2* KD worms, it was logically hypothesized that these effects were driven by substantial molecular changes, including gene expression and sncRNA pool. To investigate this, a comprehensive transcriptomic analysis was conducted using next-generation sequencing (NGS) to characterize both the gene expression profiles and the sncRNA repertoire. While sncRNAs were central to the study, placing them within the wider context of transcriptomic changes was important to depict the molecular background and essential for the functional analysis of the sncRNAs identified as being involved in regeneration.

Long RNA fractions (>200 nt) and small RNA fractions (≤80 nt) were isolated from *Smed ELAC2* KD, GFP mock, and WT regenerating worms at 3dpa and 5dpa. Sequencing libraries were prepared from these samples. The long RNA sequencing dataset facilitated the analysis of overall gene expression and mitochondrial pre-tRNA processing, while the small RNA dataset was used to examine changes in the sncRNA pool. The experimental workflow is illustrated in **Figure 21**.

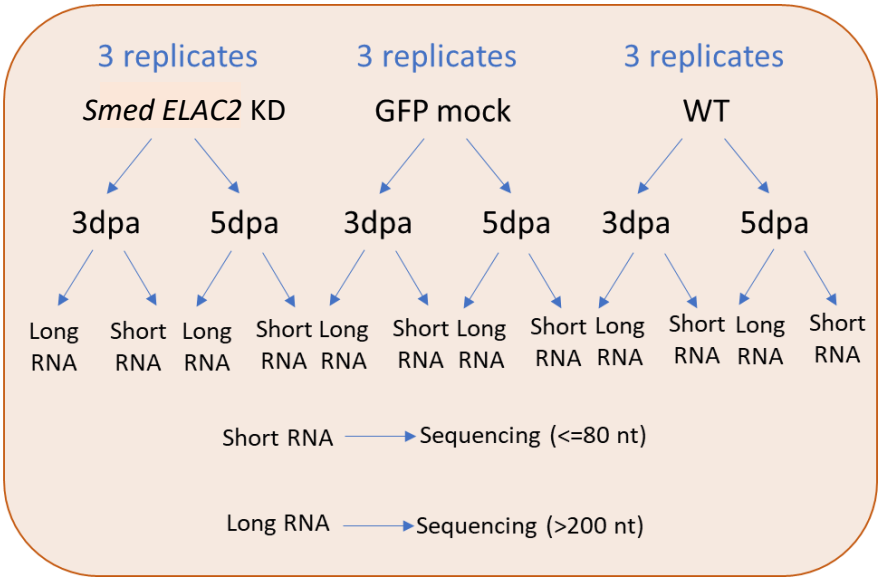

Figure 21. Experimental scheme to study the gene expression upon Smed ELAC2 silencing. Long RNA (>200 nt) and small RNA (<80 nt) fractions were sequenced from *Smed ELAC2* KD, GFP mock and WT samples.

5.3.1. Prediction of functional domains of the Smed Elac2 protein based on amino acid sequence homology

The long RNA sequencing dataset was first used to compare the *Smed ELAC2* transcript sequences obtained from the dd_Smed_v6 and SMEST transcriptomes available in the PlanMine database with the actual transcript present in the worms raised under the current laboratory setting. This step is essential when studying human gene homologs in unconventional model organisms like *S. mediterranea*, whose genome and transcriptome remain incompletely annotated and are continuously being updated. The amino acid sequence of the protein from both dd_Smed_v6 and SMEST transcripts was derived from the respective longest ORFs predicted by the NCBI ORFfinder tool. Protein sequence predicted from both these sequences were defective: the one from dd_Smed_v6 lacked the mitochondrial targeting sequence (MTS), due to two missense mutations, and the one from SMEST was severely truncated lacking multiple protein domains (due to a single insertion) (**Figure 22A**). Therefore, the *Smed ELAC2* transcript sequence was further bioinformatically developed upon using in-house produced transcriptomic datasets – this work was done by Anastasiia Zaremba, MSc, from the same research group, within the scope of her doctoral dissertation (Zaremba et al.: submitted). Multiple sequence alignment of the protein sequence derived from the newly refined transcript with other Elac2 homologs from organisms like *H. sapiens*, *C. elegans*, and *S. cerevisiae* revealed that it retained all critical C-terminal domains (CTD) necessary for catalytic function, as well as

the amino-terminal MTS required for subcellular localization. However, other motifs on the amino terminal domain (NTD) of Elac2 showed far less conservation across all organisms under study (**Figure 22B**).

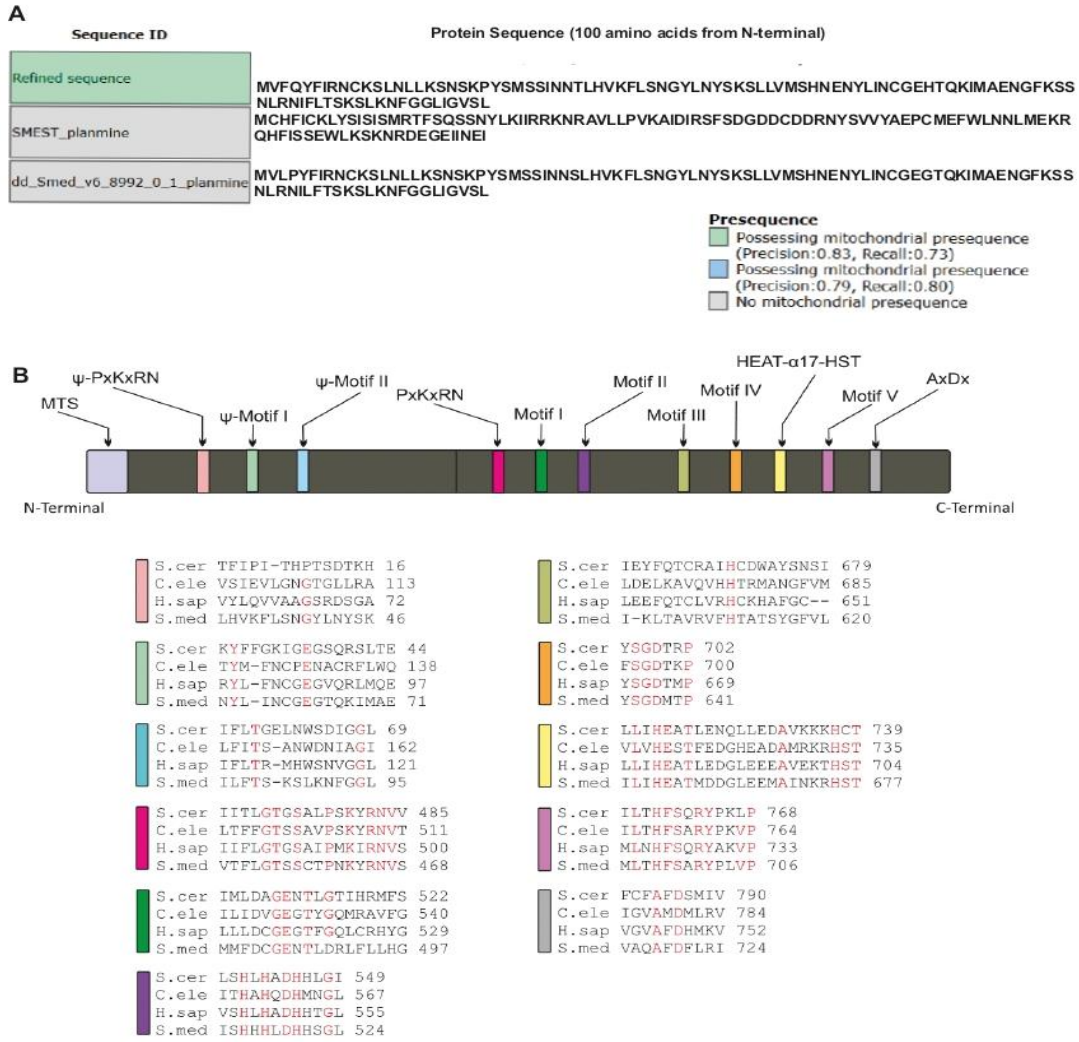

Figure 22. Prediction of Smed Elac2 protein sequence. A) Screenshot showing the presence of MTS in N-terminal of the protein predicted from the in-house refinement of *Smed ELAC2* transcript sequence. B) Homology of crucial CTD motifs of predicted Smed Elac2 protein with homologs present in other organisms - *H. sapiens*, *C. elegans* and *S. cerevisiae*.

5.3.2. Impact of *Smed ELAC2* silencing on mitochondrial pre-tRNA processing

Mitochondrial (mt-) transcripts are synthesized as polycistronic molecules containing mt-tRNA, mt-rRNA, and mt-mRNA (Basu et al., 2020). Elac2 and its homologs are known to play a crucial role in processing the 3' ends of mt-tRNAs, a key step in mt-tRNA maturation. Based on this, it was hypothesized that kockdown of *Smed ELAC2* would lead to defects in mt-tRNA processing, in turn validating Elac2 homologs in planarians also have similar function as in other organisms.

Using the *S. mediterranea* mitochondrial genome, 10 regions where the 3' end of an mt-tRNA gene directly precedes the 5' end of another gene of mRNA, rRNA or lncRNA were identified bioinformatically (regions 1–10). Polycistronic transcripts, composed of mt-tRNA and another downstream mt-RNA, were expected to originate from these regions in *Smed ELAC2* knockdown conditions. Sequencing read coverage of these regions were analysed across all experimental groups using the >200 nt sequencing dataset. This analysis revealed that there was a significant accumulation of unprocessed mt-tRNA transcripts in regions 2, 4, 8, and 9 in *Smed ELAC2* KD samples compared to controls. To confirm the observed defects in mt-tRNA processing, the findings were experimentally validated using qRT-PCR. To determine whether the release of mature mt-tRNA molecules was specifically hindered by *Smed ELAC2* disruption , the focus was placed on accurately capturing junction products that encompassed a particular mt-tRNA and its downstream other RNA neighbour (**Figure 23A**). Junction transcripts from the 4 regions identified based on NGS data were found to be significantly increased in *Smed ELAC2* KD worms compared to both control groups (**Figure 22C**), reflecting disrupted mt-tRNA processing at these specific regions. To determine whether the over-accumulation of unprocessed transcripts from the 4 regions was not caused by overexpression of mitochondrial genes, a primer set was specifically designed to amplify only the regions located downstream of mt-tRNA (**Figure 22B**). This analysis showed that the mitochondrial gene expression itself was not affected and thus the observed effect was the result of disruptions in transcript processing, not of expression changes. Similar experiments were performed for an unaffected region, region 3 as a control (**Figure 22C**, region 3 panel).

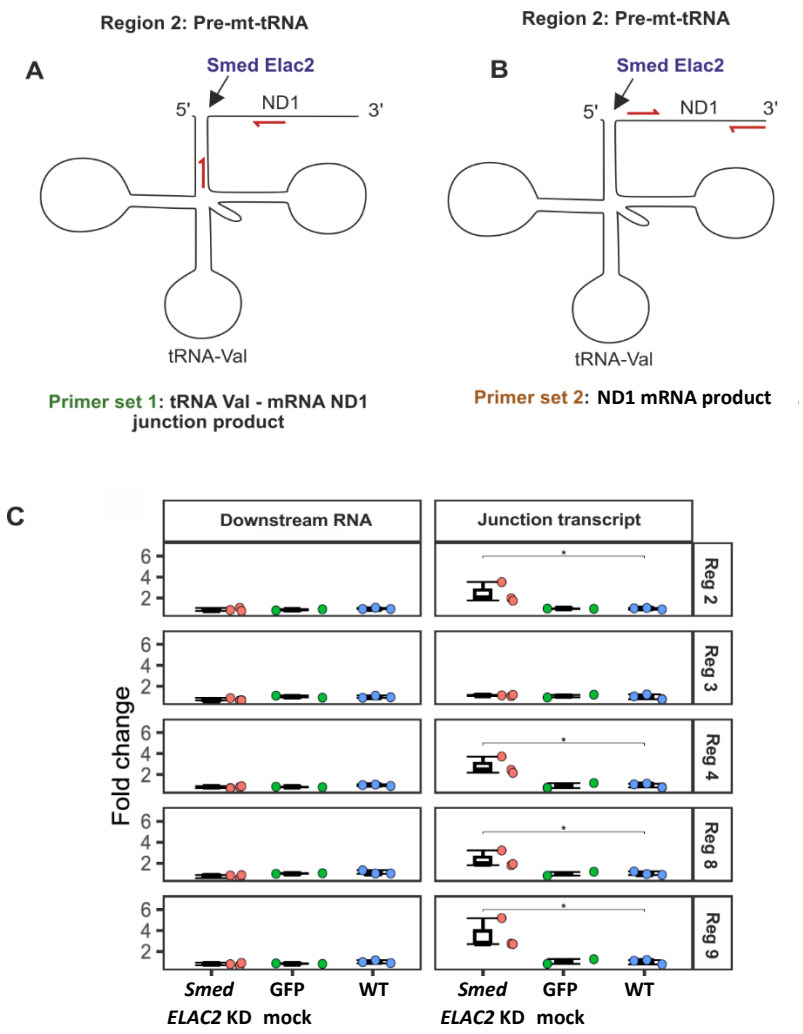

Figure 23. Validation of unprocessed mt-tRNA transcripts identified in NGS data analysis. A) Primer set to capture junction transcripts using example of region 2. B) Primer set to capture transcripts located downstream of mt-tRNA using example of region 2. C) qRT-PCR analysis plots showing levels of accumulation of junction transcripts and of downstream RNA molecules, from regions 2,4,8,9 and 3 – in *Smed ELAC2* KD, GFP mock and WT samples. Statistical analyses were performed using one-way ANOVA followed by Tukey's post hoc + Bonferroni method (*p-value: 0.05*).

Overall, these results confirmed that Smed Elac2, like its homologs in other organisms, participates in maturation of specific mitochondrial RNAs, as this process was disrupted upon depletion of this RNase.

5.3.3. Impact of *Smed ELAC2* silencing on gene expression

The long RNA NGS results were then used to analyse changes in the overall gene expression patterns in *Smed ELAC2* KD worms compared to control conditions. The total number of differentially expressed genes (DEGs) at each regenerative time point was quite

low. At 3 dpa, 19 genes were upregulated, and 27 were downregulated. By 5 dpa, these numbers increased to 25 upregulated and 58 downregulated genes.

To extract meaningful insights from the DEG list, a bioinformatic workflow was applied including, a) assigning Gene Ontology GO terms to each DEG to describe its cellular functions, b) clustering GO terms based on similarities in associated cellular and physiological pathways and, c) assigning cell type enrichment information to each DEG. Of these analyses, only results from GO clustering and cell type-specific DGE enrichment are presented, as they are only crucial for drawing relevant biological conclusions.

The identified GO clusters included: developmental processes, extracellular regions, immune response, blood-related processes, cell proliferation and differentiation, signalling pathways, metabolic processes, binding activities, membrane structures and transport, iron/metal/oxygen binding, organellar regions and activities, specialized structures, protein folding and processing, lipid processes, neuronal processes, miscellaneous activities, and response to stimuli and stress. Enriched GO clusters were analysed for four different gene sets: overexpressed at 3 dpa, overexpressed at 5 dpa, underexpressed at 3 dpa and underexpressed at 5 dpa respectively (**Figure 24**). Among these, the *metabolic processes* cluster appeared across all four sets. This cluster encompassed genes involved in a diverse range of metabolic pathways and physiological metabolite production, making it highly heterogeneous and challenging to derive specific conclusions from. Another consistently present cluster across all gene sets was *neuronal processes*, where most associated genes were linked to the negative regulation of synaptic transmission. *Developmental processes* cluster was mainly associated with underexpressed genes at 3 dpa. A cumulative analysis of these genes revealed an enrichment of GO terms associated with the negative regulation of mammalian organ and tissue development. This pattern emerged because the GO analysis was performed based on gene sequence homology with higher organisms. While planarians lack many of these organs and tissues, these GO terms suggest that key pathways regulating *S. mediterranea*-specific organ and tissue development and regeneration may be disrupted. Clusters such as *extracellular regions* and *membrane structures & transport* were consistently present in both scenarios associated with underexpressed genes (3 and 5 dpa). Again, a detailed assessment revealed that these clusters were comprised of GO terms associated with extracellular receptors and membrane ion transport, indicating an effect on the membrane transport pathways. Elsewhere, clusters related to *cell proliferation & differentiation* and *signalling pathways* were associated with overexpressed genes at both time points.

Assessment of particular GO terms assigned to genes within these clusters indicated an overall negative regulation of cellular growth processes.

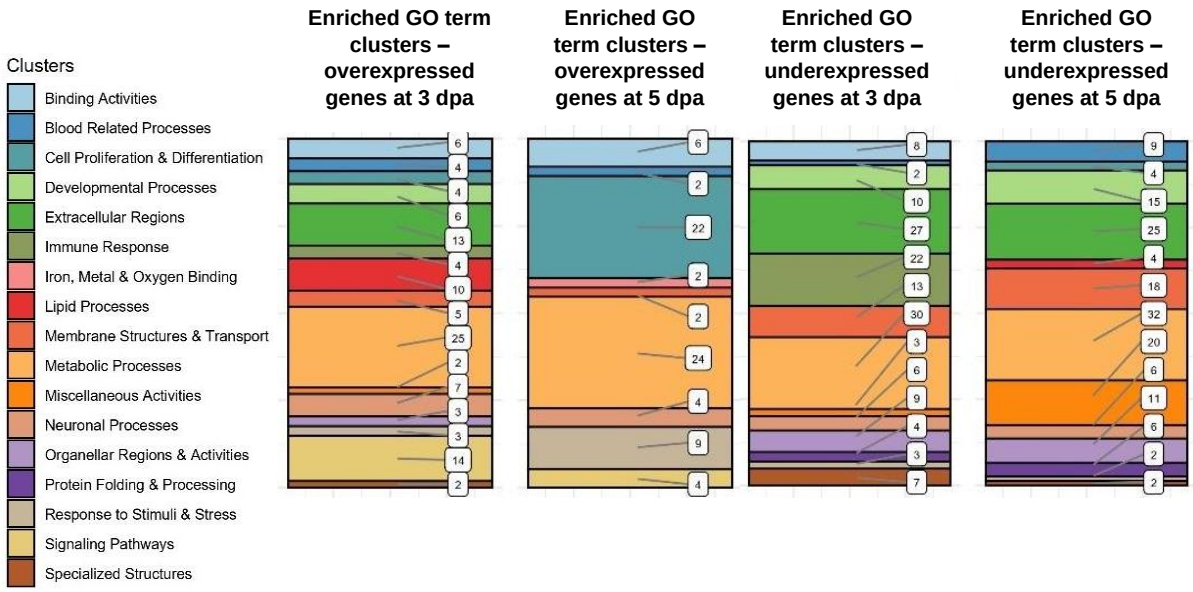

Figure 24. GO analysis of genes differentially expressed in Smed ELAC2* KD *worms versus controls, based on NGS data. Stacked bar plots indicating the number of GO terms per GO cluster at each condition, viz., genes upregulated at 3 dpa; upregulated at 5 dpa; downregulated at 3 dpa; downregulated at 5 dpa.

Next, DEGs were categorized based on the cell types in which they are primarily expressed, using publicly available single-cell RNA sequencing (scRNA-seq) datasets (**Figure 25**). This analysis revealed an intriguing pattern. The genes differentially expressed at 3 dpa were characteristic for just two major cell types: overexpressed genes are known to be expressed in parenchymal cells, while underexpressed genes are primarily associated with goblet cells. However, by 5 dpa, as regeneration progressed, both the overexpressed and underexpressed genes became more diverse in terms of the cell types in which they are primarily expressed in. At 5 dpa, the set of overexpressed genes contained not only those that are associated with parenchymal cells but also those that are expressed in neural, epidermal, and phagocytic cells. In contrast, for underexpressed genes no apparent pattern could be observed, as this group contained genes representing a broader range of cell types, including neural, goblet, secretory, parapharyngeal, epidermal, and protonephridia cells.

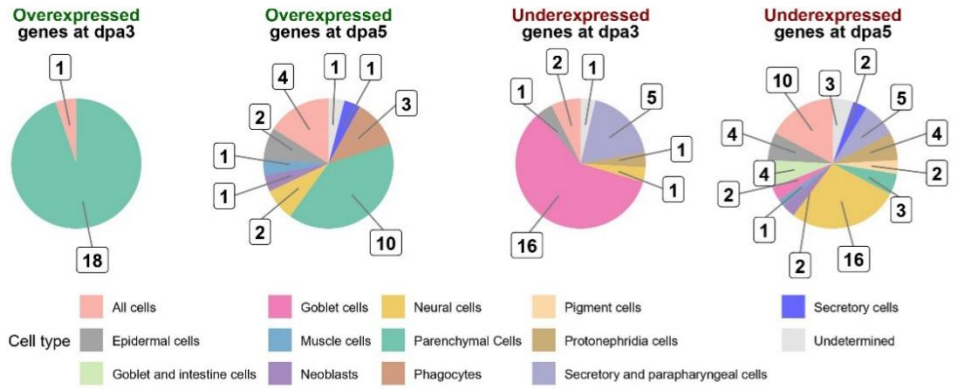

Figure 25. Differentially expressed genes in Smed ELAC2 KD worms versus controls, grouped according to the cell types in which they are expressed. Pie charts showing the distribution of DEGs across cell types at 3 and 5 dpa.

In summary, genes involved in developmental processes and cell proliferation were found to be negatively regulated. Many of the identified pathways are associated with organ function and biological processes in higher organisms, suggesting either the presence of homologous mechanisms in planarians or a role for these pathways in planaria-specific processes. Additionally, at 3 dpa, a distinct cell type-specific pattern emerged among DEGs. This pattern suggests that early gene expression abnormalities in parenchymal and goblet cells initiate regenerative defects, which later manifest at the cellular level by 5 dpa, as evidenced by the diversification of cell type-specific expression patterns of overexpressed and underexpressed genes. This conclusion is further reinforced by previous observations across multiple physiological levels, all occurring around 5 dpa.

5.3.4. Impact of *Smed ELAC2* silencing on sncRNA pool

According to the adopted research strategy, a comparative analysis of the sncRNA pool in planarians with *Smed ELAC2* knockdown versus controls was central to identifying sncRNAs involved in regenerative processes. The small RNA (<80 nt) sequencing dataset was used for this analysis. Bioinformatic analyses were done in our research group, outside of the scope of this dissertation, but their results were evaluated. It was found that the sncRNA pool mainly consisted of RNA fragments generated from molecules representing the following classes: rRNA, tRNA, mRNA, lncRNA, snoRNA, snRNA, and others. Furthermore, both miRNA and piRNA were detected as well (**Figure 27A**). The largest proportion of the pool was comprised of rRNA fragments. The length distribution for all these molecule types was then analysed (**Figure 26**). It revealed that rRNA fragments spanned almost the entire length distribution, with the shortest molecules being the most

abundant. This pattern suggested that this collection likely represented nonspecific products of an ongoing digestion process. Accordingly, they were excluded from further analysis. For most of the other RNA types, however, there was a clear trend of accumulation of molecules with specific lengths, indicating distinct length distribution patterns.

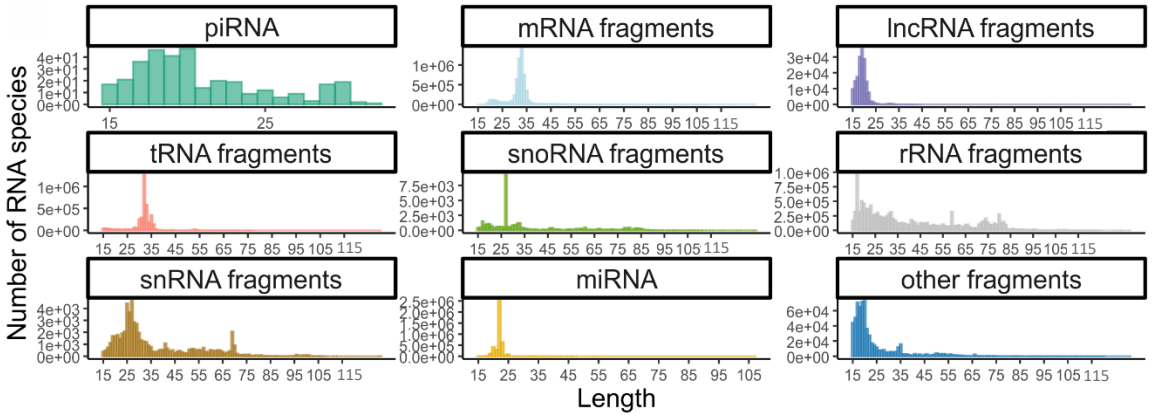

Figure 26. Read length distribution of various ncRNA classes. The peaks for major sncRNA classes were as follows: piRNAs; tRNA fragments; snoRNA fragments; snRNA fragments; miRNAs.

Overall, miRNAs comprised the largest proportion of sncRNA, followed by tRFs (**Figure 27A**). Although fluctuations in their distribution were observed across the *Smed ELAC2* KD, GFP mock and WT samples, they did not reach statistical significance. Likewise, no significant differences were observed in the proportions of the other sncRNA classes across the samples. In the next step, the results of differential accumulation analysis of individual small RNA species upon *Smed ELAC2* knockdown, compared to controls, were evaluated (**Figure 27B**). RNA species were defined as particular molecules with specific sequences, rather than general classes as a whole. At 3 dpa in *Smed ELAC2* KD worms, a total of 59 unique molecules were downregulated, and 40 molecules were upregulated. These were predominantly tRFs, among which both decreased and increased species were observed. Another class showing differential accumulation was miRNA, with the majority exhibiting an increase in accumulation. A few RNA fragments derived from snoRNA were also identified, with their accumulation levels decreasing as a result of *Smed ELAC2* silencing. At the subsequent time point, 5 dpa, differential accumulation was mainly observed in tRFs (29 unique molecules), with a particularly noticeable decrease under *Smed ELAC2* knockdown conditions.

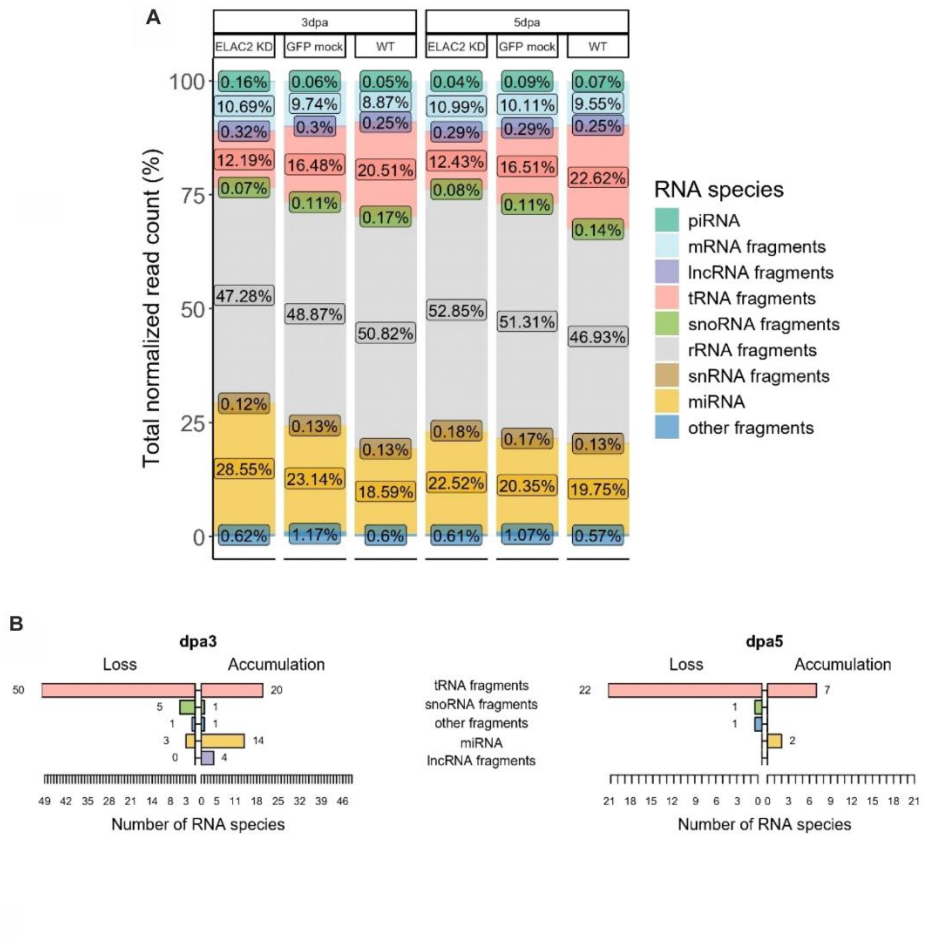

Figure 27. Profile of sncRNAs in Smed ELAC2* KD *worms. A) Percentage accumulations of various classes of sncRNAs in *Smed ELAC2* knockdown and control samples. B) Numbers of particular RNA species from specific classes of sncRNA, differentially accumulated upon *Smed ELAC2* silencing.

Subsequently, detailed analysis of the specific miRNA and tRF subtypes affected upon *Smed ELAC2* knockdown was conducted. The various subtypes of miRNA and tRF molecules found to be differentially accumulated are shown in **Figure 28A** and **B**. Accordingly, in *Smed ELAC2* KD worms at 3 dpa the following miRNA were upregulated: sme-miR-9a-5p; sme-miR-96a-5p; sme-miR-71a-5p; sme-miR-190a-3p, and downregulated: sme-miR-96b-5p; sme-miR-8b-3p; sme-miR-87c-5p; sme-miR-36a-3p; sme-miR-2153_precursor; sme-miR-125b-5p. At 5 dpa, sme-miR-71a-5p was increased and sme-miR-96b-5p decreased (**Figure 28A**). Since tRFs was the class of sncRNA most significantly remodelled as a result of *Smed ELAC2* silencing, they were subjected to a detailed characterization based on an assignment of individual fragments identified at 3 dpa and 5 dpa to specific regions of their parental molecules. In total, 24 different tRNAs gave rise to differentially accumulated fragments, showing that this was not a random

occurrence, but rather indicative of an underlying mechanism driving this pattern. As mentioned above, at 3 dpa the changes in tRF accumulation levels were more pronounced than at 5 dpa, with more RNA species being deregulated (**Figure 28B**). The tRFs with elevated accumulation originated from several parental molecules. Primarily, although not exclusively, they were derived from the 3' regions of the parental RNAs, with 3'-tRFs being the most predominant. The situation was markedly different for the tRFs whose accumulation was reduced upon *Smed ELAC2* knockdown. Most of these species were classified as 5'-tRNA halves, originating predominantly from tRNA-Gly-GCC (**Figure 28B**). 5'-tRFs and i-tRFs derived from the same parental molecule were also downregulated. Apart from these, only a limited number of other tRFs exhibited downregulation, with most of them also corresponding to 5'-tRNA halves. However, the pattern of the drastic reduction observed for fragments derived from tRNA-Gly-GCC, especially for 5' tRNA half Gly-GCC, was particularly striking.

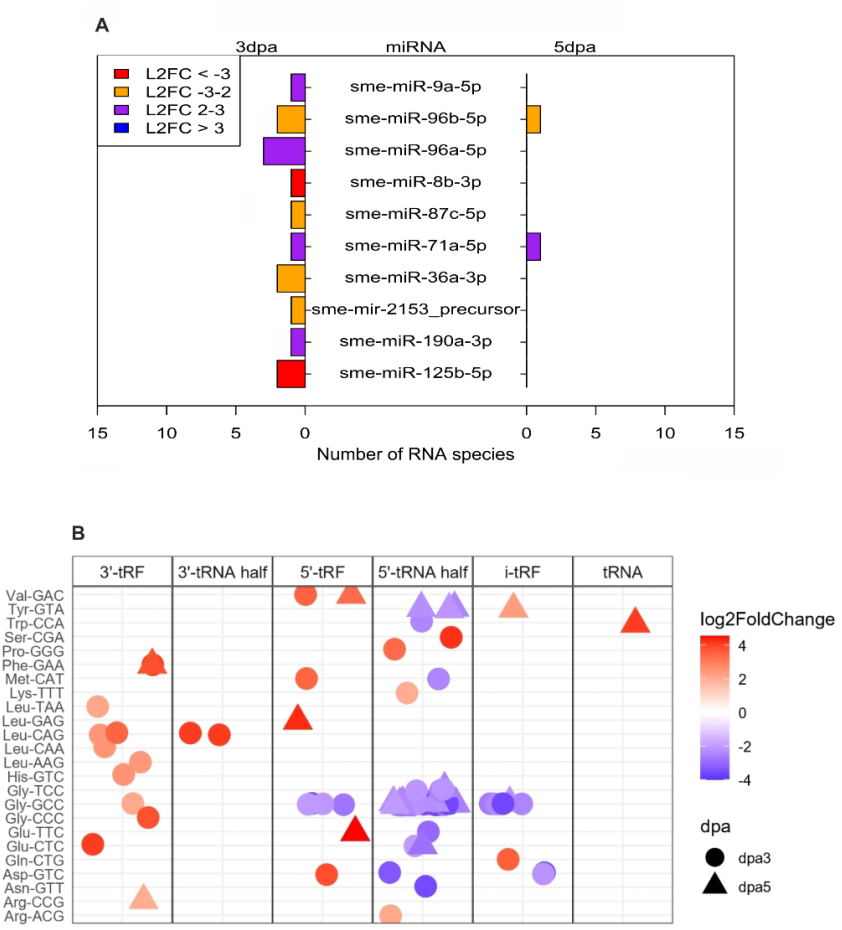

Figure 28. Smed ELAC2 knockdown effects on specific tRNA fragments and miRNA molecules. A) miRNA and B) tRF species differentially accumulated upon *Smed ELAC2* silencing.

To validate the NGS results, the accumulation of selected deregulated miRNA and tRF molecules was experimentally analysed using qRT-PCR. However, as these molecules are ~22-40 nt, the qRT-PCR methodology, previously applied to assess gene expression, had to be optimized. To detect such small RNA molecules using qRT-PCR, a manoeuvre was devised where small RNA samples underwent adapter ligation at the 5' and 3' ends using the TruSeq Small RNA Library Prep Kit (section **4.15.3**).

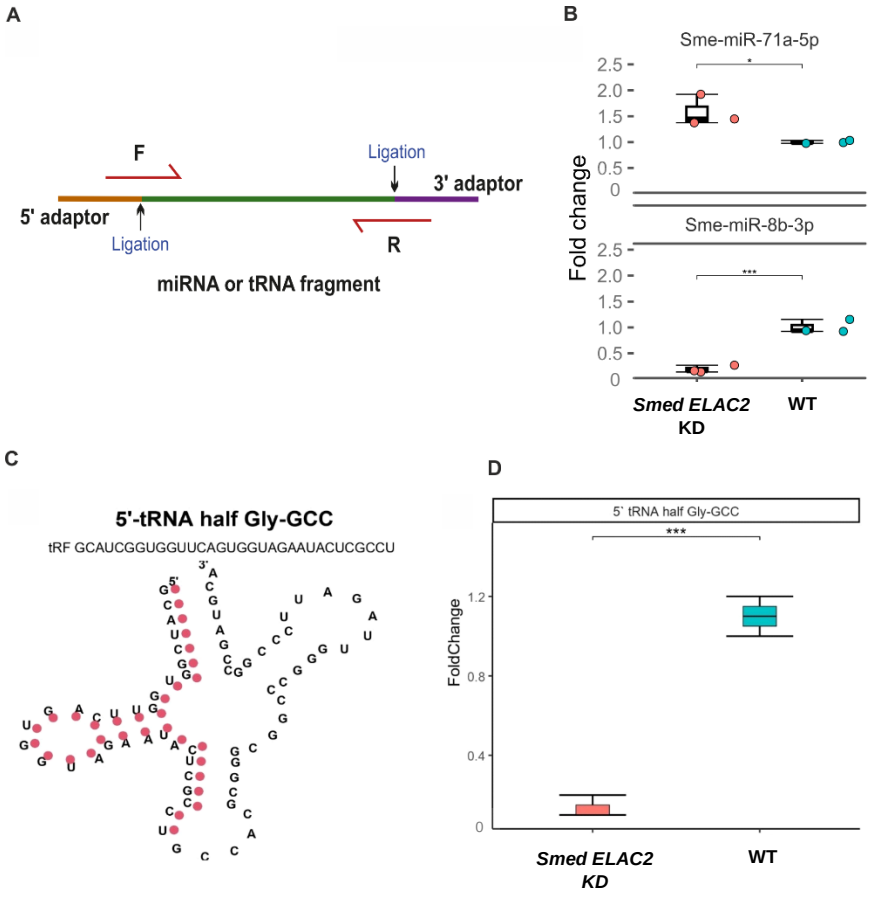

Figure 29. qRT-PCR validation of selected differentially accumulated sncRNA molecules. A) Scheme of primer design for small RNA qRT-PCR. B) Experimental validation of upregulation of sme-miR-71a-5p and downregulation of sme-miR-8b-3p. Statistical analyses were performed using Welch two Sample two-sided t-test (*p-value <0.05*) C) Location of 5' tRNA half Gly-GCC within the parent tRNA molecule. D) Experimental validation of pronounced downregulation of 5' tRNA half Gly-GCC. Statistical analyses were performed using Welch Two Sample two-sided t-test (*p-value <0.05*)

Primers for each small RNA molecule of concern were designed in a way that both forward and reverse primers encompass the junction region between the small RNA and 5' and 3' adaptor sequences, respectively (**Figure 29A**). qRT-PCR analyses validated the differential accumulation of specific miRNA molecules – upregulation of sme-miR-71a-

5p and downregulation of sme-miR-8b-3p – and downregulation of a species of 5'tRNA half Gly-GCC **Figure 29B** and **D**. The location of this specific 5' tRNA half within the secondary structure of the parental molecule is shown in **Figure 29C**.

Overall, changes in the sncRNA pool upon *Smed ELAC2* knockdown were characterized using NGS, with selected results validated with qRT-PCR. While the miRNA and tRF classes were the most affected, with specific deregulated molecules identified within these groups, the tRNA half Gly-GCC emerged as a particularly significant example.

5.4. Functional analysis of 5'tRNA half Gly-GCC *in vivo*

Given the significant reduction of 5' tRNA half Gly-GCC upon *Smed ELAC2* knockdown, it was hypothesized that Smed Elac2 ribonuclease is directly involved in the biogenesis of this molecule. Furthermore, the drastic loss of this specific sncRNA was proposed to contribute—partially or entirely—to the phenotypic, cellular, or molecular changes observed in *Smed ELAC2 KD* worms. Consequently, this sncRNA was selected for further functional analysis *in vivo*.

A critical component of this analysis involved the identification of potential target molecules for the 5'tRNA half Gly-GCC through bioinformatics approaches. Based on the current state of knowledge, two mechanisms of action for this small RNA were considered. The first mechanism assumes that the ribonuclease Smed Elac2 cleaves tRNA and uses the resulting 5'tRNA half as a short guide RNA to find and cleave its target transcript (Elbarbary et al., 2009). According to the second mechanism, the tRNA half generated by Smed Elac2, functions as a non-canonical miRNA in the RNA interference pathway (Kuscu et al., 2018). These two mechanisms differ in terms of the structural determinants of the interaction between the tRNA half and its target; however, in both cases, the target transcript is ultimately downregulated by 5' tRNA half Gly-GCC. Therefore, it was expected that its targets would be among the overexpressed genes under *Smed ELAC2 KD* conditions, where the level of 5' tRNA half Gly-GCC molecule was reduced.

These two theoretical pathways provided the foundation for *in silico* functional analyses conducted in our research group, which will not be discussed in detail in this dissertation. The results of these analyses did not identify any potential targets for the first mechanism; however, two candidate targets were found using the miRanda tool (Kuscu et al., 2018), under the assumption that the tRNA half acts as a non-canonical miRNA. One of them was *Smed ELAC2 KD* SMESG000048842.1, encoding a receptor-type tyrosine

phosphatase. From the GO analysis it was found that this gene is associated with processes like negative regulation of cell proliferation and migration, negative regulation of excitatory synapse and negative regulation of MAPK and JAK/STAT pathways.

Following this prediction, the primary objective was to validate these results *in vivo*. To achieve this, a comprehensive experimental setup was designed and executed. The main goal was to restore 5' tRNA half Gly-GCC levels in *Smed ELAC2* KD planarians to match those of control conditions and assess whether the expression pattern of the identified target transcript was affected. To this end, a novel approach was developed to replenish 5' tRNA half Gly-GCC levels in planarians. Two synthetic 2'-OMe-RNA molecules were used: one mimicked the sequence of the sncRNA of interest (5' tRNA half Gly-GCC), while the other was a scrambled version serving as a control. Both had 5' monophosphate groups to mimic the native structure of 5' termini of 5' tRNA halves and miRNAs, as well as to enable their quantitative analysis using qRT-PCR relying on adapter ligation (section **4.15.3**). The knockdown protocol was performed as described in to establish the experimental conditions: *Smed ELAC2* KD, GFP mock, and WT. Planarians were amputated and incubated in culture solution containing either the 5' tRNA half Gly-GCC mimic, scrambled RNA, or no RNA, following the scheme outlined in section **4.19** (**Figure 30A**), until 5 dpa. In this way, the worms were soaked in small RNA solution and could absorb it, therefore increasing the levels of these molecules. At this time point, worms were collected for qRT-PCR quantification of changes in the levels of 5' tRNA half Gly-GCC and its target transcript. The reference gene used in this analysis displayed similar expression level to SMESG000048842.1 and was not differentially expressed under *Smed ELAC2 KD* conditions, as determined from the NGS data.

Based on the qRT-PCR data, it was first evaluated whether the endogenous 5' tRNA half Gly-GCC was reduced in this experimental setup to a similar extent as observed in the transcriptome profiling experiment. This was assessed by comparing *Smed ELAC2* KD no RNA samples with WT no RNA samples. Additionally, GFP mock no RNA samples were compared with WT no RNA to evaluate 5' tRNA half Gly-GCC levels in GFP dsRNA-injected samples. As shown in **Figure 30C**, the effect was most pronounced in *Smed ELAC2* KD samples, with a ~60-70% reduction—consistent with previous observations.

Next, it was necessary to determine whether 5' tRNA half Gly-GCC was adequately replenished upon soaking. The qRT-PCR results indicated that soaking *Smed ELAC2* KD worms in the 5' tRNA half Gly-GCC mimic solution successfully restored the

levels of this sncRNA to those observed under native conditions, as indicated by the absence of significant differences compared to WT no RNA samples **Figure 30B**.

These results confirmed that the treatment effectively replenished the lost 5' tRNA half Gly-GCC without exceeding physiological levels. Consequently, despite the drop of endogenous level of 5' tRNA half Gly-GCC in *Smed ELAC2* KD worms, the regeneration of these planarians progressed in the presence of exogenously administrated mimic of this sncRNA. Furthermore, the treatment did not exhibit any observable toxic effects on regenerating fragments. Therefore, any changes in target gene expression could be attributed directly to the restoration of the sncRNA molecule.

Finally, the target gene expression was analysed. In *Smed ELAC2* KD worms soaked with the tRNA half mimic, SMESG000048842.1 expression was downregulated compared to *Smed ELAC2* KD planarians treated with scrambled RNA or cultured in no RNA solution (**Figure 30D**). In other words, soaking *Smed ELAC2* KD worms in the tRNA half mimic effectively neutralized the overexpression of SMESG000048842.1, restoring its expression to WT levels. This finding, therefore, indicated that 5' tRNA half Gly-GCC directly regulates the expression of SMESG000048842.1 in *S. mediterranea*. Under physiological conditions, 5' tRNA half Gly-GCC appears to suppress the expression of SMESG000048842.1. However, when *Smed ELAC2* was knocked down, leading to a reduced abundance of 5' tRNA half Gly-GCC, SMESG000048842.1 was notably overexpressed.

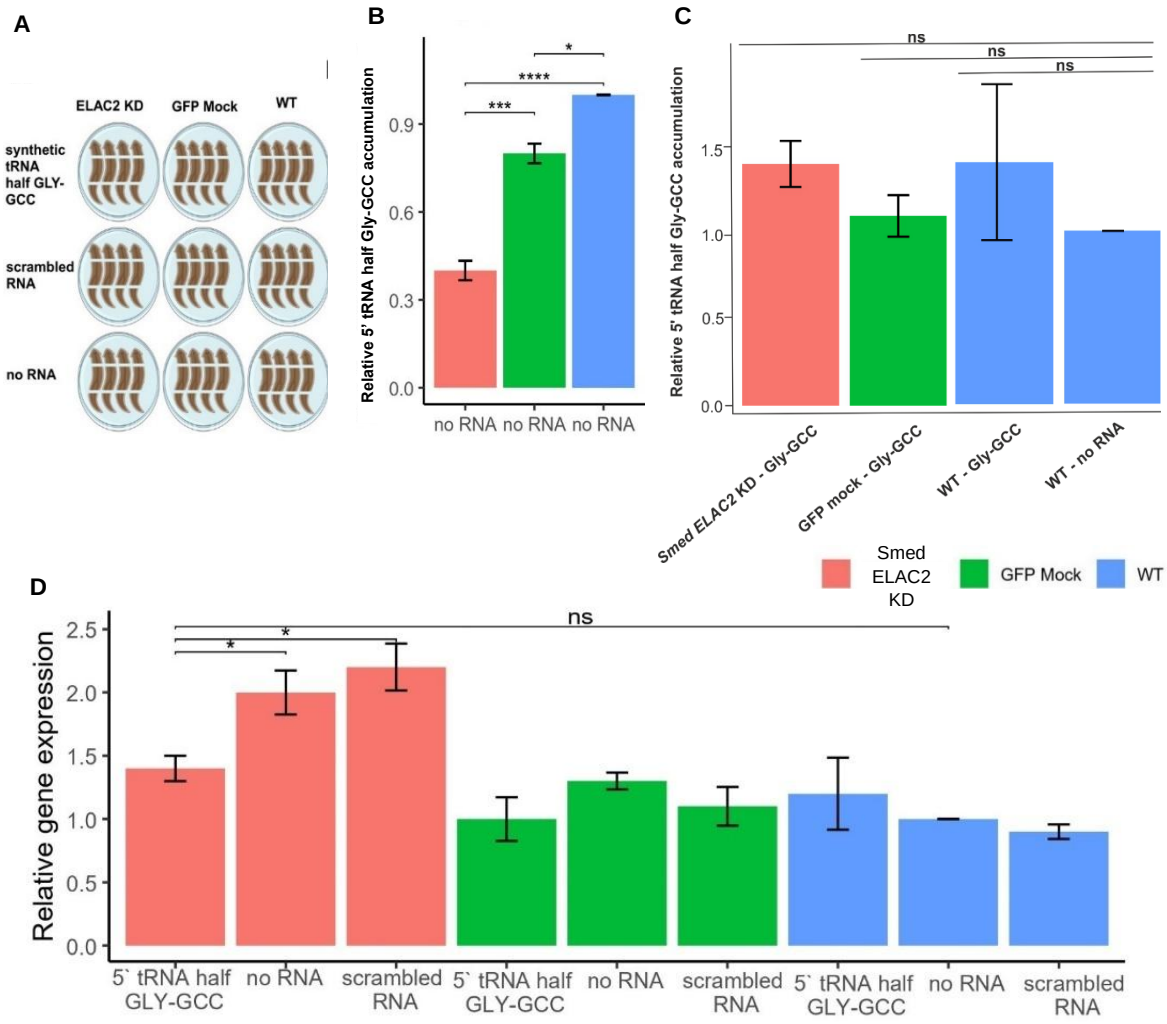

Figure 30. Impact of replenishment of 5`tRNA half Gly-GCC on target gene expression. A) Schematic representation of the mimic experiment design, illustrating three soaking conditions (5′tRNA half Gly-GCC solution, scrambled RNA, and no RNA) applied to three sample types (*Smed ELAC2* knockdown, GFP mock, and WT). B) Relative accumulation of 5′tRNA half Gly-GCC under *Smed ELAC2* knockdown no RNA conditions versus control conditions. Expression data were analyzed using a linear mixed-effects model. Then, pairwise comparisons were made using Tukey's Honest Significant Difference Test and data normality was tested using Shapiro-Wilk test (*p-value: 0.05*) - median values from 3 replicates are presented. C) Accumulation of 5′tRNA half Gly-GCC under different soaking conditions within particular sample types (normalized to WT no RNA control). Expression data were analyzed using a linear mixed-effects model. Then, pairwise comparisons were made using Tukey's Honest Significant Difference Test and data normality was tested using Shapiro-Wilk test (*p-value: 0.05*) - median values from 3 replicates are presented. D) Relative expression of SMESG000048842.1 gene across varied soaking conditions. Statistical analyses were performed using one-way ANOVA followed by Tukey's post hoc and Bonferroni method (*p-value: 0.05*) - median values from 3 replicates are presented.

Furthermore, it was hypothesized that the drastic reduction of this molecule could be a key factor contributing to the observed regeneration delay in *Smed ELAC2 KD* worms. To evaluate this, an initial phenotypic assessment was conducted on four tail-regenerating fragments per replicate for each condition: *Smed ELAC2* knockdown, GFP mock, and WT. All samples were subjected to the previously described soaking conditions. As expected, most of the tail fragments exhibited a similar delay in photoreceptor regeneration in *Smed ELAC2 KD* worms treated with scrambled RNA and no RNA solutions. However, when *Smed ELAC2 KD* worms were soaked in a 5' tRNA half Gly-GCC mimic solution, the regeneration delay phenotype was partially rescued, reducing the proportion of abnormally regenerating worms by almost half. Obviously, increasing the number of worms under study is required to enhance the robustness of this analysis and assess the statistical significance of the observed changes.

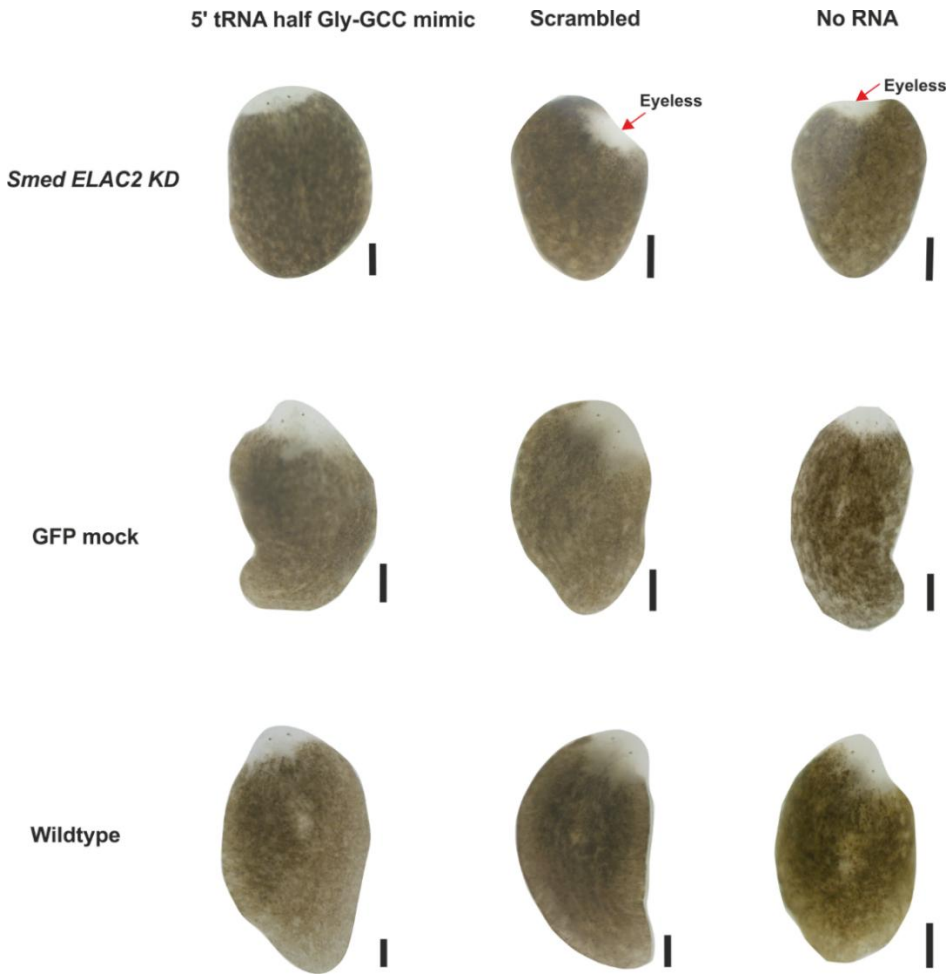

Figure 31. Phenotypic documentation of the rescue experiment. Tracking eye regeneration in *Smed ELAC2* KD, GFP mock and WT anterior regenerating fragments after being soaked in solutions comprising of either of the three components: 5' tRNA half Gly-GCC mimic or scrambled RNA or no RNA. Scale: 200 µm.

Overall, the obtained results demonstrated that 5’ tRNA half Gly-GCC has functional relevance in the context of planarian regeneration and specifically downregulates the expression of target SMESG000048842.1 gene *in vivo*, presumably acting as a non-canonical miRNA.

6. Discussion

6.1. sncRNAs in planarian regeneration

Among the regulatory RNA molecules involved in regeneration in planarians, considerable lines of evidence have been accumulated regarding miRNAs and piRNAs. In recent years, a number of specific miRNAs and piRNA pathway components have been identified as integral to the regenerative process (section **1.6.5**). In contrast, less is known about RNA fragments, with tRFs in particular, which have attracted the increasing attention of the scientific community. tRFs regulate gene expression through various pathways, including epigenetic (Wang et al., 2022) and translational (Jirström et al., 2025) mechanisms. These molecules play essential roles in both cellular homeostasis and pathology (Magee and Rigoutsos, 2020). To date, the tRF landscape in regenerating and non-regenerating planarians has been characterized in only one recent study (Lakshmanan et al., 2021). While this study provided the first-ever analysis of planarian tRF profiles, the field still lacks insights into the functional significance of their differential regulation during regeneration.

In an endeavor to bridge this gap, the current dissertation aimed at the identification and characterization of sncRNAs involved in *S. mediterranea* regeneration, with particular focus on the RNA fragments. Reaching this aim required the development of a strategy that would allow for the disruption of the sncRNA pool, and the regeneration process itself. Subsequent comparison of the disrupted and wild-type pools was conducted to identify ncRNAs essential for proper regeneration. It was assumed that the disruption of the ncRNA pool would be achieved through the silencing of a ribonuclease, whose gene displays elevated expression in neoblasts. The selection of a specific enzyme was guided by the criterion that it should be implicated in a human Mendelian disease, with its silencing leading to regeneration defects at the phenotypic level in *S. mediterranea*. As a result, *Smed ELAC2* was chosen. This strategy proved to be effective, as it has led to a successful identification of molecules undergoing differential accumulation upon impaired regeneration.

6.1.1. sncRNA differentially accumulated upon *Smed ELAC2* silencing and their impact on regeneration

The silencing of *Smed ELAC2* exerted the most pronounced effect on the pool of miRNAs and tRFs. This raises the question, to what extent the observed changes at the phenotypic, anatomical and cellular levels can be directly linked to the functions performed by these sncRNAs.

Two major studies have previously identified various planarian miRNAs (sme-miRs) that are enriched at different regenerative time points, cell types, and locations (Palakodeti et al., 2006; Sasidharan et al., 2013). These studies provide valuable insights into the spatiotemporal enrichment of specific sme-miRs identified as deregulated following *Smed ELAC2* knockdown. Neoblast-enriched sme-miR-36a and differentiated cell-enriched sme-miRs-96b were significantly downregulated following *Smed ELAC2* knockdown. Other downregulated miRNA molecules include sme-miR-8b-3p and sme-miR-87c-5p for which planarian cell-specific enrichment data are not yet available. Specifically, sme-miRs-96b was found to be enriched in the anterior regenerating blastema (Sasidharan et al., 2013). In vertebrates, the miR-96 family is known to be essential for auditory hindbrain development and influences the differentiation of cochlear hair cells in the ear (Kuhn et al., 2011; Schlüter et al., 2018). In the context of cancers, miR-96 has been found to promote cell proliferation and migration (Hong et al., 2016; Ma et al., 2018). Therefore, the downregulation of this molecule, alongside others, may contribute to the observed regeneration delay upon *Smed ELAC2* silencing. Elsewhere, the upregulated Sme-miRs include the neoblast-enriched sme-miR-71a and sme-miR-96a, as well as the differentiated cell-enriched sme-miRs-9a and sme-miR-190a. Among these, sme-miR-190a is typically downregulated during the later stages of regeneration (~3–7 dpa) in both the anterior and posterior blastema (Sasidharan et al., 2013). In the perspective of regeneration in higher vertebrates, miR-190a was found to be involved in osteoblast differentiation and bone regeneration (Lee et al., 2022). The observed upregulation of this molecule at 3 dpa during regeneration of *Smed ELAC2 KD* worms could also account for the observed regeneration abnormalities. Cumulatively, these specific effects within the sme-miR pool could potentially affect the planarian regeneration process. Furthermore, the discovery of several miRNAs whose deregulation aligns with regeneration disorders, highlights the potential for future functional studies on these molecules, aiming to determine their specific role in this process.

Among the tRFs deregulated upon the silencing of *Smed ELAC2*, 5' tRNA half Gly-GCC emerged as the most important one, displaying a profound decrease. Notably, this molecule has been described in the literature in the context of its role in developmental processes and regeneration, as well as being a biomarker for certain cancers (described earlier in **1.5.3**). There is, therefore, a wealth of evidence suggesting that this molecule is directly involved in regeneration. The most significant finding comes from a study in which silencing this tRNA half using a complementary oligonucleotide resulted in head regeneration defects in another planarian species, *D. japonica*, where the affected animals exhibited cyclopia or were eyeless (Cao et al., 2020). This provides a compelling indication that the observed phenotype of eye regeneration defects in the present study directly results from the decreased accumulation of 5' tRNA half Gly-GCC. Accordingly, the obtained results strongly support previous findings and establish 5' tRNA half Gly-GCC as a small regulatory RNA involved in planarian regeneration. Furthermore, they provide additional evidence that this molecule plays a vital role in conserved mechanisms across distant phyla.

The knockdown of *Smed ELAC2* temporarily disrupted anterior regeneration, not only affecting the eye, but also the ventral nerve cords, both being components of the planarian CNS. This aligns with findings in Drosophila, where the *ELAC2* homolog *Jhi-1* was implicated in CNS development (Bivik et al., 2015). Until now, no particular molecular mechanism underlying the conserved function of Elac2 in CNS formation has been established. In the present study, a direct association between Elac2 depletion and a reduction in 5' tRNA half Gly-GCC levels was demonstrated for the first time, with accompanying anatomical evidence of impaired CNS regeneration. Based on these results, it can be proposed that 5' tRNA half Gly-GCC mediates the CNS development in representatives of major invertebrate groups, *Ecdysozoa* (Drosophila) and *Lophotrochozoa* (*S. mediterranea*). Interestingly, the function of 5' tRNA half Gly-GCC in CNS regeneration is conserved also in mammals, as this molecule is upregulated in rat spinal cord injury, where it modulates the MAPK and neurotrophin pathways by targeting BDNF (brain-derived neurotrophic factor), thereby playing a role in injury recovery (Qin et al., 2020). Consistently, the target gene of 5’ tRNA half Gly-GCC identified in this study, a receptor-type tyrosine phosphatase, was found to negatively regulate the MAPK pathway from the GO analysis conducted.

Taken together, these findings indicated that the alteration of the planarian homeostatic levels of 5’ tRNA half Gly-GCC, elicited by *Smed ELAC2* knockdown,

disrupts anterior regeneration and CNS formation. The evidence presented here, along with previous studies, underscores the significance of this molecule in nervous system injury recovery.

6.1.2. Ribonuclease Elac2 in biogenesis of 5' tRNA half Gly-GCC

The major enzymes implicated in the biogenesis of tRFs include Angiogenin and Dicer, which have been reported to generate most types of tRNA-derived molecules, with the formation of tRNA halves being usually attributed to Angiogenin (section **1.5.3**). Elac2 is recognized for its role in producing tRF-1 through cleavage of the 3' trailer sequence of pre-tRNA (Zhu et al., 2020). While the formation of tRNA halves dependent on Angiogenin has been well-characterized, especially in the context of stress conditions, it has also been suggested that these molecules can be produced independently of Angiogenin (Liu et al., 2022). Notably, tRNA halves are evolutionarily conserved, whereas Angiogenin is a protein found only in vertebrates (Sultana et al., 2022). This suggests that tRNA halves are likely generated through several distinct pathways. In the present study, the depletion of Elac2 resulted in a specific reduction of several tRNA halves, with the most significant effect observed for 5' tRNA half Gly-GCC. Based on this, it can be proposed for the first time that Elac2 is involved in the biogenesis of 5' tRNA half Gly-GCC in planaria. Given the evolutionary conservation of both this tRNA half and Elac2, it is tempting to speculate that Elac2 plays a similar role in the production of 5' tRNA half Gly-GCC across species, including mammals. While the involvement of Elac2 in generation of tRNA half has been reported before (Choi et al., 2021), no studies have yet linked the biogenesis of the otherwise well-characterized 5' tRNA half Gly-GCC to Elac2.

Data from Planmine database indicates that *Smed ELAC2* expression is elevated in planarian stem cells, known as X1. This pattern is consistent across phyla and has also been reported in mice (Perez-Iratxeta et al., 2005). Moreover, recently the role of Elac2 in early placental trophoblast differentiation has been described (Liang et al., 2023). The increased production of Elac2 in undifferentiated cell types implies that this ribonuclease is particularly important in these specific cells. Based on the results presented here, it can be proposed that the presence of Elac2 in these cells is not only related to its role in the maturation of tRNA and mitochondrial transcripts, but also to its direct involvement in the biogenesis of the regulatory RNA 5' tRNA half Gly-GCC, which is vital for developmental and regenerative processes.

6.1.3. Downregulation of 5’ tRNA half Gly-GCC and concomitant overexpression of its target gene may cause cellular migration changes during regeneration

Insights into cell-type-specific enrichment of overexpressed genes at 3 and 5 dpa in parenchymal cells, along with associated cellular and molecular pathways, allow for certain speculations. An earlier study identified parenchymal cells as key players in guiding neoblasts during regeneration by providing a contact guidance system (Hori, 1991). More recently, specialized neoblasts particularly those associated with the CNS, were observed in close proximity to parenchymal cells. While this physical association is noteworthy, no direct regulatory role for parenchymal cells in neoblast biology has been established (Park et al., 2023). These findings suggest that parenchymal cells play a role in directing neoblast migration during regeneration. Parenchymal cells could mediate this either by influencing gene expression patterns of adjacent neoblasts or via modulating their own gene expression to indirectly affect neoblast motility. Given that the overexpressed genes in the current study are predominantly expressed in parenchymal cells, the latter scenario appears more plausible. This can be sensed from the overexpression of SMESG000048842.1. The receptor-type tyrosine phosphatase, encoded by this gene, alongside being involved in various other cellular process, was found in the conducted GO analysis to be associated with negative regulation of cell proliferation and migration/motility. Alongside other factors, crucial cell migration influencers include Rho GTPases and actin cytoskeletal remodelling. These proteins are activated through phosphorylation by Rho kinases (ROCK). Antagonistically, certain low molecular weight receptor-type tyrosine phosphatases, such as RhoA, inactivate Rho GTPases (Bidaud-Meynard et al., 2019) by dephosphorylation. It can thus be hypothesized that overexpression of SMESG000048842.1 leads to an inactivation of Rho GTPases and cytoskeletal remodelling, consequently reducing cell migration.

Another noteworthy significance of the overexpression of this particular target gene of 5’tRNA half Gly-GCC is in terms of the observed augmented nuclearity of MuNs. In Xenopus cells *in vitro*, nuclearity of multinucleated cells increased (increase of >2-nucleated cells) in the presence of a ROCK inhibitor (whose function parallels receptor-type tyrosine phosphatases), with a concomitant decrease in 2-nuc multinucleated cells (Sugita et al., 2019). Deriving from this, when considering the current scenario, the overexpression of this receptor-type tyrosine phosphatase could in fact also account for the increase of >2-nuc and decrease of 2-nuc MuNs, perhaps after the impairment of

cytokinesis. Thus, physiological levels of 5' tRNA half Gly-GCC appear to suppress the expression of this phosphatase gene, thereby promoting cell migration—an essential process for regeneration. It should be noted that the receptor-type tyrosine phosphatase family is a large group of proteins, with its members being involved in many biological processes (Tonks and Neel, 1996). The identity of SMESG000048842.1 gene and the protein it encodes was established through homology analysis based on sequence data. This gene has not been directly studied in *S. mediterranea* yet. Thus, the results obtained here regarding the hypothetical impact of the receptor-type tyrosine phosphatase on cell migration, open the possibility for new research. Further studies are necessary to ultimately determine whether and how the overexpression of this gene contributes to regeneration disorders.

6.1.4. Mechanism of 5' tRNA half Gly-GCC based gene silencing

The severe downregulation of 5' tRNA half Gly-GCC upon *Smed ELAC2* knockdown pointed towards a specific molecular role that this molecule possesses in regeneration under physiological conditions. Although 5' tRNA halves have been implicated in multiple processes, this study focused on their involvement in post-transcriptional gene repression. Two possible pathways ending up in silencing of the target gene were considered. In one of these, Elac2 ribonuclease uses specific 5' tRNA halves as guide RNA molecules to bind to the target transcripts, further cleaving the target RNA (Elbarbary et al., 2009). The other mechanism utilizes a seed-based complementarity between certain 5' tRNA halves and target RNA. However, miRNA-like seed targeting to 3'UTR region of target genes rarely applies to these molecules. Instead, 5'tRNA half molecules such Gly-GCC and Glu-CTC bind to the target within the coding sequence (CDS) or 3'UTR with a binding length of 5-10 nt, producing a gene silencing effect, via a mechanism that is not yet fully understood (Jehn et al., 2020; Luo et al., 2018). In case of the present study, both these approaches were tested to identify possible 5' tRNA half Gly-GCC targets within the list of DEGs. While the first approach yielded no target genes, portraying that Elac2 and 5' tRNA half mediated silencing might not be true in this case, the second approach did yield three potential targets (via binding to the CDS of the target genes). Of these three, one of them turned out to be the most promising candidate which could be functionally validated to be targeted by 5' tRNA half Gly-GCC – this was the gene coding for the receptor-type tyrosine phosphatase.

Based on the obtained results, the following model of 5' tRNA half Gly-GCC function can be proposed. After production by Smed Elac2, 5'tRNA half Gly-GCC is released to be bound by either an intermediary RNA-binding protein or the direct effector. The constant state of being bound by proteins is necessary to protect these single stranded naïve ncRNA molecules from random RNase cleavage (**Figure 32**).

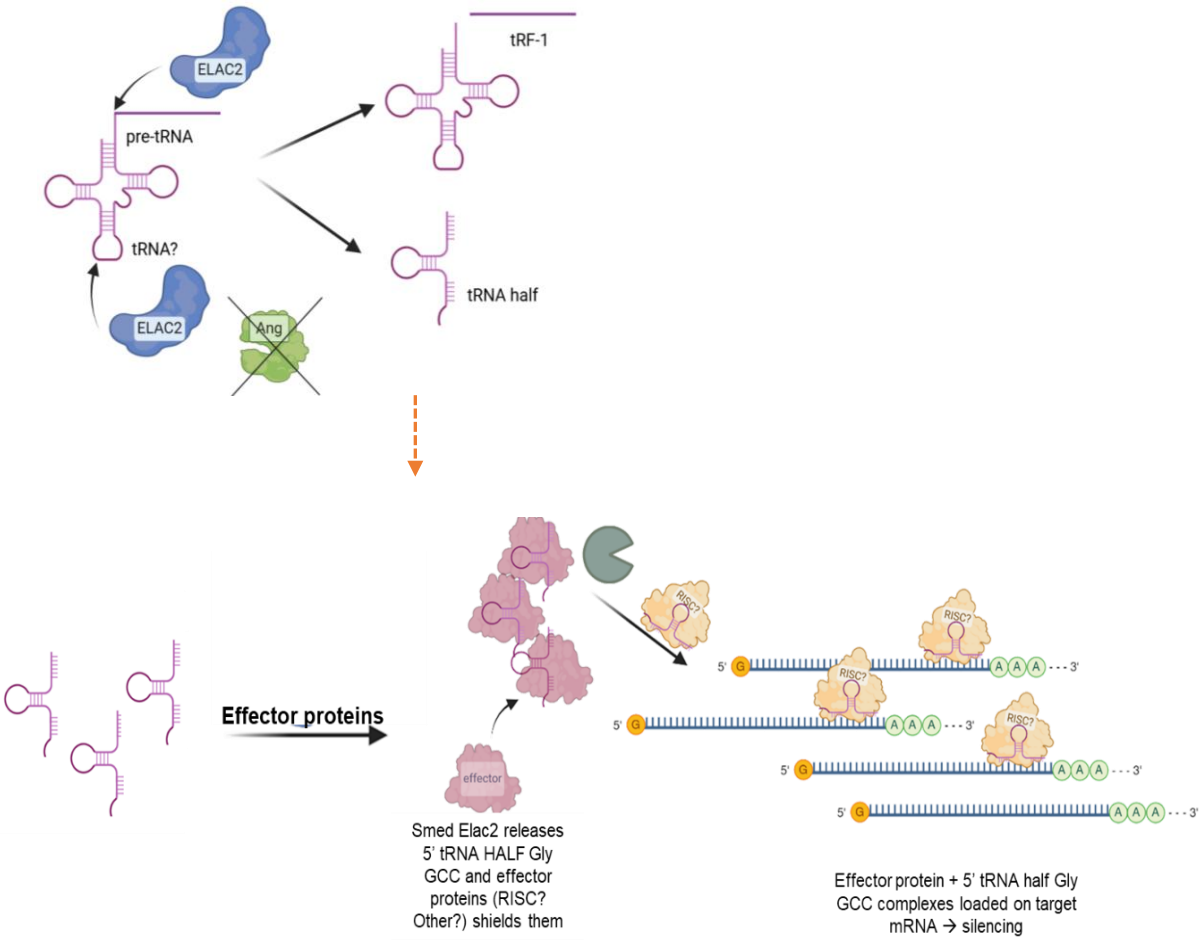

Figure 32. Proposed model for 5' tRNA half Gly-GCC formation and its silencing function. Smed Elac2 is involved in the production of 5' tRNA half Gly-GCC and after being released from Smed Elac2 protein molecules, these tRFs are bound by other effector proteins that ultimately facilitate the 5' tRNA half Gly-GCC mediated target mRNA silencing process.

This mode is supported by a set of results from the tRNA half mimic experiment, performed for the functional validation of 5'tRNA half Gly-GCC. It was observed that the level of this molecule could not exceed a certain physiological threshold in the planarian cells. This can be concluded from the observation that there was no significant increase of this molecule past this arbitrary threshold in GFP mock and WT worms soaked in the 5' tRNA half Gly-GCC mimic solution. Also, in the case of *Smed ELAC2* knockdown, where this molecule was originally severely downregulated, the exogenous administration of the

mimic led to an increase of 5’ tRNA half Gly-GCC only up to the physiological threshold, no further. This suggest that there exists a state of equilibrium between 5’ tRNA half Gly-GCC and its protein partner(s), and any additional amount of this tRF is not efficiently shielded and thus cleared. Ultimately, the complex including 5’ tRNA half Gly-GCC and effector protein binds to the CDS region of target mRNA, which leads to a post-transcriptional silencing either via target cleavage or via translational inhibition and subsequent mRNA decay (**Figure 32**). Based on this model, further research can now be initiated towards the identification of the effector protein of 5’ tRNA half Gly-GCC. The approach of target prediction applied in this study assumed a miRNA-like interaction between this tRF and mRNA, and consequently RISC emerges as a key candidate effector. However, other proteins should be considered as well, because it is not clear whether the functions of 5’ tRNA halves are necessarily Ago2-dependent (Jehn et al., 2020; Luo et al., 2018).

Overall, this study reveals several novel aspects regarding the roles of ncRNA classes such as tRFs in planarian regeneration. The study not only functionally characterised the Smed Elac2 enzyme in planarians but also revealed that depletion of this enzyme could disrupt the planarian ncRNA pool and result in alterations visible at every level of planarian physiology– from gene expression to morphology. Additionally, evidence was provided for the intricate involvement of a 5’tRNA half Gly-GCC in regenerative processes in planarians. The identification of this 5’ tRNA half under *Smed ELAC2* knockdown conditions has implications even in human Mendelian diseases associated with Elac2 functional disruptions. As for now, researchers have mostly focused on the mitochondrial aspect of Elac2 disruption in COXPD-17 (Haack et al., 2013). The present study opens an untouched avenue to be explored in this disease – the pool of tRFs, especially 5’tRNA half Gly-GCC. Future studies to validate the mechanistic details proposed here shall require the advancement in protein-level analyses in planarians.

6.2. Multinucleated cells in planarian regeneration

Polyploidization occurs in both development and disease, including cancer, with mechanisms and outcomes varying across contexts. Multinucleated cells, or MuNs, are types of polyploid cells playing crucial roles in processes like development, regeneration, and wound repair across species (Anatskaya and Vinogradov, 2022). Despite their importance, MuNs have remained largely unexplored in planarians. Prior to this study,

such cells had been documented in asexual planarians only once, linked to an externally induced abnormality (Lai et al., 2018).

This dissertation presents the first report on the identification and preliminary molecular characterization of MuNs in wild-type planarian. Conventional flow cytometry cannot resolve MuNs from events exhibiting high nuclear dye signals due to other factors, like cells in DNA synthesis (S) phase. Microscopy, while providing high-resolution imaging and information about the signal location, is limited in capturing the full diversity of cell types in organisms like planarians due to biases introduced by tissue sections, restricted field of views under study and inadequate throughput. Utilizing the imaging flow cytometry platform, combined with the traditional FACS, an innovative method was developed to overcome the limitations of microscopy and conventional flow cytometry, and study the rare planarian MuNs.

Cell diameter measurements from IS-generated BF images showed that MuNs are significantly larger than MoNs, while nuclear sizes remain consistent across cells of varied nuclearities. This suggested that MuNs are polyploid, with each nucleus containing genetic material comparable to that of diploid MoNs. Therefore, it can be proposed that planarian MuNs are formed through cell fusion and/or endomitotic events, rather than endocycling, as no nuclear enlargement was observed (Shu et al., 2018). Further supporting this, MuNs with both odd and even nuclearities were identified. The presence of MuNs in similar proportions under both wild-type regenerating and non-regenerating conditions suggests that they are physiological cell types. Additionally, the observed MuNs lacked any prominent hallmarks of pathological polyploidization often seen in cancers, such as abnormal nuclear shapes or the presence of micronuclei. Micronuclei form when lagging chromosomes fail to integrate into the main nucleus due to erroneous microtubule-kinetochore attachments. These structures lack intact nuclear envelopes, which cause nuclear content leakage (Crasta et al., 2012; Dörnen et al., 2020; Hatch et al., 2013), a feature not detected in the case of MuNs. Upon *Smed ELAC2* knockdown, a shift in the proportion of >2-nuc versus 2-nuc MuNs was observed – whereby >2-nuc ones increased with a concomitant decrease in 2-nuc ones. This can either be interpreted as: a) a negative outcome of *Smed ELAC2* knockdown, or b) a compensatory pathway in response to some of the negative effects of *Smed ELAC2* knockdown.

As discussed in details in the previous chapter (section **6.1.3**), the increase in MuNs' nuclearity may result from impaired cytoskeletal assembly and function giving rise

to increased numbers of >2-nuc cells. This scenario underlines the negative impact on regeneration of *Smed ELAC2* knockdown. In the other scenario, however, the increased nuclearity could be beneficial in context of organismal regeneration. For example, in zebrafish heart regeneration, while both mononucleated and multinucleated cells contribute to tissue repair, multinucleated cells exhibit enhanced surface coverage and migration velocities compared to their mononucleated counterparts (Cao et al., 2017). Additionally, polyploidy via endoreplication serves as a compensatory mechanism for tissue formation when cell proliferation is impaired, as observed in both zebrafish heart and murine liver regeneration (Cao et al., 2017; Lazzerini Denchi et al., 2006). Drawing from these observations, the increased nuclearity of MuNs may act as a compensatory adaptation to counteract the regeneration delay caused by *Smed ELAC2* knockdown, particularly by mitigating the negative impact on cell proliferation and migration. It is plausible that >2-nuc MuNs are more effective in compensating for these disruptions than their 2-nuc counterparts.

Next, the marker gene expression analyses and neoblast ablation studies provided initial insights into the differentiative potential and possible functions of MuNs in planarians. It can be proposed that MuNs are likely undifferentiated cells, possibly progenitors, based on several key observations. Firstly, in wild-type worms, FACS population E containing MuNs was majorly composed of undifferentiated cells (~70%) – with highest expression of the late epidermal progenitor marker *AGAT1* among all populations analysed (**Figure 18**). Secondly, the neoblast elimination via *H2B* KD had the greatest negative impact on FACS population D, where it caused a pronounced reduction of cell percentage, while population E was less affected (**Figure 20D**). Lastly, a direct visual inspection of MuNs unequivocally demonstrated that their proportion in the total cell pool declined in *H2B* KD worms (**Figure 20B**). Based on the literature data regarding the specific cell types under *H2B* KD conditions at day 5 post-RNAi, one would expect clearance of MuNs if they were neoblasts. In contrast, if these cells were differentiated, no effect would be anticipated (Solana et al., 2012). The observed pattern of their limited decline instead indicates that MuNs could be progenitors. In this context, an important question arises whether MuNs represent a single lineage and, if so, whether they are of epidermal identity.

Population E, comprising MuNs, harbors a substantial proportion of *AGAT1+* cells (**Figure 15A**), which represent late epidermal progenitors (Eisenhoffer et al., 2008).

The planarian epidermal lineage is well-characterized and originates from zeta neoblasts within the mesenchyme (van Wolfswinkel et al., 2014; Wurtzel et al., 2017). The marker genes *Smed nb_21.11e* and *Smed AGAT1* are associated with early and late epidermal progenitors, respectively, and previous study showed that their expression diminished to varying degrees upon *H2B* knockdown, with *Smed nb_21.11e* decreasing more than *Smed AGAT1*. Moreover, while *Smed nb_21.11e* became undetectable at day 10 post-RNAi, cells expressing *Smed AGAT1* persisted throughout the follow-up, as long as 20 days (Solana et al., 2012). The extent of *Smed AGAT1* reduction level in unsorted cells from *H2B* KD worms (**Figure 20A**) closely parallels the decrease in the number of MuNs (**Figure 20B**). It is tentative to speculate, based on this observation, that MuNs may be late epidermal progenitors. Currently, there are no effective methods available for the analysis of marker genes specifically in MuNs. This is due to the fact that in flow cytometry they do not form a distinctive population that could be selectively gated for cell sorting. Even with the latest imaging-based sorting instruments, little additional insight is likely to be gained unless precise automated approaches exist to identify MuNs in real time rather than post-acquisition. In addition, the application of *in situ* hybridization techniques, widely used in planarian research, is challenging, as these cells are rare, which makes it difficult to ensure reproducibility and statistical robustness.

One of the outstanding questions of the study concerns the causes of the observed decline of MuNs following *H2B* knockdown. Assuming these are indeed progenitor cells, two alternative explanations can be considered. According to the first, MuNs are a dynamic population and continuously give rise to differentiated cells, while relying on neoblasts for replenishment. When neoblasts are ablated, the population of MuNs cannot be renewed. In the second scenario, after *H2B* knockdown MuNs, undergo ploidy reduction to restore diploid progenitors or, through dedifferentiation, revert to stem cells. Both of these mechanisms warrant further investigation to determine which one is responsible for the observed effects. It would be valuable to determine whether, in an extended period following neoblast depletion, MuNs disappear completely or only decrease, while acting as a stable reservoir of cells.

Naturally occurring polyploid cells, found for example in *Drosophila* and mammalian tissues, are typically post-mitotic and rarely proliferative but exhibit high ploidy plasticity to meet functional demands (Windmueller et al., 2020). They utilize this plasticity in regeneration by functioning either as reservoirs of diploid cells or as

immediate effectors in wound healing. The first mechanism occurs during starvation in *Drosophila*, when intestinal stem cells are depleted and rapidly reappear upon feeding, largely through depolyploidization of 4n enterocyte lineage cells (Lucchetta and Ohlstein, 2017). Similarly, mammalian hepatocytes reduce ploidy under proliferative stimuli, such as during post-injury regeneration or during metabolic stress (Duncan et al., 2010). The second mechanism takes place elsewhere in *Drosophila*, where polyploidization mitigates tissue loss, from epidermal wounds to hindgut damage, via cell fusion and repeated endocycles (Losick et al., 2013). Planarian MuNs, owing to their stability in distribution under both regenerating and non-regenerating conditions (**Figure 19B**), seemingly function as diploid cell reservoirs in times of need. This hypothesis can also be supported by the observation about their drop during neoblast ablation, where they could possibly function in repopulating diploid cells pool via depolyploidization. However, it is also important to note that multinucleated cells are present under physiological conditions in various organisms, where they arise through the formation of syncytia. In *C. elegans* and *Drosophila*, syncytia play a crucial role not only in development but also in the physiology of the adult organism (Alper and Podbilewicz, 2008; Kloc et al., 2024). Thus, further studies on the mechanisms underlying the formation of planarian MuNs are necessary for a proper understanding of their functions and significance in an evolutionary context.

In conclusion, the identification of MuNs in *S. medit*erranea introduces a novel factor into the extensively studied process of planarian regeneration. Notably, the current research suggests that these newly identified cells may play a critical role in coordinating regeneration under conditions of cellular proliferation and migratory stress, such as those induced by *Smed ELAC2* knockdown. Ultimately, this discovery paves the way for a deeper and more refined understanding of this complex biological phenomenon.

7. Conclusions

The results obtained from the research conducted for this doctoral dissertation have led to the following conclusions:

1. *Smed ELAC2*, the planarian homolog of the tRNA-processing Elac2/tRNase Z gene, encodes a protein containing all domains necessary for both its ribonuclease activity and subcellular trafficking, including the mitochondrial localization signal.
2. Knockdown of *Smed ELAC2* phenotypically and anatomically manifests as eye regeneration delay and ventral nerve cord formation defect, respectively, during planarian anterior regeneration.
3. The fractions of X1, X2, and Xins cell populations remain unchanged between *Smed ELAC2 KD* worms and controls over the course of regeneration.
4. *S. mediterranea* harbors a population of multinucleated cells (MuNs), likely of progenitor identity, consistently present throughout regeneration.
5. The nuclearity (number of nuclei per cell) ratio of MuNs — categorized as >2-nuc versus 2-nuc MuNs — increases upon *Smed ELAC2* knockdown over the course of regeneration.
6. The silencing of *Smed ELAC2* disrupts the maturation of mitochondrial transcripts.
7. Differential gene expression analysis of *Smed ELAC2* knockdown versus control samples revealed negative regulation of crucial processes such as synaptic transmission, cell proliferation and migration.
8. The classes of sncRNA, most significantly affected by *Smed ELAC2* knockdown, are miRNAs and tRFs, with 5’tRNA half Gly-GCC displaying a pronounced decrease.
9. Ribonuclease Smed Elac2 emerges as being involved in biogenesis of 5’tRNA half Gly-GCC
10. 5’tRNA half Gly-GCC functions as a regulatory RNA *in vivo* and mediates posttranscriptional silencing of the receptor-type tyrosine phosphatase gene (SMESG000048842.1).

8. References

Agata, K., Saito, Y., Nakajima, E., 2007. Unifying principles of regeneration I: Epimorphosis versus morphallaxis. Dev Growth Differ 49, 73–78. https://doi.org/10.1111/j.1440-169X.2007.00919.x

Aguilar, P.S., Baylies, M.K., Fleissner, A., Helming, L., Inoue, N., Podbilewicz, B., Wang, H., Wong, M., 2013. Genetic basis of cell–cell fusion mechanisms. Trends in Genetics 29, 427–437. https://doi.org/10.1016/j.tig.2013.01.011

Akkouche, A., Grentzinger, T., Fablet, M., Armenise, C., Burlet, N., Braman, V., Chambeyron, S., Vieira, C., 2013. Maternally deposited germline piRNAs silence the *tirant* retrotransposon in somatic cells. EMBO Rep 14, 458–464. https://doi.org/10.1038/embor.2013.38

Allikka Parambil, S., Li, D., Zelko, M., Poulet, A., van Wolfswinkel, J.C., 2024. piRNA generation is associated with the pioneer round of translation in stem cells. Nucleic Acids Res 52, 2590–2608. https://doi.org/10.1093/nar/gkad1212

Al-Mukhtar, K.A.K., Webb, A.C., 1971. An ultrastructural study of primordial germ cells, oogonia and early oocytes in *Xenopus laevis*. Development 26, 195–217. https://doi.org/10.1242/dev.26.2.195

Alper, S., Podbilewicz, B., 2008. Cell Fusion in Caenorhabditis elegans. pp. 53–74. https://doi.org/10.1007/978-1-59745-250-2_4

Alvarado, A.S., 2000. Regeneration in the metazoans: why does it happen? BioEssays 22, 578–590. https://doi.org/https://doi.org/10.1002/(SICI)1521-1878(200006)22:6<578::AID-BIES11>3.0.CO;2-#

Alvarado, A.S., Newmark, P.A., Robb, S.M.C., Juste, R., 2002. The *Schmidtea mediterranea* database as a molecular resource for studying platyhelminthes, stem cells and regeneration. Development 129, 5659–5665. https://doi.org/10.1242/dev.00167

Álvarez-Presas, M., Baguñà, J., Riutort, M., 2008. Molecular phylogeny of land and freshwater planarians (Tricladida, Platyhelminthes): From freshwater to land and back. Mol Phylogenet Evol 47, 555–568. https://doi.org/10.1016/j.ympev.2008.01.032

Anatskaya, O. V., Vinogradov, A.E., 2022. Polyploidy as a Fundamental Phenomenon in Evolution, Development, Adaptation and Diseases. Int J Mol Sci 23, 3542. https://doi.org/10.3390/ijms23073542

Aránega, A.E., Lozano-Velasco, E., Rodriguez-Outeiriño, L., Ramírez de Acuña, F., Franco, D., Hernández-Torres, F., 2021. MiRNAs and Muscle Regeneration: Therapeutic Targets in Duchenne Muscular Dystrophy. Int J Mol Sci 22, 4236. https://doi.org/10.3390/ijms22084236

Aravin, A.A., Sachidanandam, R., Girard, A., Fejes-Toth, K., Hannon, G.J., 2007. Developmentally Regulated piRNA Clusters Implicate MILI in Transposon Control. Science (1979) 316, 744–747. https://doi.org/10.1126/science.1142612

Arenas Gómez, C.M., Sabin, K.Z., Echeverri, K., 2020. Wound healing across the animal kingdom: Crosstalk between the immune system and the extracellular matrix. Developmental Dynamics 249, 834–846. https://doi.org/10.1002/dvdy.178

Arendt, D., Musser, J.M., Baker, C.V.H., Bergman, A., Cepko, C., Erwin, D.H., Pavlicev, M., Schlosser, G., Widder, S., Laubichler, M.D., Wagner, G.P., 2016. The origin and evolution of cell types. Nat Rev Genet 17, 744–757. https://doi.org/10.1038/nrg.2016.127

Arora, K., Nüsslein-Volhard, C., 1992. Altered mitotic domains reveal fate map changes in *Drosophila* embryos mutant for zygotic dorsoventral patterning genes. Development 114, 1003–1024. https://doi.org/10.1242/dev.114.4.1003

Aztekin, C., 2024. Mechanisms of regeneration: to what extent do they recapitulate development? Development 151. https://doi.org/10.1242/dev.202541

Aztekin, C., Hiscock, T.W., Marioni, J.C., Gurdon, J.B., Simons, B.D., Jullien, J., 2019. Identification of a regeneration-organizing cell in the *Xenopus* tail. Science (1979) 364, 653–658. https://doi.org/10.1126/science.aav9996

Bailey, E.C., Kobielski, S., Park, J., Losick, V.P., 2021. Polyploidy in Tissue Repair and Regeneration. Cold Spring Harb Perspect Biol 13, a040881. https://doi.org/10.1101/cshperspect.a040881

Bartel, D.P., 2018. Metazoan MicroRNAs. Cell 173, 20–51. https://doi.org/10.1016/j.cell.2018.03.006

Basu, U., Bostwick, A.M., Das, K., Dittenhafer-Reed, K.E., Patel, S.S., 2020. Structure, mechanism, and regulation of mitochondrial DNA transcription initiation. Journal of Biological Chemistry 295, 18406–18425. https://doi.org/10.1074/jbc.REV120.011202

Bely, A.E., Nyberg, K.G., 2010. Evolution of animal regeneration: re-emergence of a field. Trends Ecol Evol 25, 161–170. https://doi.org/10.1016/j.tree.2009.08.005

Bidaud-Meynard, A., Binamé, F., Lagrée, V., Moreau, V., 2019. Regulation of Rho GTPase activity at the leading edge of migrating cells by p190RhoGAP. Small GTPases 10, 99–110. https://doi.org/10.1080/21541248.2017.1280584

Bivik, C., Bahrampour, S., Ulvklo, C., Nilsson, P., Angel, A., Fransson, F., Lundin, E., Renhorn, J., Thor, S., 2015. Novel Genes Involved in Controlling Specification of *Drosophila* FMRFamide Neuropeptide Cells. Genetics 200, 1229–1244. https://doi.org/10.1534/genetics.115.178483

Brodbeck, W.G., Anderson, J.M., 2009. Giant cell formation and function. Curr Opin Hematol 16, 53–57. https://doi.org/10.1097/MOH.0b013e32831ac52e

Brosnan, C.A., Palmer, A.J., Zuryn, S., 2021. Cell-type-specific profiling of loaded miRNAs from Caenorhabditis elegans reveals spatial and temporal flexibility in Argonaute loading. Nat Commun 12, 2194. https://doi.org/10.1038/s41467-021-22503-7

Burton, P.M., Finnerty, J.R., 2009. Conserved and novel gene expression between regeneration and asexual fission in Nematostella vectensis. Dev Genes Evol 219, 79–87. https://doi.org/10.1007/s00427-009-0271-2

Cao, J., Wang, J., Jackman, C.P., Cox, A.H., Trembley, M.A., Balowski, J.J., Cox, B.D., De Simone, A., Dickson, A.L., Di Talia, S., Small, E.M., Kiehart, D.P., Bursac, N., Poss, K.D., 2017. Tension Creates an Endoreplication Wavefront that Leads Regeneration of Epicardial Tissue. Dev Cell 42, 600-615.e4. https://doi.org/10.1016/j.devcel.2017.08.024

Cao, Z., Rosenkranz, D., Wu, S., Liu, H., Pang, Q., Zhang, X., Liu, B., Zhao, B., 2020. Different classes of small RNAs are essential for head regeneration in the planarian Dugesia japonica. BMC Genomics 21, 876. https://doi.org/10.1186/s12864-020-07234-1

Carranza, S., Littlewood, D.T.J., Clough, K.A., Ruiz-Trillo, I., Baguñà, J., Riutort, M., 1998. A robust molecular phylogeny of the Tricladida (Platyhelminthes: Seriata) with a discussion on morphological synapomorphies. Proc R Soc Lond B Biol Sci 265, 631–640. https://doi.org/10.1098/rspb.1998.0341

Cary, G.A., Wolff, A., Zueva, O., Pattinato, J., Hinman, V.F., 2019. Analysis of sea star larval regeneration reveals conserved processes of whole-body regeneration across the metazoa. BMC Biol 17, 16. https://doi.org/10.1186/s12915-019-0633-9

Cazet, J., Juliano, C., 2020. Oral Regeneration Is the Default Pathway Triggered by Injury in *Hydra*. https://doi.org/10.1101/2020.07.06.189811

Chen, C.-Y., Yueh, W.-T., Chen, J.-H., 2020. Canonical Wnt Signaling is Involved in Anterior Regeneration of the Annelid *Aeolosoma viride*. https://doi.org/10.1101/2020.03.01.972448

Chen, P.Y., Manninga, H., Slanchev, K., Chien, M., Russo, J.J., Ju, J., Sheridan, R., John, B., Marks, D.S., Gaidatzis, D., Sander, C., Zavolan, M., Tuschl, T., 2005. The developmental miRNA profiles of zebrafish as determined by small RNA cloning. Genes Dev 19, 1288–1293. https://doi.org/10.1101/gad.1310605

Chen, Q., Yan, M., Cao, Z., Li, X., Zhang, Yunfang, Shi, J., Feng, G., Peng, H., Zhang, X., Zhang, Ying, Qian, J., Duan, E., Zhai, Q., Zhou, Q., 2016. Sperm tsRNAs contribute to intergenerational inheritance of an acquired metabolic disorder. Science (1979) 351, 397–400. https://doi.org/10.1126/science.aad7977

Chen, S., Ben, S., Xin, J., Li, S., Zheng, R., Wang, H., Fan, L., Du, M., Zhang, Z., Wang, M., 2021. The biogenesis and biological function of PIWI-interacting RNA in cancer. J Hematol Oncol 14, 93. https://doi.org/10.1186/s13045-021-01104-3

Chen, X., 2025. Stem cells (neoblasts) and positional information jointly dominate regeneration in planarians. Heliyon 11, e41833. https://doi.org/10.1016/j.heliyon.2025.e41833

Cheng, E.-C., Kang, D., Wang, Z., Lin, H., 2014. PIWI Proteins Are Dispensable for Mouse Somatic Development and Reprogramming of Fibroblasts into Pluripotent Stem Cells. PLoS One 9, e97821. https://doi.org/10.1371/journal.pone.0097821

Choi, E.-J., Wu, W., Zhang, K., Lee, I., Kim, I.-H., Lee, Y.S., Bao, X., 2021. ELAC2, an Enzyme for tRNA Maturation, Plays a Role in the Cleavage of a Mature tRNA to Produce a tRNA-Derived RNA Fragment During Respiratory Syncytial Virus Infection. Front Mol Biosci 7. https://doi.org/10.3389/fmolb.2020.609732

Cohen, E., Allen, S.R., Sawyer, J.K., Fox, D.T., 2018. Fizzy-Related dictates A cell cycle switch during organ repair and tissue growth responses in the Drosophila hindgut. Elife 7. https://doi.org/10.7554/eLife.38327

Crasta, K., Ganem, N.J., Dagher, R., Lantermann, A.B., Ivanova, E. V., Pan, Y., Nezi, L., Protopopov, A., Chowdhury, D., Pellman, D., 2012. DNA breaks and chromosome pulverization from errors in mitosis. Nature 482, 53–58. https://doi.org/10.1038/nature10802

Dallaire, A., Frédérick, P.-M., Simard, M.J., 2018. Somatic and Germline MicroRNAs Form Distinct Silencing Complexes to Regulate Their Target mRNAs Differently. Dev Cell 47, 239-247.e4. https://doi.org/10.1016/j.devcel.2018.08.022

Daughters, R.S., Chen, Y., Slack, J.M.W., 2011. Origin of muscle satellite cells in the *Xenopus* embryo. Development 138, 821–830. https://doi.org/10.1242/dev.056481

De Robertis, E.M., 2010. Wnt Signaling in Axial Patterning and Regeneration: Lessons from Planaria. Sci Signal 3. https://doi.org/10.1126/scisignal.3127pe21

Dean, M.R.P., Duncan, E.M., 2020. Laboratory Maintenance and Propagation of Freshwater Planarians. Curr Protoc Microbiol 59. https://doi.org/10.1002/cpmc.120

Dexheimer, P.J., Cochella, L., 2020. MicroRNAs: From Mechanism to Organism. Front Cell Dev Biol 8. https://doi.org/10.3389/fcell.2020.00409

Dhahbi, J.M., Spindler, S.R., Atamna, H., Yamakawa, A., Boffelli, D., Mote, P., Martin, D.I., 2013. 5′ tRNA halves are present as abundant complexes in serum, concentrated in blood cells, and modulated by aging and calorie restriction. BMC Genomics 14, 298. https://doi.org/10.1186/1471-2164-14-298

Di Leva, G., Croce, C.M., 2010. Roles of small RNAs in tumor formation. Trends Mol Med 16, 257–267. https://doi.org/10.1016/j.molmed.2010.04.001

Dippold, R.P., Vadigepalli, R., Gonye, G.E., Hoek, J.B., 2012. Chronic ethanol feeding enhances miR-21 induction during liver regeneration while inhibiting proliferation in rats. American Journal of Physiology-Gastrointestinal and Liver Physiology 303, G733–G743. https://doi.org/10.1152/ajpgi.00019.2012

Donne, R., Saroul-Aïnama, M., Cordier, P., Celton-Morizur, S., Desdouets, C., 2020. Polyploidy in liver development, homeostasis and disease. Nat Rev Gastroenterol Hepatol 17, 391–405. https://doi.org/10.1038/s41575-020-0284-x

Dörnen, J., Sieler, M., Weiler, J., Keil, S., Dittmar, T., 2020. Cell Fusion-Mediated Tissue Regeneration as an Inducer of Polyploidy and Aneuploidy. Int J Mol Sci 21, 1811. https://doi.org/10.3390/ijms21051811

Duncan, A.W., Hanlon Newell, A.E., Bi, W., Finegold, M.J., Olson, S.B., Beaudet, A.L., Grompe, M., 2012. Aneuploidy as a mechanism for stress-induced liver adaptation. Journal of Clinical Investigation 122, 3307–3315. https://doi.org/10.1172/JCI64026

Duncan, A.W., Taylor, M.H., Hickey, R.D., Hanlon Newell, A.E., Lenzi, M.L., Olson, S.B., Finegold, M.J., Grompe, M., 2010. The ploidy conveyor of mature hepatocytes as a source of genetic variation. Nature 467, 707–710. https://doi.org/10.1038/nature09414

Dutta A., Zaremba A., Jackowiak P., 2025. Ribonucleases in Mendelian disease – characterization and insight from model organisms. Genes & Diseases.

Echeverri, K., Tanaka, E.M., 2002. Ectoderm to Mesoderm Lineage Switching During Axolotl Tail Regeneration. Science (1979) 298, 1993–1996. https://doi.org/10.1126/science.1077804

Eddy, E.M., 1974. Fine structural observations on the form and distribution of nuage in germ cells of the rat. Anat Rec 178, 731–757. https://doi.org/10.1002/ar.1091780406

Eisenhoffer, G.T., Kang, H., Alvarado, A.S., 2008. Molecular Analysis of Stem Cells and Their Descendants during Cell Turnover and Regeneration in the Planarian *Schmidtea mediterranea*. Cell Stem Cell 3, 327–339. https://doi.org/10.1016/j.stem.2008.07.002

Elbarbary, R.A., Takaku, H., Uchiumi, N., Tamiya, H., Abe, M., Takahashi, M., Nishida, H., Nashimoto, M., 2009. Modulation of Gene Expression by Human Cytosolic tRNase ZL through 5′-Half-tRNA. PLoS One 4, e5908. https://doi.org/10.1371/journal.pone.0005908

Fan, Y., Bergmann, A., 2008. Apoptosis-induced compensatory proliferation. The Cell is dead. Long live the Cell! Trends Cell Biol 18, 467–473. https://doi.org/10.1016/j.tcb.2008.08.001

Fang, Y., Liu, Y., Yan, Y., Shen, Y., Li, Z., Li, X., Zhang, Y., Xue, Z., Peng, C., Chen, X., Cao, K., Zhou, J., 2021. Differential Expression Profiles and Function Predictions for tRFs & tiRNAs in Skin Injury Induced by Ultraviolet Irradiation. Front Cell Dev Biol 9. https://doi.org/10.3389/fcell.2021.707572

Farrell, J.A., O'Farrell, P.H., 2014. From Egg to Gastrula: How the Cell Cycle Is Remodeled During the *Drosophila* Mid-Blastula Transition. Annu Rev Genet 48, 269–294. https://doi.org/10.1146/annurev-genet-111212-133531

Ffrench, B., O'Leary, J.J., Gallagher, M.F., 2015. Therapeutically Targeting Epigenetic Regulation of Cancer Stem Cells, in: Epigenetic Cancer Therapy. Elsevier, pp. 639–664. https://doi.org/10.1016/B978-0-12-800206-3.00027-6

Fincher, C.T., Wurtzel, O., de Hoog, T., Kravarik, K.M., Reddien, P.W., 2018. Cell type transcriptome atlas for the planarian *Schmidtea mediterranea*. Science (1979) 360. https://doi.org/10.1126/science.aaq1736

Fox, D.T., Duronio, R.J., 2013. Endoreplication and polyploidy: insights into development and disease. Development 140, 3–12. https://doi.org/10.1242/dev.080531

Friedländer, M.R., Adamidi, C., Han, T., Lebedeva, S., Isenbarger, T.A., Hirst, M., Marra, M., Nusbaum, C., Lee, W.L., Jenkin, J.C., Alvarado, A.S., Kim, J.K., Rajewsky, N., 2009. High-resolution profiling and discovery of planarian small RNAs. Proceedings of the National Academy of Sciences 106, 11546–11551. https://doi.org/10.1073/pnas.0905222106

Fu, M., Gu, J., Wang, M., Zhang, J., Chen, Y., Jiang, P., Zhu, T., Zhang, X., 2023. Emerging roles of tRNA-derived fragments in cancer. Mol Cancer 22, 30. https://doi.org/10.1186/s12943-023-01739-5

Fuchs, Y., Steller, H., 2011. Programmed Cell Death in Animal Development and Disease. Cell 147, 742–758. https://doi.org/10.1016/j.cell.2011.10.033

Fuller-Carter, P.I., Carter, K.W., Anderson, D., Harvey, A.R., Giles, K.M., Rodger, J., 2015. Integrated analyses of zebrafish miRNA and mRNA expression profiles identify miR-29b and miR-223 as potential regulators of optic nerve regeneration. BMC Genomics 16, 591. https://doi.org/10.1186/s12864-015-1772-1

Funayama, N., Nakatsukasa, M., Mohri, K., Masuda, Y., Agata, K., 2010. *Piwi* expression in archeocytes and choanocytes in demosponges: insights into the stem cell system in demosponges. Evol Dev 12, 275–287. https://doi.org/10.1111/j.1525-142X.2010.00413.x

Gangaraju, V.K., Lin, H., 2009. MicroRNAs: key regulators of stem cells. Nat Rev Mol Cell Biol 10, 116–125. https://doi.org/10.1038/nrm2621

Gehrke, A.R., Neverett, E., Luo, Y.-J., Brandt, A., Ricci, L., Hulett, R.E., Gompers, A., Ruby, J.G., Rokhsar, D.S., Reddien, P.W., Srivastava, M., 2019. Acoel genome reveals the regulatory landscape of whole-body regeneration. Science (1979) 363. https://doi.org/10.1126/science.aau6173

Gerber, T., Murawala, P., Knapp, D., Masselink, W., Schuez, M., Hermann, S., Gac-Santel, M., Nowoshilow, S., Kageyama, J., Khattak, S., Currie, J.D., Camp, J.G., Tanaka, E.M., Treutlein, B., 2018. Single-cell analysis uncovers convergence of cell identities during axolotl limb regeneration. Science (1979) 362. https://doi.org/10.1126/science.aaq0681

González-Rosa, J.M., Sharpe, M., Field, D., Soonpaa, M.H., Field, L.J., Burns, C.E., Burns, C.G., 2018. Myocardial Polyploidization Creates a Barrier to Heart Regeneration in Zebrafish. Dev Cell 44, 433-446.e7. https://doi.org/10.1016/j.devcel.2018.01.021

Grohme, M.A., Schloissnig, S., Rozanski, A., Pippel, M., Young, G.R., Winkler, S., Brandl, H., Henry, I., Dahl, A., Powell, S., Hiller, M., Myers, E., Rink, J.C., 2018. The genome of *Schmidtea mediterranea* and the evolution of core cellular mechanisms. Nature 554, 56–61. https://doi.org/10.1038/nature25473

Gu, T., Elgin, S.C.R., 2013. Maternal Depletion of Piwi, a Component of the RNAi System, Impacts Heterochromatin Formation in *Drosophila*. PLoS Genet 9, e1003780. https://doi.org/10.1371/journal.pgen.1003780

Guo, L., Bloom, J.S., Dols-Serrate, D., Boocock, J., Ben-David, E., Schubert, O.T., Kozuma, K., Ho, K., Warda, E., Chui, C., Wei, Y., Leighton, D., Lemus Vergara, T., Riutort, M., Sánchez Alvarado, A., Kruglyak, L., 2022. Island-specific evolution of a sex-primed autosome in a sexual planarian. Nature 606, 329–334. https://doi.org/10.1038/s41586-022-04757-3

Gurley, K.A., Elliott, S.A., Simakov, O., Schmidt, H.A., Holstein, T.W., Alvarado, A.S., 2010. Expression of secreted Wnt pathway components reveals unexpected complexity of the planarian amputation response. Dev Biol 347, 24–39. https://doi.org/10.1016/j.ydbio.2010.08.007

Guzzi, N., Cieśla, M., Ngoc, P.C.T., Lang, S., Arora, S., Dimitriou, M., Pimková, K., Sommarin, M.N.E., Munita, R., Lubas, M., Lim, Y., Okuyama, K., Soneji, S., Karlsson, G., Hansson, J., Jönsson, G., Lund, A.H., Sigvardsson, M., Hellström-Lindberg, E., Hsieh, A.C., Bellodi, C., 2018. Pseudouridylation of tRNA-Derived Fragments Steers Translational Control in Stem Cells. Cell 173, 1204-1216.e26. https://doi.org/10.1016/j.cell.2018.03.008

Ha, H., Song, J., Wang, S., Kapusta, A., Feschotte, C., Chen, K.C., Xing, J., 2014. A comprehensive analysis of piRNAs from adult human testis and their relationship with genes and mobile elements. BMC Genomics 15, 545. https://doi.org/10.1186/1471-2164-15-545

Haack, T.B., Kopajtich, R., Freisinger, P., Wieland, T., Rorbach, J., Nicholls, T.J., Baruffini, E., Walther, A., Danhauser, K., Zimmermann, F.A., Husain, R.A., Schum, J., Mundy, H., Ferrero, I., Strom, T.M., Meitinger, T., Taylor, R.W., Minczuk, M., Mayr, J.A., Prokisch, H., 2013. ELAC2 Mutations Cause a Mitochondrial RNA Processing Defect Associated with Hypertrophic Cardiomyopathy. The American Journal of Human Genetics 93, 211–223. https://doi.org/10.1016/j.ajhg.2013.06.006

Hallez, Paul., 1894. Catalogue des rhabdoclides, triclades & polyclades du nord de la France / par Paul Hallez. Impr. L. Danel, Lille: https://doi.org/10.5962/bhl.title.11545

Hatch, E.M., Fischer, A.H., Deerinck, T.J., Hetzer, M.W., 2013. Catastrophic Nuclear Envelope Collapse in Cancer Cell Micronuclei. Cell 154, 47–60. https://doi.org/10.1016/j.cell.2013.06.007

Hayashi, T., Asami, M., Higuchi, S., Shibata, N., Agata, K., 2006. Isolation of planarian X-ray-sensitive stem cells by fluorescence-activated cell sorting. Dev Growth Differ 48, 371–380. https://doi.org/10.1111/j.1440-169X.2006.00876.x

Holland, A.J., Cleveland, D.W., 2009. Boveri revisited: chromosomal instability, aneuploidy and tumorigenesis. Nat Rev Mol Cell Biol 10, 478–487. https://doi.org/10.1038/nrm2718

Holland, N.D., 2021. Vincenzo Colucci's 1886 memoir, *Intorno alla rigenerazione degli arti e della coda nei tritoni*, annotated and translated into English as: Concerning regeneration of the limbs and tail in salamanders. Eur Zool J 88, 837–890. https://doi.org/10.1080/24750263.2021.1943549

Hong, A., Narbonne-Reveau, K., Riesgo-Escovar, J., Fu, H., Aladjem, M.I., Lilly, M.A., 2007. The cyclin-dependent kinase inhibitor Dacapo promotes replication licensing during Drosophila endocycles. EMBO J 26, 2071–2082. https://doi.org/10.1038/sj.emboj.7601648

Hong, Y., Liang, H., Uzair-ur-Rehman, Wang, Y., Zhang, W., Zhou, Y., Chen, S., Yu, M., Cui, S., Liu, M., Wang, N., Ye, C., Zhao, C., Liu, Y., Fan, Q., Zhang, C.-Y., Sang, J., Zen, K., Chen, X., 2016. miR-96 promotes cell proliferation, migration and invasion by targeting PTPN9 in breast cancer. Sci Rep 6, 37421. https://doi.org/10.1038/srep37421

Hori, I., 1991. Role of fixed parenchyma cells in blastema formation of the planarian *Dugesia japonica*. Int J Dev Biol 35, 101–108.

Houwing, S., Berezikov, E., Ketting, R.F., 2008. Zili is required for germ cell differentiation and meiosis in zebrafish. EMBO J 27, 2702–2711. https://doi.org/10.1038/emboj.2008.204

Huang, Y., Ren, H.T., Xiong, J.L., Gao, X.C., Sun, X.H., 2017. Identification and characterization of known and novel microRNAs in three tissues of Chinese giant salamander base on deep sequencing approach. Genomics 109, 258–264. https://doi.org/10.1016/j.ygeno.2017.04.007

Huang, Z., Du, Y., Wen, J., Lu, B., Zhao, Y., 2022. snoRNAs: functions and mechanisms in biological processes, and roles in tumor pathophysiology. Cell Death Discov 8, 259. https://doi.org/10.1038/s41420-022-01056-8

Ivanković, M., Brand, J.N., Pandolfini, L., Brown, T., Pippel, M., Rozanski, A., Schubert, T., Grohme, M.A., Winkler, S., Robledillo, L., Zhang, M., Codino, A., Gustincich, S., Vila-Farré, M., Zhang, S., Papantonis, A., Marques, A., Rink, J.C., 2024. A comparative analysis of planarian genomes reveals regulatory conservation in the face of rapid structural divergence. Nat Commun 15, 8215. https://doi.org/10.1038/s41467-024-52380-9

Ivankovic, M., Haneckova, R., Thommen, A., Grohme, M.A., Vila-Farré, M., Werner, S., Rink, J.C., 2019. Model systems for regeneration: planarians. Development 146. https://doi.org/10.1242/dev.167684

Janssen, R., Le Gouar, M., Pechmann, M., Poulin, F., Bolognesi, R., Schwager, E.E., Hopfen, C., Colbourne, J.K., Budd, G.E., Brown, S.J., Prpic, N.-M., Kosiol, C., Vervoort, M., Damen, W.G., Balavoine, G., McGregor, A.P., 2010. Conservation, loss, and redeployment of Wnt ligands in protostomes: implications for understanding the evolution of segment formation. BMC Evol Biol 10, 374. https://doi.org/10.1186/1471-2148-10-374

Jehn, J., Treml, J., Wulsch, S., Ottum, B., Erb, V., Hewel, C., Kooijmans, R.N., Wester, L., Fast, I., Rosenkranz, D., 2020. 5′ tRNA halves are highly expressed in the

primate hippocampus and might sequence-specifically regulate gene expression. RNA 26, 694–707. https://doi.org/10.1261/rna.073395.119

Jirström, E., Matveeva, A., Baindoor, S., Donovan, P., Ma, Q., Morrissey, E.P., Arijs, I., Boeckx, B., Lambrechts, D., Garcia-Munoz, A., Dillon, E.T., Wynne, K., Ying, Z., Matallanas, D., Hogg, M.C., Prehn, J.H.M., 2025. Effects of ALS-associated 5'tiRNAGly-GCC on the transcriptomic and proteomic profile of primary neurons in vitro. Exp Neurol 385, 115128. https://doi.org/10.1016/j.expneurol.2024.115128

Johnson, G.L., Masias, E.J., Lehoczky, J.A., 2020. Cellular Heterogeneity and Lineage Restriction during Mouse Digit Tip Regeneration at Single-Cell Resolution. Dev Cell 52, 525-540.e5. https://doi.org/10.1016/j.devcel.2020.01.026

Jopling, C., Boue, S., Belmonte, J.C.I., 2011. Dedifferentiation, transdifferentiation and reprogramming: three routes to regeneration. Nat Rev Mol Cell Biol 12, 79–89. https://doi.org/10.1038/nrm3043

Juliano, C., Wessel, G., 2010. Versatile Germline Genes. Science (1979) 329, 640–641. https://doi.org/10.1126/science.1194037

Juliano, C.E., Swartz, S.Z., Wessel, G.M., 2010. A conserved germline multipotency program. Development 137, 4113–4126. https://doi.org/10.1242/dev.047969

Kaikkonen, M.U., Lam, M.T.Y., Glass, C.K., 2011. Non-coding RNAs as regulators of gene expression and epigenetics. Cardiovasc Res 90, 430–440. https://doi.org/10.1093/cvr/cvr097

Kane, D.A., Warga, R.M., Kimmel, C.B., 1992. Mitotic domains in the early embryo of the zebrafish. Nature 360, 735–737. https://doi.org/10.1038/360735a0

Karami, A., Tebyanian, H., Goodarzi, V., Shiri, S., 2015. Planarians: an *In Vivo* Model for Regenerative Medicine. Int J Stem Cells 8, 128–133. https://doi.org/10.15283/ijsc.2015.8.2.128

Kim, I. V., Duncan, E.M., Ross, E.J., Gorbovytska, V., Nowotarski, S.H., Elliott, S.A., Sánchez Alvarado, A., Kuhn, C.-D., 2019. Planarians recruit piRNAs for mRNA turnover in adult stem cells. Genes Dev 33, 1575–1590. https://doi.org/10.1101/gad.322776.118

Kim, I. V., Riedelbauch, S., Kuhn, C.-D., 2020. The piRNA pathway in planarian flatworms: new model, new insights. Biol Chem 401, 1123–1141. https://doi.org/10.1515/hsz-2019-0445

King, B.L., Yin, V.P., 2016. A Conserved MicroRNA Regulatory Circuit Is Differentially Controlled during Limb/Appendage Regeneration. PLoS One 11, e0157106. https://doi.org/10.1371/journal.pone.0157106

King, H.O., Owusu-Boaitey, K.E., Fincher, C.T., Reddien, P.W., 2024. A transcription factor atlas of stem cell fate in planarians. Cell Rep 43, 113843. https://doi.org/10.1016/j.celrep.2024.113843

King, R.S., Newmark, P.A., 2012. The cell biology of regeneration. Journal of Cell Biology 196, 553–562. https://doi.org/10.1083/jcb.201105099

Kloc, M., Tworzydło, W., Szklarzewicz, T., 2024. Germline and Somatic Cell Syncytia in Insects. Syncytia: Origin, Structure, and Functions. pp. 47–63. https://doi.org/10.1007/978-3-031-37936-9_3

Kodama, J., Kaito, T., 2020. Osteoclast Multinucleation: Review of Current Literature. Int J Mol Sci 21. https://doi.org/10.3390/ijms21165685

Krishna, S., Nair, A., Cheedipudi, S., Poduval, D., Dhawan, J., Palakodeti, D., Ghanekar, Y., 2013. Deep sequencing reveals unique small RNA repertoire that is regulated during head regeneration in *Hydra magnipapillata*. Nucleic Acids Res 41, 599–616. https://doi.org/10.1093/nar/gks1020

Krishna, S., Raghavan, S., DasGupta, R., Palakodeti, D., 2021. tRNA-derived fragments (tRFs): establishing their turf in post-transcriptional gene regulation. Cellular and Molecular Life Sciences 78, 2607–2619. https://doi.org/10.1007/s00018-020-03720-7

Krishna, S., Yim, D.G., Lakshmanan, V., Tirumalai, V., Koh, J.L., Park, J.E., Cheong, J.K., Low, J.L., Lim, M.J., Sze, S.K., Shivaprasad, P., Gulyani, A., Raghavan, S., Palakodeti, D., DasGupta, R., 2019. Dynamic expression of tRNA-derived small RNAs define cellular states. EMBO Rep 20. https://doi.org/10.15252/embr.201947789

Krishnan, D., Ghosh, S.K., 2018. Cellular Events of Multinucleated Giant Cells Formation During the Encystation of *Entamoeba invadens*. Front Cell Infect Microbiol 8, 262. https://doi.org/10.3389/fcimb.2018.00262

Kuhn, S., Johnson, S.L., Furness, D.N., Chen, J., Ingham, N., Hilton, J.M., Steffes, G., Lewis, M.A., Zampini, V., Hackney, C.M., Masetto, S., Holley, M.C., Steel, K.P., Marcotti, W., 2011. miR-96 regulates the progression of differentiation in mammalian cochlear inner and outer hair cells. Proceedings of the National Academy of Sciences 108, 2355–2360. https://doi.org/10.1073/pnas.1016646108

Kumar, P., Kuscu, C., Dutta, A., 2016. Biogenesis and Function of Transfer RNA-Related Fragments (tRFs). Trends Biochem Sci 41, 679–689. https://doi.org/10.1016/j.tibs.2016.05.004

Kuscu, C., Kumar, P., Kiran, M., Su, Z., Malik, A., Dutta, A., 2018. tRNA fragments (tRFs) guide Ago to regulate gene expression post-transcriptionally in a Dicer-independent manner. RNA 24, 1093–1105. https://doi.org/10.1261/rna.066126.118

Lai, A.G., Aboobaker, A.A., 2018. EvoRegen in animals: Time to uncover deep conservation or convergence of adult stem cell evolution and regenerative processes. Dev Biol 433, 118–131. https://doi.org/10.1016/j.ydbio.2017.10.010

Lai, A.G., Kosaka, N., Abnave, P., Sahu, S., Aboobaker, A.A., 2018. The abrogation of condensin function provides independent evidence for defining the self-renewing population of pluripotent stem cells. Dev Biol 433, 218–226. https://doi.org/10.1016/j.ydbio.2017.07.023

Lakshmanan, V., Sujith, T.N., Bansal, D., Shivaprasad, P. V., Palakodeti, D., Krishna, S., 2021. Comprehensive annotation and characterization of planarian tRNA and

tRNA-derived fragments (tRFs). RNA 27, 477–495. https://doi.org/10.1261/rna.077701.120

Lau, N.C., Ohsumi, T., Borowsky, M., Kingston, R.E., Blower, M.D., 2009. Systematic and single cell analysis of *Xenopus* Piwi-interacting RNAs and Xiwi. EMBO J 28, 2945–2958. https://doi.org/10.1038/emboj.2009.237

Lazzeri, E., Angelotti, M.L., Peired, A., Conte, C., Marschner, J.A., Maggi, L., Mazzinghi, B., Lombardi, D., Melica, M.E., Nardi, S., Ronconi, E., Sisti, A., Antonelli, G., Becherucci, F., De Chiara, L., Guevara, R.R., Burger, A., Schaefer, B., Annunziato, F., Anders, H.-J., Lasagni, L., Romagnani, P., 2018. Endocycle-related tubular cell hypertrophy and progenitor proliferation recover renal function after acute kidney injury. Nat Commun 9, 1344. https://doi.org/10.1038/s41467-018-03753-4

Lazzerini Denchi, E., Celli, G., de Lange, T., 2006. Hepatocytes with extensive telomere deprotection and fusion remain viable and regenerate liver mass through endoreduplication. Genes Dev 20, 2648–2653. https://doi.org/10.1101/gad.1453606

Lee, S.-K., Jung, S.-H., Song, S.-J., Lee, I.-G., Choi, J.-Y., Zadeh, H., Lee, D.-W., Pi, S.-H., You, H.-K., 2022. miRNA-Based Early Healing Mechanism of Extraction Sockets: miR-190a-5p, a Potential Enhancer of Bone Healing. Biomed Res Int 2022. https://doi.org/10.1155/2022/7194640

Lee, Y.S., Shibata, Y., Malhotra, A., Dutta, A., 2009. A novel class of small RNAs: tRNA-derived RNA fragments (tRFs). Genes Dev 23, 2639–2649. https://doi.org/10.1101/gad.1837609

Lengfeld, T., Watanabe, H., Simakov, O., Lindgens, D., Gee, L., Law, L., Schmidt, H.A., Özbek, S., Bode, H., Holstein, T.W., 2009. Multiple Wnts are involved in *Hydra* organizer formation and regeneration. Dev Biol 330, 186–199. https://doi.org/10.1016/j.ydbio.2009.02.004

Li, X.Z., Roy, C.K., Dong, X., Bolcun-Filas, E., Wang, J., Han, B.W., Xu, J., Moore, M.J., Schimenti, J.C., Weng, Z., Zamore, P.D., 2013. An Ancient Transcription Factor Initiates the Burst of piRNA Production during Early Meiosis in Mouse Testes. Mol Cell 50, 67–81. https://doi.org/10.1016/j.molcel.2013.02.016

Li, Y.-Q., Zeng, A., Han, X.-S., Wang, C., Li, G., Zhang, Z.-C., Wang, J.-Y., Qin, Y.-W., Jing, Q., 2011. Argonaute-2 regulates the proliferation of adult stem cells in planarian. Cell Res 21, 1750–1754. https://doi.org/10.1038/cr.2011.151

Liang, Junyong, Liang, Jingjie, Tan, Q., Wang, Z., 2023. ELAC2 Functions as a Key Gene in the Early Development of Placental Formation Based on WGCNA. Cells 12, 613. https://doi.org/10.3390/cells12040613

Lim, R.S.M., Anand, A., Nishimiya-Fujisawa, C., Kobayashi, S., Kai, T., 2014. Analysis of Hydra PIWI proteins and piRNAs uncover early evolutionary origins of the piRNA pathway. Dev Biol 386, 237–251. https://doi.org/10.1016/j.ydbio.2013.12.007

Lim, R.S.M., Kai, T., 2015. A piece of the pi(e): The diverse roles of animal piRNAs and their PIWI partners. Semin Cell Dev Biol 47–48, 17–31. https://doi.org/10.1016/j.semcdb.2015.10.025

Liu, X., Mei, W., Padmanaban, V., Alwaseem, H., Molina, H., Passarelli, M.C., Tavora, B., Tavazoie, S.F., 2022. A pro-metastatic tRNA fragment drives Nucleolin oligomerization and stabilization of its bound metabolic mRNAs. Mol Cell 82, 2604-2617.e8. https://doi.org/10.1016/j.molcel.2022.05.008

Losick, V.P., Fox, D.T., Spradling, A.C., 2013. Polyploidization and Cell Fusion Contribute to Wound Healing in the Adult *Drosophila* Epithelium. Current Biology 23, 2224–2232. https://doi.org/10.1016/j.cub.2013.09.029

Lovely, A.M., Duerr, T.J., Qiu, Q., Galvan, S., Voss, S.R., Monaghan, J.R., 2022. Wnt Signaling Coordinates the Expression of Limb Patterning Genes During Axolotl Forelimb Development and Regeneration. Front Cell Dev Biol 10. https://doi.org/10.3389/fcell.2022.814250

Lucchetta, E.M., Ohlstein, B., 2017. Amitosis of Polyploid Cells Regenerates Functional Stem Cells in the Drosophila Intestine. Cell Stem Cell 20, 609-620.e6. https://doi.org/10.1016/j.stem.2017.02.012

Luo, S., He, F., Luo, J., Dou, S., Wang, Y., Guo, A., Lu, J., 2018. Drosophila tsRNAs preferentially suppress general translation machinery via antisense pairing and participate in cellular starvation response. Nucleic Acids Res 46, 5250–5268. https://doi.org/10.1093/nar/gky189

Ma, B., Wang, S., Wu, W., Shan, P., Chen, Y., Meng, J., Xing, L., Yun, J., Hao, L., Wang, X., Li, S., Guo, Y., 2023. Mechanisms of circRNA/lncRNA-miRNA interactions and applications in disease and drug research. Biomedicine & Pharmacotherapy 162, 114672. https://doi.org/10.1016/j.biopha.2023.114672

Ma, X., Shi, W., Peng, L., Qin, X., Hui, Y., 2018. MiR-96 enhances cellular proliferation and tumorigenicity of human cervical carcinoma cells through PTPN9. Saudi J Biol Sci 25, 863–867. https://doi.org/10.1016/j.sjbs.2017.10.020

Magee, R., Rigoutsos, I., 2020. On the expanding roles of tRNA fragments in modulating cell behavior. Nucleic Acids Res 48, 9433–9448. https://doi.org/10.1093/nar/gkaa657

Mahowald, A.P., 1968. Polar granules of *Drosophila*. II. Ultrastructural changes during early embryogenesis. Journal of Experimental Zoology 167, 237–261. https://doi.org/10.1002/jez.1401670211

Mani, S.R., Megosh, H., Lin, H., 2014. PIWI proteins are essential for early *Drosophila* embryogenesis. Dev Biol 385, 340–349. https://doi.org/10.1016/j.ydbio.2013.10.017

Matsumoto, T., Wakefield, L., Tarlow, B.D., Grompe, M., 2020. In Vivo Lineage Tracing of Polyploid Hepatocytes Reveals Extensive Proliferation during Liver Regeneration. Cell Stem Cell 26, 34-47.e3. https://doi.org/10.1016/j.stem.2019.11.014

Mauri, M., Kirchner, M., Aharoni, R., Ciolli Mattioli, C., van den Bruck, D., Gutkovitch, N., Modepalli, V., Selbach, M., Moran, Y., Chekulaeva, M., 2017. Conservation of miRNA-mediated silencing mechanisms across 600 million years of animal evolution. Nucleic Acids Res 45, 938–950. https://doi.org/10.1093/nar/gkw792

McCusker, C., Bryant, S. V., Gardiner, D.M., 2015. The axolotl limb blastema: cellular and molecular mechanisms driving blastema formation and limb regeneration in tetrapods. Regeneration 2, 54–71. https://doi.org/10.1002/reg2.32

Mehrotra, S., Maqbool, S.B., Kolpakas, A., Murnen, K., Calvi, B.R., 2008. Endocycling cells do not apoptose in response to DNA rereplication genotoxic stress. Genes Dev 22, 3158–3171. https://doi.org/10.1101/gad.1710208

Merryman, M.S., Alvarado, A.S., Jenkin, J.C., 2018. Culturing Planarians in the Laboratory. pp. 241–258. https://doi.org/10.1007/978-1-4939-7802-1_5

Mescher, A.L., White, G.W., Brokaw, J.J., 2000. Apoptosis in regenerating and denervated, nonregenerating urodele forelimbs. Wound Repair and Regeneration 8, 110–116. https://doi.org/10.1046/j.1524-475x.2000.00110.x

Moein, S., Ahmadbeigi, N., Adibi, R., Kamali, S., Moradzadeh, K., Nematollahi, P., Nardi, N.B., Gheisari, Y., 2023. Regenerative potential of multinucleated cells: bone marrow adiponectin-positive multinucleated cells take the lead. Stem Cell Res Ther 14, 173. https://doi.org/10.1186/s13287-023-03400-w

Molina, M.D., Cebrià, F., 2021. Decoding Stem Cells: An Overview on Planarian Stem Cell Heterogeneity and Lineage Progression. Biomolecules 11, 1532. https://doi.org/10.3390/biom11101532

Morgan, T.H., 1898. Experimental studies of the regeneration of Planaria *maculata*. Archiv für Entwickelungsmechanik der Organismen 7, 364–397. https://doi.org/10.1007/BF02161491

Mullins, L.J., Mullins, J.J., 2004. Insights from the rat genome sequence. Genome Biol 5, 221. https://doi.org/10.1186/gb-2004-5-5-221

Murakami, M.S., Moody, S.A., Daar, I.O., Morrison, D.K., 2004. Morphogenesis during *Xenopus* gastrulation requires Wee1-mediated inhibition of cell proliferation. Development 131, 571–580. https://doi.org/10.1242/dev.00971

Nahar, S., Morales Moya, L.J., Brunner, J., Hendriks, G.-J., Towbin, B., Hauser, Y.P., Brancati, G., Gaidatzis, D., Großhans, H., 2024. Dynamics of miRNA accumulation during *C. elegans* larval development. Nucleic Acids Res 52, 5336–5355. https://doi.org/10.1093/nar/gkae115

Nakasa, T., Yoshizuka, M., Usman, M., Mahmoud, E., Ochi, M., 2015. MicroRNAs and Bone Regeneration. Curr Genomics 16, 441–452. https://doi.org/10.2174/1389202916666150817213630

O'Farrell, P.H., 2015. Growing an Embryo from a Single Cell: A Hurdle in Animal Life. Cold Spring Harb Perspect Biol 7, a019042. https://doi.org/10.1101/cshperspect.a019042

Ong, S.-G., Lee, W.H., Kodo, K., Wu, J.C., 2015. MicroRNA-mediated regulation of differentiation and trans-differentiation in stem cells. Adv Drug Deliv Rev 88, 3–15. https://doi.org/10.1016/j.addr.2015.04.004

Orii, H., Ito, H., Watanabe, K., 2002. Anatomy of the Planarian *Dugesia japonica* I. The Muscular System Revealed by Antisera against Myosin Heavy Chains. Zoolog Sci 19, 1123–1131. https://doi.org/10.2108/zsj.19.1123

Ouyang, Z., Wei, K., 2021. miRNA in cardiac development and regeneration. Cell Regeneration 10, 14. https://doi.org/10.1186/s13619-021-00077-5

Oviedo, N.J., Nicolas, C.L., Adams, D.S., Levin, M., 2008a. Planarians: A Versatile and Powerful Model System for Molecular Studies of Regeneration, Adult Stem Cell Regulation, Aging, and Behavior. Cold Spring Harb Protoc 2008, pdb.emo101. https://doi.org/10.1101/pdb.emo101

Oviedo, N.J., Pearson, B.J., Levin, M., Sánchez Alvarado, A., 2008b. Planarian PTEN homologs regulate stem cells and regeneration through TOR signaling. Dis Model Mech 1, 131–143. https://doi.org/10.1242/dmm.000117

Palakodeti, D., Smielewska, M., Graveley, B.R., 2006. MicroRNAs from the Planarian *Schmidtea mediterranea* : A model system for stem cell biology. RNA 12, 1640–1649. https://doi.org/10.1261/rna.117206

Palakodeti, D., Smielewska, M., Lu, Y.-C., Yeo, G.W., Graveley, B.R., 2008. The PIWI proteins SMEDWI-2 and SMEDWI-3 are required for stem cell function and piRNA expression in planarians. RNA 14, 1174–1186. https://doi.org/10.1261/rna.1085008

Park, C., Owusu-Boaitey, K.E., Valdes, G.M., Reddien, P.W., 2023. Fate specification is spatially intermingled across planarian stem cells. Nat Commun 14, 7422. https://doi.org/10.1038/s41467-023-43267-2

Pellettieri, J., Alvarado, A.S., 2007. Cell Turnover and Adult Tissue Homeostasis: From Humans to Planarians. Annu Rev Genet 41, 83–105. https://doi.org/10.1146/annurev.genet.41.110306.130244

Pellettieri, J., Fitzgerald, P., Watanabe, S., Mancuso, J., Green, D.R., Sánchez Alvarado, A., 2010. Cell death and tissue remodeling in planarian regeneration. Dev Biol 338, 76–85. https://doi.org/10.1016/j.ydbio.2009.09.015

Peng, H., Shi, J., Zhang, Y., Zhang, H., Liao, S., Li, W., Lei, L., Han, C., Ning, L., Cao, Y., Zhou, Q., Chen, Q., Duan, E., 2012. A novel class of tRNA-derived small RNAs extremely enriched in mature mouse sperm. Cell Res 22, 1609–1612. https://doi.org/10.1038/cr.2012.141

Perez-Iratxeta, C., Palidwor, G., Porter, C.J., Sanche, N.A., Huska, M.R., Suomela, B.P., Muro, E.M., Krzyzanowski, P.M., Hughes, E., Campbell, P.A., Rudnicki, M.A., Andrade, M.A., 2005. Study of stem cell function using microarray experiments. FEBS Lett 579, 1795–1801. https://doi.org/10.1016/j.febslet.2005.02.020

Petersen, C.P., Reddien, P.W., 2009. A wound-induced Wnt expression program controls planarian regeneration polarity. Proceedings of the National Academy of Sciences 106, 17061–17066. https://doi.org/10.1073/pnas.0906823106

Peterson, N.G., Fox, D.T., 2021. Communal living: the role of polyploidy and syncytia in tissue biology. Chromosome Research 29, 245–260. https://doi.org/10.1007/s10577-021-09664-3

Piovesan, A., Pelleri, M.C., Antonaros, F., Strippoli, P., Caracausi, M., Vitale, L., 2019. On the length, weight and GC content of the human genome. BMC Res Notes 12, 106. https://doi.org/10.1186/s13104-019-4137-z

Plass, M., Solana, J., Wolf, F.A., Ayoub, S., Misios, A., Glažar, P., Obermayer, B., Theis, F.J., Kocks, C., Rajewsky, N., 2018. Cell type atlas and lineage tree of a whole complex animal by single-cell transcriptomics. Science (1979) 360. https://doi.org/10.1126/science.aaq1723

Poliwoda, S., Noor, N., Downs, E., Schaaf, A., Cantwell, A., Ganti, L., Kaye, A.D., Mosel, L.I., Carroll, C.B., Viswanath, O., Urits, I., 2022. Stem cells: a comprehensive review of origins and emerging clinical roles in medical practice. Orthop Rev (Pavia) 14. https://doi.org/10.52965/001c.37498

Qin, C., Feng, H., Zhang, C., Zhang, X., Liu, Y., Yang, D.-G., Du, L.-J., Sun, Y.-C., Yang, M.-L., Gao, F., Li, J.-J., 2020. Differential Expression Profiles and Functional Prediction of tRNA-Derived Small RNAs in Rats After Traumatic Spinal Cord Injury. Front Mol Neurosci 12. https://doi.org/10.3389/fnmol.2019.00326

Ramirez, A.N., Loubet-Senear, K., Srivastava, M., 2020. A Regulatory Program for Initiation of Wnt Signaling during Posterior Regeneration. Cell Rep 32, 108098. https://doi.org/10.1016/j.celrep.2020.108098

Reddien, Peter W., 2018. The Cellular and Molecular Basis for Planarian Regeneration. Cell 175, 327–345. https://doi.org/10.1016/j.cell.2018.09.021

Reddien, Peter W, 2018. The Cellular and Molecular Basis for Planarian Regeneration. Cell 175, 327–345. https://doi.org/10.1016/j.cell.2018.09.021

Reichman, O.J., 1984. Evolution of Regeneration Capabilities. Am Nat 123, 752–763. https://doi.org/10.1086/284237

Ribeiro, A.O., de Oliveira, A.C., Costa, J.M., Nachtigall, P.G., Herkenhoff, M.E., Campos, V.F., Delella, F.K., Pinhal, D., 2022. <scp>MicroRNA</scp> roles in regeneration: Multiple lessons from zebrafish. Developmental Dynamics 251, 556–576. https://doi.org/10.1002/dvdy.421

Richardson, B.E., Nowak, S.J., Baylies, M.K., 2008. Myoblast Fusion in Fly and Vertebrates: New Genes, New Processes and New Perspectives. Traffic 9, 1050–1059. https://doi.org/10.1111/j.1600-0854.2008.00756.x

Riedmann, L.T., Schwentner, R., 2010. miRNA, siRNA, piRNA and Argonautes: News in small matters. RNA Biol 7, 133–139. https://doi.org/10.4161/rna.7.2.11288

Rink, J.C. (Ed.), 2018. Planarian Regeneration. Springer New York, New York, NY. https://doi.org/10.1007/978-1-4939-7802-1

Robine, N., Lau, N.C., Balla, S., Jin, Z., Okamura, K., Kuramochi-Miyagawa, S., Blower, M.D., Lai, E.C., 2009. A Broadly Conserved Pathway Generates 3′UTR-Directed Primary piRNAs. Current Biology 19, 2066–2076. https://doi.org/10.1016/j.cub.2009.11.064

Rodriguez, A.J., Seipel, S.A., Hamill, D.R., Romancino, D.P., Di carlo, M., Suprenant, K.A., Bonder, E.M., 2005. Seawi—a sea urchin piwi/argonaute family member is a component of MT-RNP complexes. RNA 11, 646–656. https://doi.org/10.1261/rna.7198205

Rouget, C., Papin, C., Boureux, A., Meunier, A.-C., Franco, B., Robine, N., Lai, E.C., Pelisson, A., Simonelig, M., 2010. Maternal mRNA deadenylation and decay by the piRNA pathway in the early Drosophila embryo. Nature 467, 1128–1132. https://doi.org/10.1038/nature09465

Saito, K., Siomi, M.C., 2010. Small RNA-Mediated Quiescence of Transposable Elements in Animals. Dev Cell 19, 687–697. https://doi.org/10.1016/j.devcel.2010.10.011

Samarfard, S., Ghorbani, A., Karbanowicz, T.P., Lim, Z.X., Saedi, M., Fariborzi, N., McTaggart, A.R., Izadpanah, K., 2022. Regulatory non-coding RNA: The core defense mechanism against plant pathogens. J Biotechnol 359, 82–94. https://doi.org/10.1016/j.jbiotec.2022.09.014

Sánchez Alvarado, A., 2012. Q&A: What is regeneration, and why look to planarians for answers? BMC Biol 10, 88. https://doi.org/10.1186/1741-7007-10-88

Sandoval-Guzmán, T., Currie, J.D., 2018. The journey of cells through regeneration. Curr Opin Cell Biol 55, 36–41. https://doi.org/10.1016/j.ceb.2018.05.008

Sarais, F., Perdomo-Sabogal, A., Wimmers, K., Ponsuksili, S., 2022. tiRNAs: Insights into Their Biogenesis, Functions, and Future Applications in Livestock Research. Noncoding RNA 8, 37. https://doi.org/10.3390/ncrna8030037

Sasidharan, V., Lu, Y.-C., Bansal, D., Dasari, P., Poduval, D., Seshasayee, A., Resch, A.M., Graveley, B.R., Palakodeti, D., 2013. Identification of neoblast- and regeneration-specific miRNAs in the planarian *Schmidtea mediterranea*. RNA 19, 1394–1404. https://doi.org/10.1261/rna.038653.113

Saxena, A.K., 2010. Congenital Anomalies of Soft Tissues: Birth Defects Depending on Tissue Engineering Solutions and Present Advances in Regenerative Medicine. Tissue Eng Part B Rev 16, 455–466. https://doi.org/10.1089/ten.teb.2009.0700

Schlüter, T., Berger, C., Rosengauer, E., Fieth, P., Krohs, C., Ushakov, K., Steel, K.P., Avraham, K.B., Hartmann, A.K., Felmy, F., Nothwang, H.G., 2018. miR-96 is required for normal development of the auditory hindbrain. Hum Mol Genet 27, 860–874. https://doi.org/10.1093/hmg/ddy007

Schoenfelder, K.P., Fox, D.T., 2015. The expanding implications of polyploidy. Journal of Cell Biology 209, 485–491. https://doi.org/10.1083/jcb.201502016

Scimone, M.L., Kravarik, K.M., Lapan, S.W., Reddien, P.W., 2014. Neoblast Specialization in Regeneration of the Planarian *Schmidtea mediterranea*. Stem Cell Reports 3, 339–352. https://doi.org/10.1016/j.stemcr.2014.06.001

Scimone, M.L., Srivastava, M., Bell, G.W., Reddien, P.W., 2011. A regulatory program for excretory system regeneration in planarians. Development 138, 4387–4398. https://doi.org/10.1242/dev.068098

Sclavi, B., Herrick, J., 2019. Genome size variation and species diversity in salamanders. J Evol Biol 32, 278–286. https://doi.org/10.1111/jeb.13412

Sen, C.K., Ghatak, S., 2015. miRNA Control of Tissue Repair and Regeneration. Am J Pathol 185, 2629–2640. https://doi.org/10.1016/j.ajpath.2015.04.001

Sharma, U., Conine, C.C., Shea, J.M., Boskovic, A., Derr, A.G., Bing, X.Y., Belleannee, C., Kucukural, A., Serra, R.W., Sun, F., Song, L., Carone, B.R., Ricci, E.P., Li, X.Z., Fauquier, L., Moore, M.J., Sullivan, R., Mello, C.C., Garber, M., Rando, O.J., 2016. Biogenesis and function of tRNA fragments during sperm maturation and fertilization in mammals. Science (1979) 351, 391–396. https://doi.org/10.1126/science.aad6780

Shen, L., Liao, T., Chen, Q., Lei, Y., Wang, L., Gu, H., Qiu, Y., Zheng, T., Yang, Y., Wei, C., Chen, L., Zhao, Y., Niu, L., Zhang, S., Zhu, Y., Li, M., Wang, J., Li, X., Gan, M., Zhu, L., 2023. tRNA -derived small RNA, 5'tiRNA-Gly-CCC, promotes skeletal muscle regeneration through the inflammatory response. J Cachexia Sarcopenia Muscle 14, 1033–1045. https://doi.org/10.1002/jcsm.13187

Shi, J., Xu, J., Ma, J., He, F., 2023. tRNA-derived small RNAs are embedded in the gene regulatory network instructing *Drosophila* metamorphosis. Genome Res 33, 2119–2132. https://doi.org/10.1101/gr.278128.123

Shu, Z., Row, S., Deng, W.-M., 2018. Endoreplication: The Good, the Bad, and the Ugly. Trends Cell Biol 28, 465–474. https://doi.org/10.1016/j.tcb.2018.02.006

Siira, S.J., Rossetti, G., Richman, T.R., Perks, K., Ermer, J.A., Kuznetsova, I., Hughes, L., Shearwood, A.J., Viola, H.M., Hool, L.C., Rackham, O., Filipovska, A., 2018. Concerted regulation of mitochondrial and nuclear non-coding RNA by a dual-targeted RNase Z. EMBO Rep 19. https://doi.org/10.15252/embr.201846198

Sluys, R., Kawakatsu, M., 2006. Towards a phylogenetic classification of dendrocoelid freshwater planarians (Platyhelminthes): a morphological and eclectic approach. Journal of Zoological Systematics and Evolutionary Research 44, 274–284. https://doi.org/10.1111/j.1439-0469.2006.00371.x

Sluys, R., Kawakatsu, M., Riutort, M., Baguñà, J., 2009. A new higher classification of planarian flatworms (Platyhelminthes, Tricladida). J Nat Hist 43, 1763–1777. https://doi.org/10.1080/00222930902741669

Sluys, R., Riutort, M., 2018. Planarian Diversity and Phylogeny. pp. 1–56. https://doi.org/10.1007/978-1-4939-7802-1_1

Solana, J., Kao, D., Mihaylova, Y., Jaber-Hijazi, F., Malla, S., Wilson, R., Aboobaker, A., 2012. Defining the molecular profile of planarian pluripotent stem cells using a

combinatorial RNA-seq, RNA interference and irradiation approach. Genome Biol 13, R19. https://doi.org/10.1186/gb-2012-13-3-r19

Srivastava, M., 2021. Beyond Casual Resemblance: Rigorous Frameworks for Comparing Regeneration Across Species. Annu Rev Cell Dev Biol 37, 415–440. https://doi.org/10.1146/annurev-cellbio-120319-114716

Srivastava, M., Mazza-Curll, K.L., van Wolfswinkel, J.C., Reddien, P.W., 2014. Whole-Body Acoel Regeneration Is Controlled by Wnt and Bmp-Admp Signaling. Current Biology 24, 1107–1113. https://doi.org/10.1016/j.cub.2014.03.042

Sugita, S., Munechika, R., Nakamura, M., 2019. Multinucleation of Incubated Cells and Their Morphological Differences Compared to Mononuclear Cells. Micromachines (Basel) 10, 156. https://doi.org/10.3390/mi10020156

Sugiura, T., Taniguchi, Y., Tazaki, A., Ueno, N., Watanabe, K., Mochii, M., 2004. Differential gene expression between the embryonic tail bud and regenerating larval tail in *Xenopus laevis*. Dev Growth Differ 46, 97–105. https://doi.org/10.1111/j.1440-169X.2004.00727.x

Sultana, Mst.F., Abo, H., Kawashima, H., 2022. Human and mouse angiogenins: Emerging insights and potential opportunities. Front Microbiol 13. https://doi.org/10.3389/fmicb.2022.1022945

Sun, C., Shepard, D.B., Chong, R.A., López Arriaza, J., Hall, K., Castoe, T.A., Feschotte, C., Pollock, D.D., Mueller, R.L., 2012. LTR Retrotransposons Contribute to Genomic Gigantism in Plethodontid Salamanders. Genome Biol Evol 4, 168–183. https://doi.org/10.1093/gbe/evr139

Swanson, C.I., Meserve, J.H., McCarter, P.C., Thieme, A., Mathew, T., Elston, T.C., Duronio, R.J., 2015. Expression of an S phase-stabilized version of the CDK inhibitor Dacapo can alter endoreplication. Development. https://doi.org/10.1242/dev.115006

Tanaka, E.M., Reddien, P.W., 2011. The Cellular Basis for Animal Regeneration. Dev Cell 21, 172–185. https://doi.org/10.1016/j.devcel.2011.06.016

Thatcher, E.J., Patton, J.G., 2010. Small RNAs have a big impact on regeneration. RNA Biol 7, 333–338. https://doi.org/10.4161/rna.7.3.12085

Thompson, D.M., Parker, R., 2009. Stressing Out over tRNA Cleavage. Cell 138, 215–219. https://doi.org/10.1016/j.cell.2009.07.001

Tiozzo, S., Copley, R.R., 2015. Reconsidering regeneration in metazoans: an evo-devo approach. Front Ecol Evol 3. https://doi.org/10.3389/fevo.2015.00067

Todorov, H., Weißbach, S., Schlichtholz, L., Mueller, H., Hartwich, D., Gerber, S., Winter, J., 2024. Stage-specific expression patterns and co-targeting relationships among miRNAs in the developing mouse cerebral cortex. Commun Biol 7, 1366. https://doi.org/10.1038/s42003-024-07092-7

Tonks, N.K., Neel, B.G., 1996. From Form to Function: Signaling by Protein Tyrosine Phosphatases. Cell 87, 365–368. https://doi.org/10.1016/S0092-8674(00)81357-4

Trakala, M., Rodríguez-Acebes, S., Maroto, M., Symonds, C.E., Santamaría, D., Ortega, S., Barbacid, M., Méndez, J., Malumbres, M., 2015. Functional Reprogramming of Polyploidization in Megakaryocytes. Dev Cell 32, 155–167. https://doi.org/10.1016/j.devcel.2014.12.015

Tu, S., Johnson, S.L., 2011. Fate Restriction in the Growing and Regenerating Zebrafish Fin. Dev Cell 20, 725–732. https://doi.org/10.1016/j.devcel.2011.04.013

Tuck, A.C., Tollervey, D., 2011. RNA in pieces. Trends in Genetics 27, 422–432. https://doi.org/10.1016/j.tig.2011.06.001

Tursch, A., Holstein, T.W., 2023. From injury to patterning—MAPKs and Wnt signaling in Hydra. pp. 381–417. https://doi.org/10.1016/bs.ctdb.2023.01.003

van Wolfswinkel, J.C., 2014. Piwi and Potency: PIWI Proteins in Animal Stem Cells and Regeneration. Integr Comp Biol 54, 700–713. https://doi.org/10.1093/icb/icu084

van Wolfswinkel, J.C., Wagner, D.E., Reddien, P.W., 2014. Single-Cell Analysis Reveals Functionally Distinct Classes within the Planarian Stem Cell Compartment. Cell Stem Cell 15, 326–339. https://doi.org/10.1016/j.stem.2014.06.007

Vervoort, M., 2011. Regeneration and Development in Animals. Biol Theory 6, 25–35. https://doi.org/10.1007/s13752-011-0005-3

Vogg, M.C., Beccari, L., Iglesias Ollé, L., Rampon, C., Vriz, S., Perruchoud, C., Wenger, Y., Galliot, B., 2019. An evolutionarily-conserved Wnt3/β-catenin/Sp5 feedback loop restricts head organizer activity in Hydra. Nat Commun 10, 312. https://doi.org/10.1038/s41467-018-08242-2

Von Stetina, J.R., Frawley, L.E., Unhavaithaya, Y., Orr-Weaver, T.L., 2018. Variant cell cycles regulated by Notch signaling control cell size and ensure a functional blood-brain barrier. Development 145. https://doi.org/10.1242/dev.157115

Vorobjev, I.A., Bekbayev, S., Temirgaliyev, A., Tlegenova, M., Barteneva, N.S., 2023. Imaging Flow Cytometry of Multi-Nuclearity. pp. 87–101. https://doi.org/10.1007/978-1-0716-3020-4_5

Wagner, D.E., Wang, I.E., Reddien, P.W., 2011. Clonogenic neoblasts are pluripotent adult stem cells that underlie planarian regeneration. Science 332, 811–6. https://doi.org/10.1126/science.1203983

Wajahat, M., Bracken, C.P., Orang, A., 2021. Emerging Functions for snoRNAs and snoRNA-Derived Fragments. Int J Mol Sci 22, 10193. https://doi.org/10.3390/ijms221910193

Walczyńska, K.S., Zhu, L., Liang, Y., 2023. Insights into the role of the Wnt signaling pathway in the regeneration of animal model systems. Int J Dev Biol 67, 65–78. https://doi.org/10.1387/ijdb.220144yl

Wang, C., Lin, H., 2021. Roles of piRNAs in transposon and pseudogene regulation of germline mRNAs and lncRNAs. Genome Biol 22, 27. https://doi.org/10.1186/s13059-020-02221-x

Wang, J., Batourina, E., Schneider, K., Souza, S., Swayne, T., Liu, C., George, C.D., Tate, T., Dan, H., Wiessner, G., Zhuravlev, Y., Canman, J.C., Mysorekar, I.U., Mendelsohn, C.L., 2018. Polyploid Superficial Cells that Maintain the Urothelial Barrier Are Produced via Incomplete Cytokinesis and Endoreplication. Cell Rep 25, 464-477.e4. https://doi.org/10.1016/j.celrep.2018.09.042

Wang, L., Owusu-Hammond, C., Sievert, D., Gleeson, J.G., 2023. Stem Cell–Based Organoid Models of Neurodevelopmental Disorders. Biol Psychiatry 93, 622–631. https://doi.org/10.1016/j.biopsych.2023.01.012

Wehner, D., Cizelsky, W., Vasudevaro, M.D., Özhan, G., Haase, C., Kagermeier-Schenk, B., Röder, A., Dorsky, R.I., Moro, E., Argenton, F., Kühl, M., Weidinger, G., 2014. Wnt/β-Catenin Signaling Defines Organizing Centers that Orchestrate Growth and Differentiation of the Regenerating Zebrafish Caudal Fin. Cell Rep 6, 467–481. https://doi.org/10.1016/j.celrep.2013.12.036

Wei, C., Salichos, L., Wittgrove, C.M., Rokas, A., Patton, J.G., 2012. Transcriptome-wide analysis of small RNA expression in early zebrafish development. RNA 18, 915–929. https://doi.org/10.1261/rna.029090.111

Weidensdorfer, D., Stöhr, N., Baude, A., Lederer, M., Köhn, M., Schierhorn, A., Buchmeier, S., Wahle, E., Hüttelmaier, S., 2009. Control of c-myc mRNA stability by IGF2BP1-associated cytoplasmic RNPs. RNA 15, 104–115. https://doi.org/10.1261/rna.1175909

Weissman, I.L., Anderson, D.J., Gage, F., 2001. Stem and Progenitor Cells: Origins, Phenotypes, Lineage Commitments, and Transdifferentiations. Annu Rev Cell Dev Biol 17, 387–403. https://doi.org/10.1146/annurev.cellbio.17.1.387

Wen, J., Huang, Z., Li, Q., Chen, X., Qin, H., Zhao, Y., 2021. Research progress on the tsRNA classification, function, and application in gynecological malignant tumors. Cell Death Discov 7, 388. https://doi.org/10.1038/s41420-021-00789-2

Wenemoser, D., Lapan, S.W., Wilkinson, A.W., Bell, G.W., Reddien, P.W., 2012. A molecular wound response program associated with regeneration initiation in planarians. Genes Dev 26, 988–1002. https://doi.org/10.1101/gad.187377.112

Wenemoser, D., Reddien, P.W., 2010. Planarian regeneration involves distinct stem cell responses to wounds and tissue absence. Dev Biol 344, 979–91. https://doi.org/10.1016/j.ydbio.2010.06.017

Wilkinson, P.D., Delgado, E.R., Alencastro, F., Leek, M.P., Roy, N., Weirich, M.P., Stahl, E.C., Otero, P.A., Chen, M.I., Brown, W.K., Duncan, A.W., 2019. The Polyploid State Restricts Hepatocyte Proliferation and Liver Regeneration in Mice. Hepatology 69, 1242–1258. https://doi.org/10.1002/hep.30286

Windmueller, R., Leach, J.P., Babu, A., Zhou, S., Morley, M.P., Wakabayashi, A., Petrenko, N.B., Viatour, P., Morrisey, E.E., 2020. Direct Comparison of Mononucleated and Binucleated Cardiomyocytes Reveals Molecular Mechanisms Underlying Distinct Proliferative Competencies. Cell Rep 30, 3105-3116.e4. https://doi.org/10.1016/j.celrep.2020.02.034

Wu, X., Pan, Y., Fang, Y., Zhang, J., Xie, M., Yang, F., Yu, T., Ma, P., Li, W., Shu, Y., 2020. The Biogenesis and Functions of piRNAs in Human Diseases. Mol Ther Nucleic Acids 21, 108–120. https://doi.org/10.1016/j.omtn.2020.05.023

Wu, Y., Lou, Q.-Y., Ge, F., Xiong, Q., 2017. Quantitative Proteomics Analysis Reveals Novel Targets of miR-21 in Zebrafish Embryos. Sci Rep 7, 4022. https://doi.org/10.1038/s41598-017-04166-x

Wurtzel, O., Oderberg, I.M., Reddien, P.W., 2017. Planarian Epidermal Stem Cells Respond to Positional Cues to Promote Cell-Type Diversity. Dev Cell 40, 491-504.e5. https://doi.org/10.1016/j.devcel.2017.02.008

Yu, M., Lu, B., Zhang, J., Ding, J., Liu, P., Lu, Y., 2020. tRNA-derived RNA fragments in cancer: current status and future perspectives. J Hematol Oncol 13, 121. https://doi.org/10.1186/s13045-020-00955-6

Yu, Y., Xiao, J., Hann, S.S., 2019. The emerging roles of PIWI-interacting RNA in human cancers . Cancer Manag Res Volume 11, 5895–5909. https://doi.org/10.2147/CMAR.S209300

Zeng, A., Li, H., Guo, L., Gao, X., McKinney, S., Wang, Y., Yu, Z., Park, J., Semerad, C., Ross, E., Cheng, L.-C., Davies, E., Lei, K., Wang, W., Perera, A., Hall, K., Peak, A., Box, A., Sánchez Alvarado, A., 2018. Prospectively Isolated Tetraspanin+ Neoblasts Are Adult Pluripotent Stem Cells Underlying Planaria Regeneration. Cell 173, 1593-1608.e20. https://doi.org/10.1016/j.cell.2018.05.006

Zhang, P., Wu, W., Chen, Q., Chen, M., 2019. Non-Coding RNAs and their Integrated Networks. J Integr Bioinform 16. https://doi.org/10.1515/jib-2019-0027

Zhang, Q., Lu, B., 2024. The mRNA and microRNA Landscape of the Blastema Niche in Regenerating Newt Limbs. Int J Mol Sci 25, 9225. https://doi.org/10.3390/ijms25179225

Zhang, X.-T., Mao, Z.-Y., Jin, X.-Y., Wang, Y.-G., Dong, Y.-Q., Zhang, C., 2023. Identification of a tsRNA Contributor to Impaired Diabetic Wound Healing via High Glucose-Induced Endothelial Dysfunction. Diabetes, Metabolic Syndrome and Obesity Volume 16, 285–298. https://doi.org/10.2147/DMSO.S379473

Zhou, X., Platt, J.L., 2011. Molecular and Cellular Mechanisms of Mammalian Cell Fusion. pp. 33–64. https://doi.org/10.1007/978-94-007-0763-4_4

Zhu, P., Yu, J., Zhou, P., 2020. Role of tRNA-derived fragments in cancer: novel diagnostic and therapeutic targets tRFs in cancer. Am J Cancer Res 10, 393–402.

Zhu, S.J., Hallows, S.E., Currie, K.W., Xu, C., Pearson, B.J., 2015. A mex3 homolog is required for differentiation during planarian stem cell lineage development. Elife 4. https://doi.org/10.7554/eLife.07025

Zhu, W., Pao, G.M., Satoh, A., Cummings, G., Monaghan, J.R., Harkins, T.T., Bryant, S. V., Randal Voss, S., Gardiner, D.M., Hunter, T., 2012. Activation of germline-specific genes is required for limb regeneration in the Mexican axolotl. Dev Biol 370, 42–51. https://doi.org/10.1016/j.ydbio.2012.07.021